8-18 GHz RADAR SPECTROMETER

CRES Technical Report 177-43

Thomas F. Bush
Fawwaz T. Ulaby

September, 1973

Supported by:
NATIONAL AERONAUTICS AND SPACE ADMINISTRATION
Lyndon B. Johnson Space Center
Houston, Texas 77058
CONTRACT NAS 9-10261

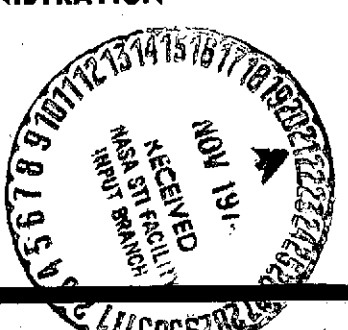

THE UNIVERSITY OF KANSAS CENTER FOR RESEARCH, INC.
2385 Irving Hill Rd.— Campus West Lawrence, Kansas 66044

THE UNIVERSITY OF KANSAS SPACE TECHNOLOGY LABORATORIES
2291 Irving Hill Dr.— Campus West Lawrence, Kansas 66044

Telephone:

8 - 18 GHz RADAR SPECTROMETER

CRES Technical Report 177-43

Thomas F. Bush
Fawwaz T. Ulaby

September 1973

Supported by:

NATIONAL AERONAUTICS AND SPACE ADMINISTRATION
Lyndon B. Johnson Space Center
Houston, Texas 77058

CONTRACT NAS 9-10261

TABLE OF CONTENTS

TABLE OF CONTENTS (CONTINUED)

LIST OF FIGURES

LIST OF FIGURES (CONTINUED)

ABSTRACT

This report discusses the design, construction, testing and accuracy of an 8-18 GHz radar spectrometer. The spectrometer is an FM-CW system employing a dual antenna system. The antennas, transmitter and a portion of the receiver are mounted at the top of a 26 meter hydraulic boom which is in turn mounted on a truck for system mobility. HH and VV polarized measurements are possible at incidence angles ranging from 0° to 80°. Calibration is accomplished by referencing the measurements against a Luneberg lens of known radar cross section.

1.0 INTRODUCTION

Remote Sensing is one of the youngest, yet one of the most dynamic fields in the scientific community today. The term "youngest," however, should not be construed as absolute since the advent of the camera provided one of the most valuable sensors available at the present day. It was not until the past decade, however, that remote sensing came of age as a science recognized as a valuable tool with the potential to solve many of the present and future resources problems facing mankind (1, 2, 20).

Remote Sensing advocates do not claim to have answers to all of man's problems but they do offer solutions to many of the most pressing questions At this time one of the most real problems for many people is the world's diminishing energy supply. Remote sensing has been shown to be an extremely effective tool for the study of lithologic and geological structures, important keys in the exploration for oil (3, 4, 19, 20). Other applications of remote sensing include land-use inventories, detection of crop insect pests and diseases, weather forecasting and a variety of others too numerous to be presented in detail. Luney and Dill (2) present a discussion of many of the applications of remote sensing with particular attention to agriculture and forestry. The Water Resources Research Catalog (41) provides a useful index to the many applications of remote sensing to the field of hydrology.

The ocean, covering 75 per cent of our planet, provides food and transportation for all nations and constitutes the major link in the earths water cycle. Thus it is not surprising that the sea is a major target of study for many investigators. These investigations indicate an extreme potential in remotely sensing the ocean (5, 6).

As the popularity of remote sensing increases, more and more effort is being made to design new sensors and to apply existing sensors. A number of sensors were developed for usage in other fields but were recognized as important instruments to be used in remote sensing. The obvious example of the aerial camera found its first applications in the military which has helped it to develop into one of the primary sensors. Its popularity stems from the fact that it is flexible, can provide high resolution images and is available to most people. Its major disadvantages stem from the fact that it requires solar illumination and clear weather (7, 8).

The radiometer has found application in the visible, infrared and microwave portions of the electro-magnetic spectrum. Its ability to measure target emission, an indicator of target temperature, has shown it to be an effective tool in geoscience investigations and in the study of thermal pollutants (9, 10).

A multitude of other sensors are available to scientists such as sonar, gamma ray spectrometers and magnetometers, each possessing unique capabilities. Although each sensor provides its own particular type of data, the integration of a number of these unique sensors into an operational system provides the potential for realizing more information than any one could provide alone. To fully utilize an operational system, each element of the system must be dependable and fully understood (11). Radar is one such element and may play the central role in an operational system.

2.0 RADAR AS A REMOTE SENSOR

Radar is a unique device in that it provides its own source of illumination. It has its origins during World War II when it was developed by the military for aircraft detection and tracking. Since then it has developed as both a military tool and as a civilian tool.

Being self-illuminating and thus independent of external illumination, radar provides distinct advantages over passive sensors. The angle at which the illumination intersects the target can be varied so as to produce a number of desired effects such as shadowing (12). Radar is also nearly weather and time independent. The designer's control of frequency allows him to place the signal in an atmospheric window so that signal attenuation due to rain, cloud cover and gaseous absorption is minimized.

The frequency and polarization of the illumination can be chosen to provide optimum results for a particular investigation. Experimental results have shown that both parameters can be extremely important in the detection and separation of targets (13, 14, 15). Control of the illumination phase is also important, particularly in the synthetic aperture imaging radars.

2.1 Imaging Radar

Radar technology has continued at a rapid pace since its beginnings. The present state of the art has produced an ultra-sophisticated imaging system known as a synthetic aperture side looking airborne radar. This radar illuminates a target from a number of positions along its flight path and extracts both amplitude and phase information from the signal at each position. This information is then stored and finally processed to produce an image. Although this is an extremely costly and complicated process, it results in very fine resolution which in theory can under some conditions top that of a high quality photographic system (16)!

Needless to say, synthetic aperture radars are not commonplace. Real aperture side looking imaging systems are available for civilian use but even these are not yet readily available. They have, however, exhibited their capabilities and are the topic of many investigations (4, 12, 15, 17).

A distinct advantage of state of the art side look radar is that it is an imaging system. The image resemblance to a photograph allows it to be interpreted by a photo interpreter after minimal instructions. All of his inclinations to look for sizes, shapes and patterns in the image are applicable. Tone, shadow and texture are highly dependent on the imaging system, a critical point that must be realized (18).

A second capability of a side looking imaging system is that it produces a synoptic presentation of a rather extensive area while providing resolution acceptable for most applications. Typically, a real aperture side looking system can provide cross track resolution of 10 meters and along track resolution of 15 meters while covering a 65 km swath from an aircraft at a few km altitude.

Another advantage of SLAR is that of relief enhancement. This is the effect of shadowing which is especially pronounced in the far range. As with photography, stereoscopic coverage is available as is the ability to mosaic radar imagery (19).

These advantages of SLAR are suggestive of an extremely effective tool in remote sensing (21). Yet the effectiveness of side looking airborne radar has not been fully realized. Although the sophistication of synthetic aperture radar is a reality, information available on the parameter which is ultimately measured, the radar cross section, is sadly quite limited.

2.2 Non-Imaging Radar

In the field of remote sensing, non-imaging radars are normally known as scatterometers. The purpose of any scatterometer is to measure the scattering cross section, σ, of a target of interest. Knowing σ, the ultimate goal is to extract from it a maximum of information pertinent to that particular target. Hopefully this would permit use of σ as a target identifier.

Again as with imaging systems, scatterometers have displayed their effectiveness in remote sensing (22). Scatterometers are not usually imaging devices although an imaging system may be calibrated for this purpose. Scatterometers are, however, often simpler in design, making them less costly in terms of initial expense.

2.3 The Radar Cross Section

In most cases in remote sensing, radar backscatter is described in terms of σ^o, the differential radar cross section rather than σ, the total radar cross section. This representation is correct only if it is assumed that the backscatter is contributed by a very large number of independent scatterers so that the signal is essentially incoherent. If this assumption is indeed applicable, superposition of power is possible and we can write the radar equation in the form

$$P_r = \sum_{i=1}^{n} \frac{P_{ti}\, G_{ti}\, G_{ri}\, (\sigma_i/\Delta A_i)\, \Delta A_i\, \lambda^2}{(4\pi)^3\, R^4} \qquad 2.3.1$$

where ΔA_i is an element of the scattering surface and n is the number of scattering elements. For the i^{th} element, $\sigma_i/\Delta A_i$ is the incremental scattering cross section. By our initial assumption we can only consider the average case so we write

$$\sigma^o = \left\langle \frac{\sigma_i}{\Delta A_i} \right\rangle \qquad 2.3.2$$

where $\langle\ \rangle$ denotes the average value. This parameter, σ^o, was introduced in an attempt to describe a scattering cross section independent of illuminated area, a variable totally dependent on the particular system being used (23).

Two target parameters control the value σ^o will assume. The first is target geometry, while the second is target complex permittivity. Both are equally important when an attempt is made to characterize a target in terms of σ^o.

2.3.1 σ^o as a Function of Target Geometry

Target geometry is the more difficult parameter to describe. In an attempt to define the cutoff point between a smooth and rough surface, Rayleigh proposed a criterion which is commonly accepted among investigators. Rayleigh states that in order to consider a target as "smooth,"

$$h < \frac{\lambda}{8 \cos \theta} \qquad 2.3.3$$

where h is the maximum height difference between points on a surface, λ is the wavelength and θ is the angle of incidence. After applying this criterion, however, the question remains as to the degree of smoothness or roughness presented by a particular target and finally, how to describe the target.

Many investigators have presented mathematical models for particular classes of targets in an attempt to describe their scattering behavior. A useful summary of many of the earlier models is given by Janza (24).

Because of the complexities of natural targets, both the physical and statistical models are extremely idealized resulting in a gross target description. In some cases this may be appropriate but for most targets an actual measurement is the ultimate description.

2.3.2 σ^o as a Function of Complex Permitivity

In collecting data on complex permittivity, most investigators have taken an experimental rather than a theoretical approach (25, 26, 27, 28). The methods employed in compiling these data are generally quite controlled and the measurements are usually made in the laboratory. In studying many materials such as synthetic insulators, these methods are perfectly acceptable, but when studying naturally occurring targets whose properties vary as a function of their environment, these methods may not be easily employed.

An important example of this is found in the measurement of complex permittivity of soils. The permittivity of a soil will be a function of soil type, moisture content and soil density. In samples collected for laboratory study, both moisture content and soil density may be disturbed,making an analysis somewhat unreliable.

2.3.3 σ^o as a Function of System Parameters

Although target geometry and permittivity are basic to the description of σ^o, the characteristics of the illumination are equally important. These characteristics are frequency, polarization and incidence angle. Although investigators have made an effort to study the effects of these variables on σ^o, no coordinated program has been initiated to study this problem in a comprehensive manner (13, 14, 15). Combined with the effects of target parameters, the addition of these three variables presents an almost impossible task to the theoretician attempting to devise an adequate mathematical description of σ^o, even for the simpler naturally occurring targets.

2.4 Lack of Adequate Scattering Data

Radar has already exhibited its worth as a useful remote sensor and certainly has much unrealized potential. In attempting to realize this potential, however, it is most frustrating to attempt radar design with little or no a priori knowledge of the parameter being studied, the scattering coefficient (23, 24).

Most of the studies made of σ^{o}, as of this writing, suffer from serious disadvantages. These may be lack of polarization agility, limited range of incidence angle, limited size of resolution cell, limited variety of targets and so on. One of the most serious drawbacks to nearly all studies, however, is that measurements were made at single frequencies rather than continuously over wide bands. This is in contrast to measurements made in the visible and infrared bands where continuous spectral responses are available.

The Goodyear program (35) was initiated in order to study the backscatter of vegetation. Measurements, however, were restricted in terms of frequency, look angle and variety of targets. Ohio State University (14) studied an extensive variety of targets at four frequencies but was seriously hampered by the small size of the resolution cell and the lack of continuous frequency coverage. In an attempt to measure the ability of radar to study subsurface soil interfaces, Lundien (25) constructed a system for making controlled laboratory studies. It was discovered however that multiple reflections within the radar facility and his method of sample preparation made signature analysis, an important phase of his study, impossible. Similar problems plagued most of the reported studies such as de Loor (36) whose system produced useful data but only over a small range of incident angles.

In 1969, Moore, Waite and Rouse published an article (37) describing the advantages of transmitting a broad band signal. The term "panchromatic" was coined to describe such a system. Subsequently, much effort was made to realize a panchromatic radar and to experimentally exhibit these advantages. Initial studies of panchromatic illumination were made by Rouse (42), Thomann (38) and Waite (29). Thomann made an acoustical simulation of a panchromatic imaging system and showed the effect to be that of speckle reduction in radar imagery. Similarly , Waite constructed a polypanchromatic microwave system and exhibited the same reduction in speckle along with octave bandwidth spectral response curves for a very small range of targets.

During the summer of 1971, octave bandwidth spectral response data were produced by a frequency modulated system. Calibration difficulties were a problem so that only relative data was reported (39). The system was rebuilt and octave bandwidth data with better absolute calibration were finally collected during the summer of 1972 by Ulaby (34).

In view of the success achieved by this system, it was decided to expand the system to cover the spectrum from 2-18 GHz. It was proposed to cover this range of frequencies with two systems, one covering the band from 2-8 GHz and a second covering the band from 8-18 GHz. This report discusses the design, construction and testing of a system operating between 8 and 18 GHz.

3.0 RADAR SPECTROMETER DESIGN AND CONSTRUCTION

3.1 Specific Design Objectives

The original design objectives of the scatterometer are presented below in the form of a listing.

(a) Absolute measurement of σ^o.

(b) Continuous frequency coverage from 8 GHz to 18 GHz.

(c) Continuous incident angle coverage from 0^o (normal) to 80^o.

(d) Maximum polarization agility.

(e) Adequate frequency averaging without excessive loss of spectral resolution.

(f) Ranging capabilities.

(g) Adequate dynamic range for targets of interest.

(h) Semi-continuous calibration capabilities.

(i) Sufficient angular resolution so as not to sacrifice angular information.

(j) System mobility for coverage of a variety of targets.

The following sections explain how the above objectives were met.

3.2 Choice of an FM-CW System

The choice of an FM-CW system was based on its ability to satisfy a number of the objectives set forth in the previous section. These are discussed below.

3.2.1 Frequency Averaging

If we assume that the targets of interest can be represented by a random collection of independent scatterers, then we can describe the fading signal by a Rayleigh distribution (23). If we do indeed make this assumption, the number of independent samples required for a particular accuracy is shown in Figure 1. In this case, the deviation from the median value between the 5 per cent and 95 per cent points on the distribution is plotted against the number of independent samples. Clearly averaging is needed for an acceptable amount of accuracy.

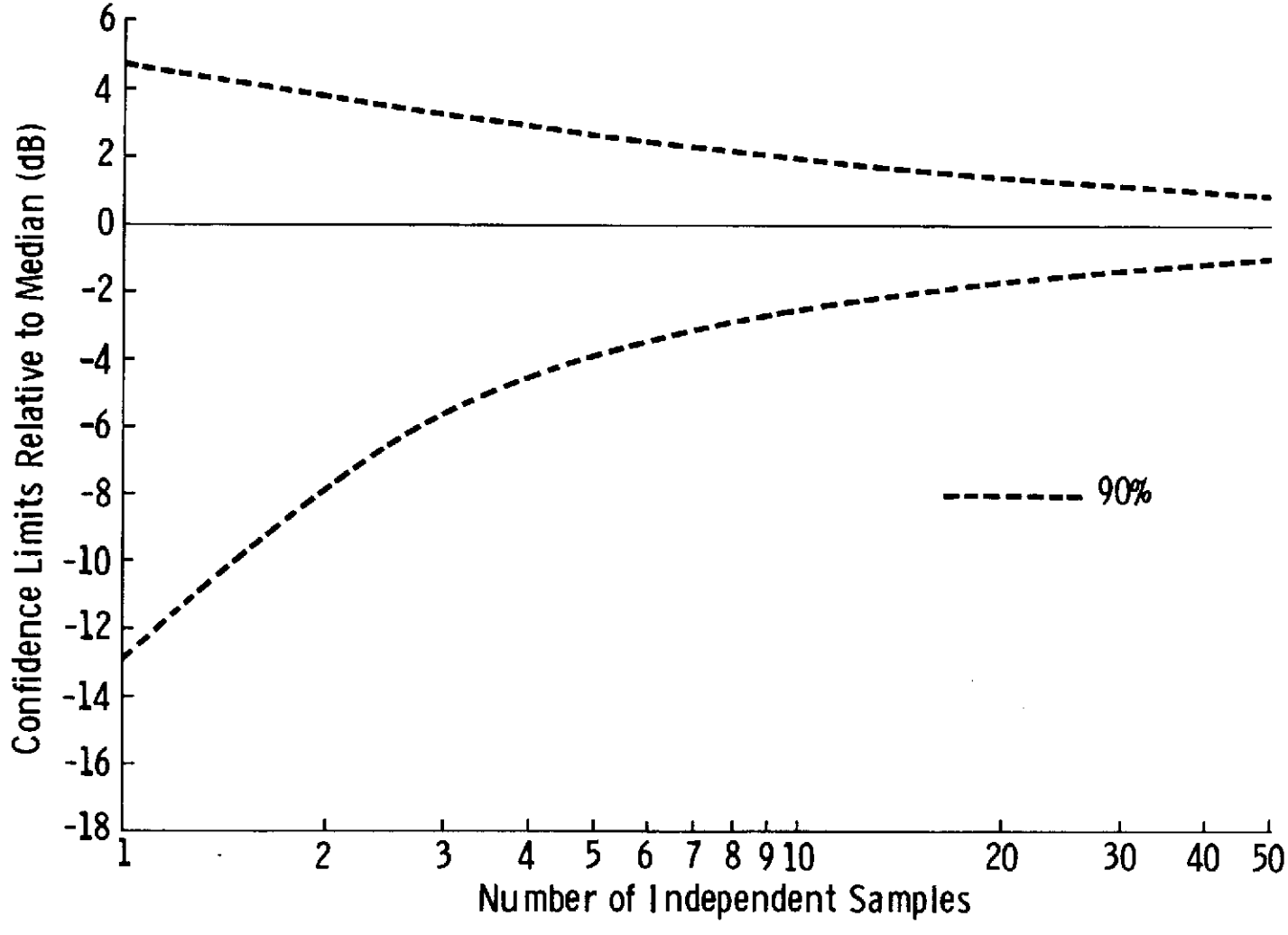

FIGURE 1. 90 PER CENT CONFIDENCE INTERVAL FOR RAYLEIGH DISTRIBUTION.

Since the accuracy depends upon the number of independent samples, not the total number of samples, it is necessary to determine the frequency spacing between independent samples. Under the conditions that the fading distribution is Rayleigh, this spacing is given by (29)

$$\Delta F_s = \frac{150}{D} \text{ MHz} \qquad 3.2.1.1$$

where D is the difference of the minimum and maximum distance (measured radially from the antenna) between the scatterers in an illuminated cell contributing to the return. For any radar, the maximum value of D can never exceed the range resolution of the system although D can be less than the range resolution.

For an FM-CW radar, range resolution is determined either by the angular resolution of the beam or by the limiting effect of the IF filter on the measured return (see sections 6.3).

If the IF filter is not limiting the return, ΔR can be calculated from pure geometrical considerations. In this case, (see Figure 2).

where $\Delta R = h \left[\sec(\theta + \beta/2) - \sec(\theta - \beta/2)\right]$

ΔR = range resolution

h = antenna height above the target

θ = pointing angle of antenna relative to vertical

β = antenna beamwidth in the elevation plane.

If the IF filter limits the measured return

$$\Delta R = R \frac{\Delta f_{if}}{f_{if}} \qquad 3.2.1.2$$

where R = slant range

Δf_{if} = IF filter bandwidth

f_{if} = intermediate frequency

Usually, the minimum value of D occurs at normal incidence. When looking at bare soil, for example, D may be in the range of 5-10 cm depending on surface roughness and penetration. In this case, ΔF_s will range from 3 to 1.5 GHz. The maximum value of D occurs at a look angle of 70° at which point the range resolution of the system (4.53 m) is the controlling factor. For this case, ΔF_s = 33 MHz.

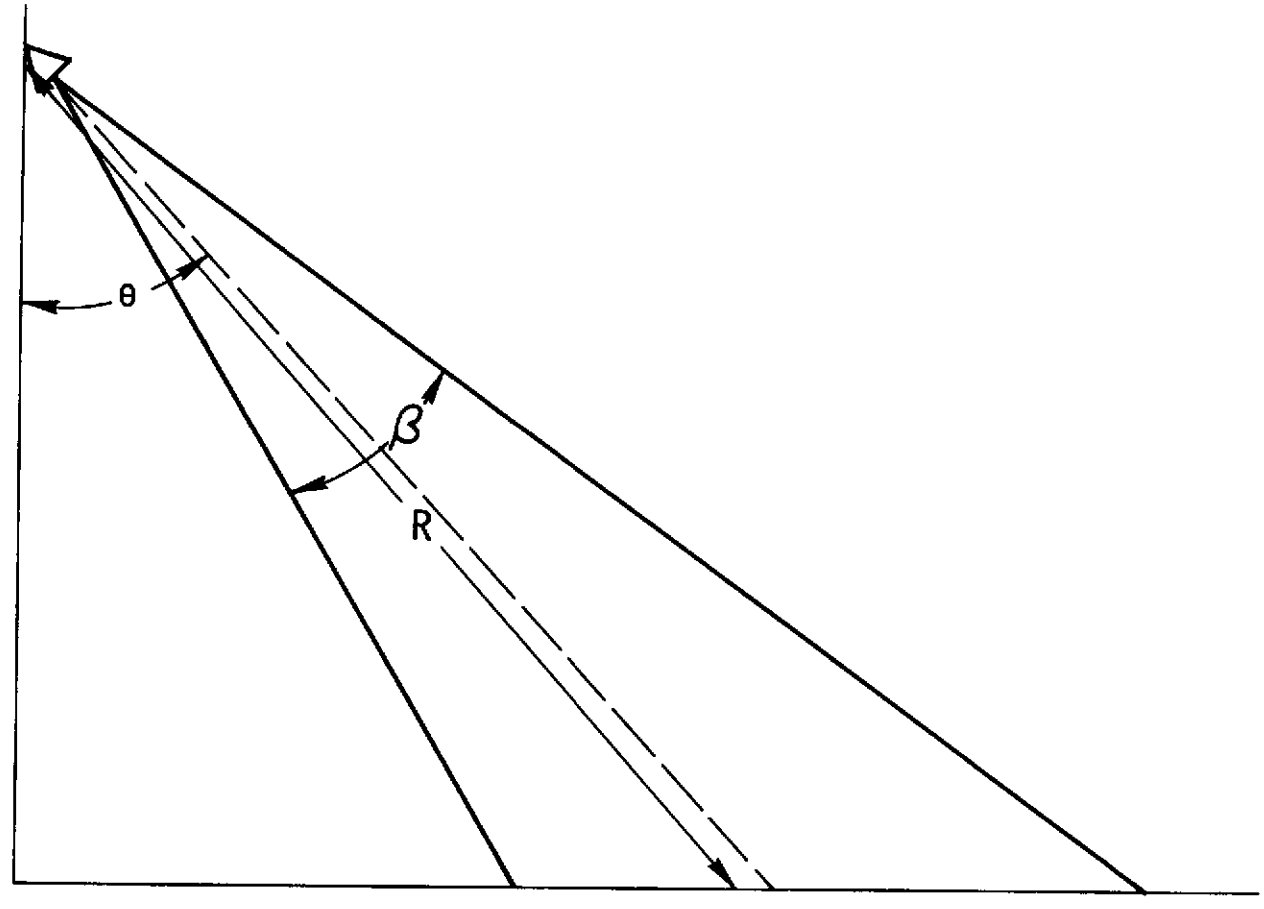

FIGURE 2. ILLUSTRATION DEFINING INCIDENT ANGLE, θ BEAMWIDTH, β, AND RANGE, R.

Based upon these figures a decision was made on the band over which averaging would be done. It was felt that 400 MHz was acceptable in terms of spectral resolution and in terms of the number of independent samples provided at larger incident angles. Although only 1 independent sample would be provided at vertical, 12 independent samples would be provided when a target exceeded the range resolution of the system at 70°.

3.2.2 Ranging Capabilities

To permit control over the size of the resolution cell, it was felt that ranging capabilities were necessary. The resolution ability of an FM-CW radar is determined by the IF filter which is discussed in section 6.3.

3.2.3 System Simplicity

To reduce both cost and construction time and to increase reliability it was felt a relatively uncomplicated system was desirable. Although a pulse system such as that used by Waite (29) would have provided the necessary system capabilities it was felt that the problems associated with such a system were undesirable. To keep track of individual pulses, some sort of timing scheme would be necessary. This in itself would have been a major subsystem causing a substantial increase in system complexity. Adding to this would be the problem of the ringing of pulses within the system making it even more difficult to distinguish the actual signal from decayed remnants of the transmitter pulse.

Often, an FM-CW radar suffers the problem of transmitter leakage through the duplexer of a single antenna system. This can be solved, however, by use of a dual antenna system.

4.0 ANTENNAS

4.1 Reflectors

The choice of reflectors was based on a compromise among three basic criteria.

(a) Antenna Beamwidth $\beta = \frac{\lambda}{D}$

(b) Placement of target in far field $R_M = \frac{2D^2}{\lambda}$

(c) Antenna Gain $G = \frac{4\pi\eta A_e}{\lambda^2}$

where

β = beamwidth

λ = wavelength

D = aperture diameter

G = gain

η = antenna efficiency

A_e = effective aperture area

R_M = minimum range to far field

4.1.1 Antenna Beamwidth

For the radar backscatter to be representative of a particular target, the illuminated cell must include several scatterers contributing to the measured return. Yet, if the iliuminated area is increased, too much angular information concerning σ^o would be lost.

In view of this, 61 cm. spun aluminum parabolic reflectors with an f/d ratio of 0.3 were chosen for both transmitting and receiving antennas. At vertical indicence the reflectors would theoretically provide an effective beamwidth ($G_t \cdot G_r$) of approximately 2.2^o and 1.2^o at 8 and 18 GHz respectively. This forces the illuminated area to vary from 1 m^2 to 0.5 m^2. These values increase with the incident angle.

4.1.2 Far Field

Figure 3 shows the far field distance as a function of frequency for the standard criteria, (30)

$$R_M = \frac{2D^2}{\lambda}$$

and the less stringent criteria (30).

$$R_M = \frac{D^2}{\lambda}$$

Note that the reflectors satisfy the more stringent requirement at 8 GHz and the less stringent requirement at 18 GHz.

4.1.3 Antenna Gain

For any antenna, gain is an important parameter to be considered when a choice of reflector is being made. This was true in our case but a more stringent requirement was that of beamwidth, discussed above. Since beamwidth and gain are related by

$$G = \frac{4\pi\eta}{\theta_\theta \, \phi_\phi}$$

where

η = antenna efficiency

θ_θ, ϕ_ϕ = half power beamwidths measured in radians

the gain was dictated by the beamwidths. For a beamwidth of 3.0° in both planes, and an antenna efficiency of 0.5, the gain would be 33.5 dB, the figure used in calculating the expected power returned.

4.2 Antenna Feeds

Because of the limited availability of feeds covering the 8-18 GHz regions, the choice was somewhat simplified. Both log periodic and spiral types were available but because a spiral is circularly polarized rather than linearly polarized a log periodic feed was chosen.

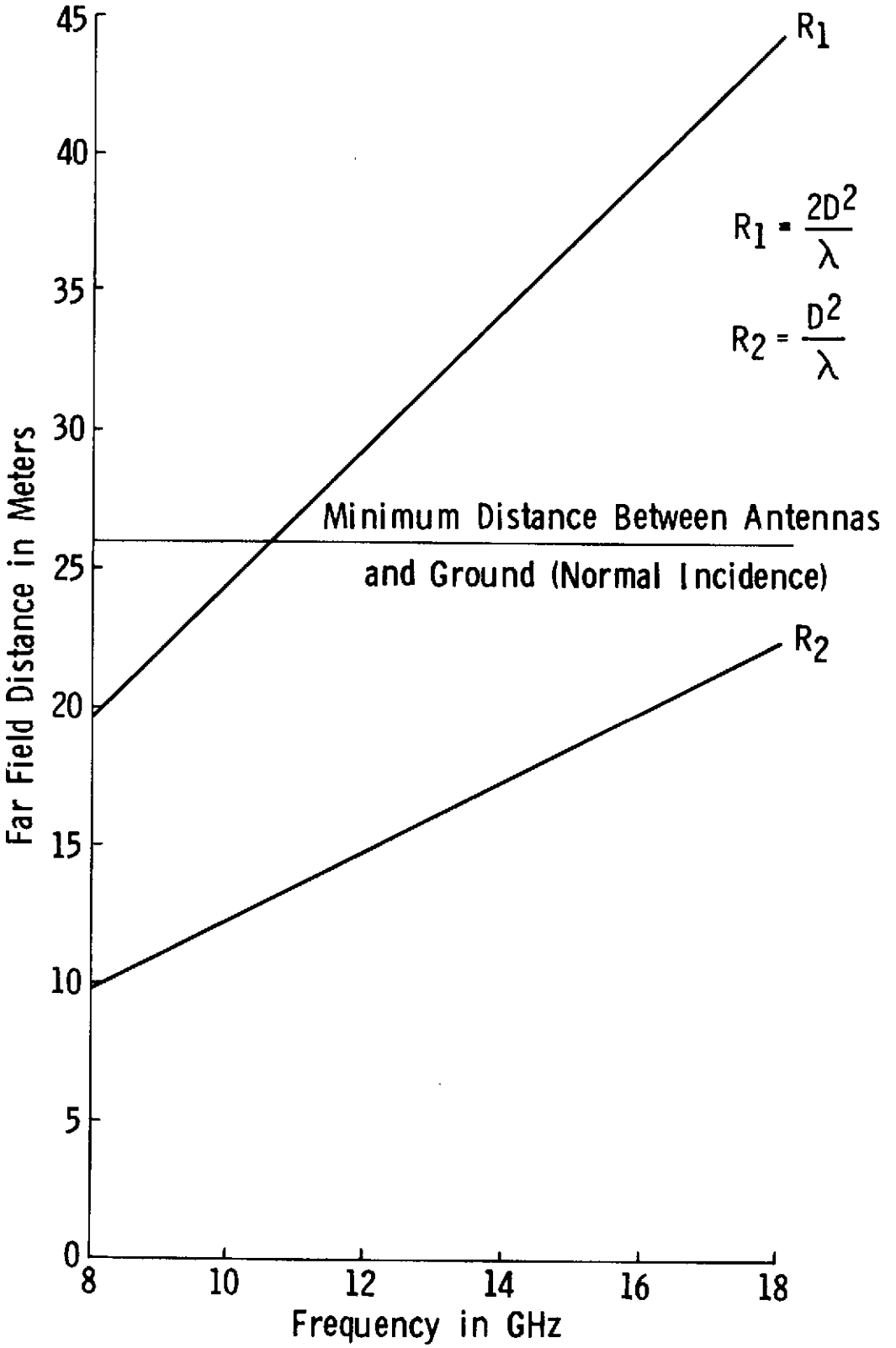

FIGURE 3. FAR FIELD DISTANCE FOR THE ANTENNAS AS A FUNCTION OF FREQUENCY.

The primary patterns of the feeds are shown in Appendix A . Appendix B shows VSWR vs. frequency, cross polarization level vs. frequency and gain vs. frequency.

The feed mount was constructed entirely from nylon and plexiglass, both having a dielectric constant far below that of a metal mount, to minimize pattern distortion.

4.3 Polarization Capabilities

To maximize the polarization agility of the system, both dishes were mounted on the shafts of small electric motors. Limit switches were installed such that the dishes were permitted to rotate only 90°. Each motor was independently remotely controlled so that all four polarization combinations, HH, HV, VH, VV were possible.

4.4 Antenna Pattern Measurement Procedure

Both antennas were mounted on an aluminum frame so that their position relative to one another could be fixed (see Figure 4). Provisions were made on the transmitting antenna so that it could be adjusted in both the azimuth and elevation planes. The entire frame was then mounted on the receiving antenna tower on an outdoor antenna range at The University of Kansas. Between the antennas, a small television camera was mounted so that visual indication of what the antennas were "seeing" was available. After accomplishing this, the following procedure was followed:

a. To correctly focus each antenna feed, principal plane power patterns were made at frequencies from 8-18 GHz in 2 GHz increments. Feed adjustments and patterns were made alternately so that the patterns were optimized in terms of beamwidth, sidelobe level and symmetry.

b. After focusing, principal plane power patterns were made at the above mentioned frequencies. These patterns are shown in Appendices C and D.

c. Next, the transmitting antenna was mechanically adjusted by means of adjustment bolts so that the beams of the antennas were coincident in both planes. This was done by alternately switching each antenna to the antenna range receiver and plotting both patterns on the same paper. After alignment was insured, dual patterns were made at frequencies from 8-18 GHz in 2 GHz increments and are shown in Appendix E.

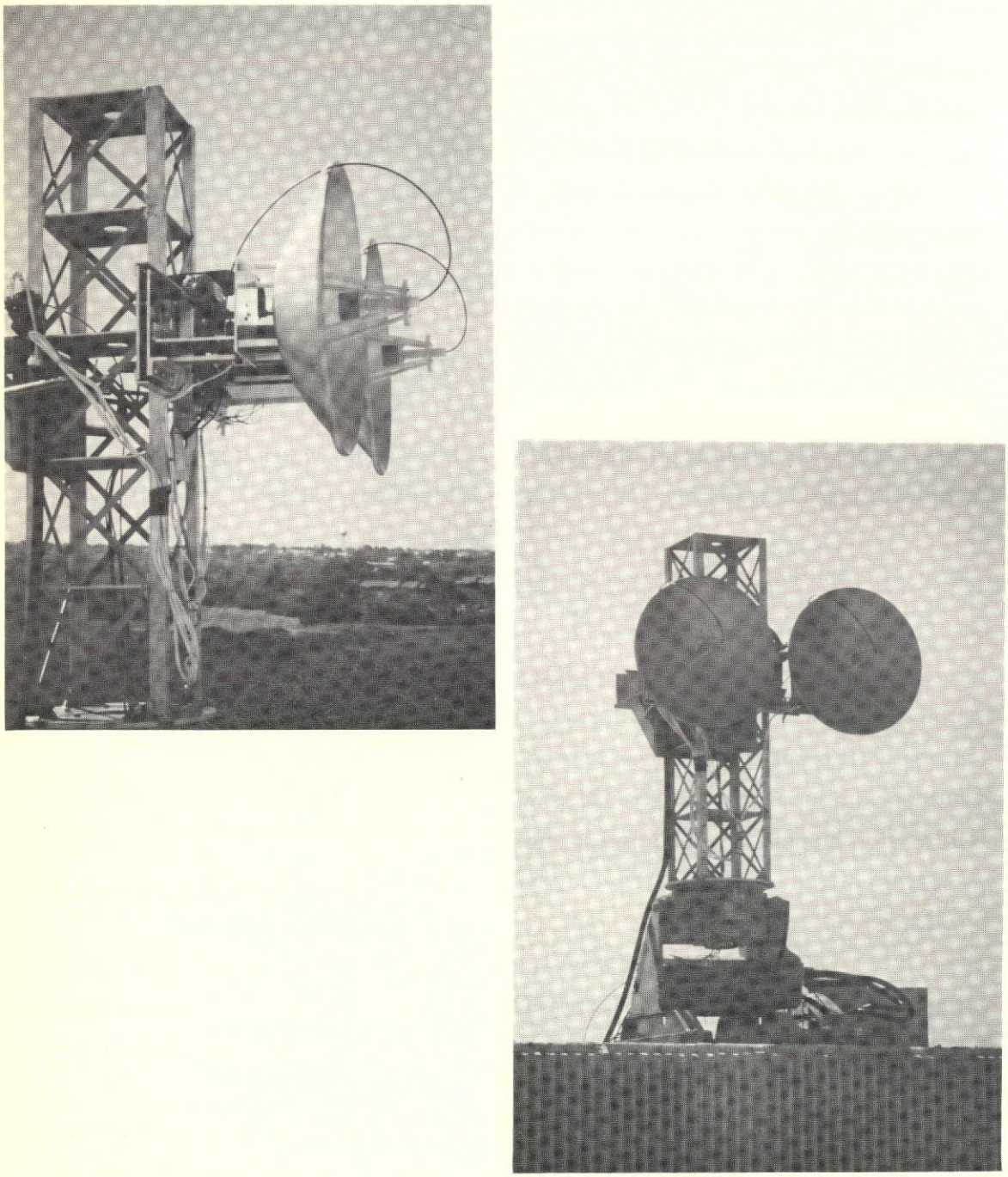

FIGURE 4. PHOTOGRAPHS SHOWING ANTENNAS MOUNTED ON ANTENNA RANGE TOWER.

d. Finally, adjustments were made on the television camera. With the antennas positioned at the point of maximum signal, the camera was fixed such that the cross hairs on the television monitor centered on the image of the transmitting horn.

Although not presented here, preliminary cross polarized patterns were made. These patterns indicate that the main beam of the cross polarized pattern averaged only 13 dB down from the main beam of the like-polarized pattern. The cause of this rather poor isolation can be seen by referring to Figure B4, in Appendix B which shows the poor cross polarization isolation level of the antenna feeds as a function of frequency. This problem made it impossible to make cross-polarized scattering measurements.

4.5 Calculation of Effective Antenna Beamwidth

Since the average scattering coefficient is defined in terms of the illuminated area,

$$\sigma^o = \left\langle \frac{\sigma_i}{\Delta A_i} \right\rangle \qquad 2.3.2$$

it is necessary to determine the effective illuminated area. This calculation is contingent on the knowledge of the product pattern of the antennas at each frequency.

To obtain these patterns, the product of the gain of the antennas was calculated at 0.5^o increments from the maximum and then plotted to obtain the effective patterns. These are shown in Appendix F . An effective beamwidth was determined by integrating the area under the pattern bounded by a -20 dB reference and then divided by 100. All integration was done with a Hewlett-Packard 9125 B calculator-plotter.

The illuminated area is an ellipse if the beam is conical. The axes of these ellipses are functions of look angle , range and beamwidth. Since the illuminated area contributing to the measured return is confined by the IF filter (see section 6.3), the general expression for the area must be modified. The derivation of the necessary expressions is provided by Batlivala and Khamsi (31).

5.0 TRANSMITTER

Shown in Figure 5 is a simplified block diagram of the basic components presently under discussion. Further discussion of supporting hardware is given in section 7.0.

The transmitter power is provided by two Hewlett-Packard 8690 series sweep oscillators. One covers 8-12.4 GHz while the second covers 12.4-18.0 GHz. An RF single-pole, double-throw switch was used to direct the power from the required oscillator.

Following this switch was a 3 dB power divider. The choice of a 3 dB divider was dictated by the local oscillator power requirements of the mixer. Thus, half the signal was used as the actual transmitted signal while the second half comprised the local oscillator signal. As shown in Figure 5 , two RF SPDT switches allowed a delay line to be used as a calibration device (see section 8.0).

Both oscillators were modulated by a triangular waveform provided by a function generator. The peak to peak voltage of this signal determined the frequency swing, Δf, of the RF signal around the carrier frequency, f, while the triangular waveform frequency, F_M, determined the IF frequency.

This is shown graphically in Figure 6. Considering like triangles we can write

$$\frac{f_{if}}{2R/c} = \frac{\Delta f/2}{1/4\, F_M} \qquad 5.0.1$$

where

f_{if} = intermediate frequency
R = range
Δf = RF frequency deviation
F_M = frequency of modulation
c = speed of light

Hence,

$$f_{if} = \frac{4\Delta f\, R\, F_M}{c} \qquad 5.0.2$$

Note that for a fixed intermediate frequency, (determined by the IF filter) the range and F_M are inversely related by the constant

$$\frac{f_{if}\, c}{4f}$$

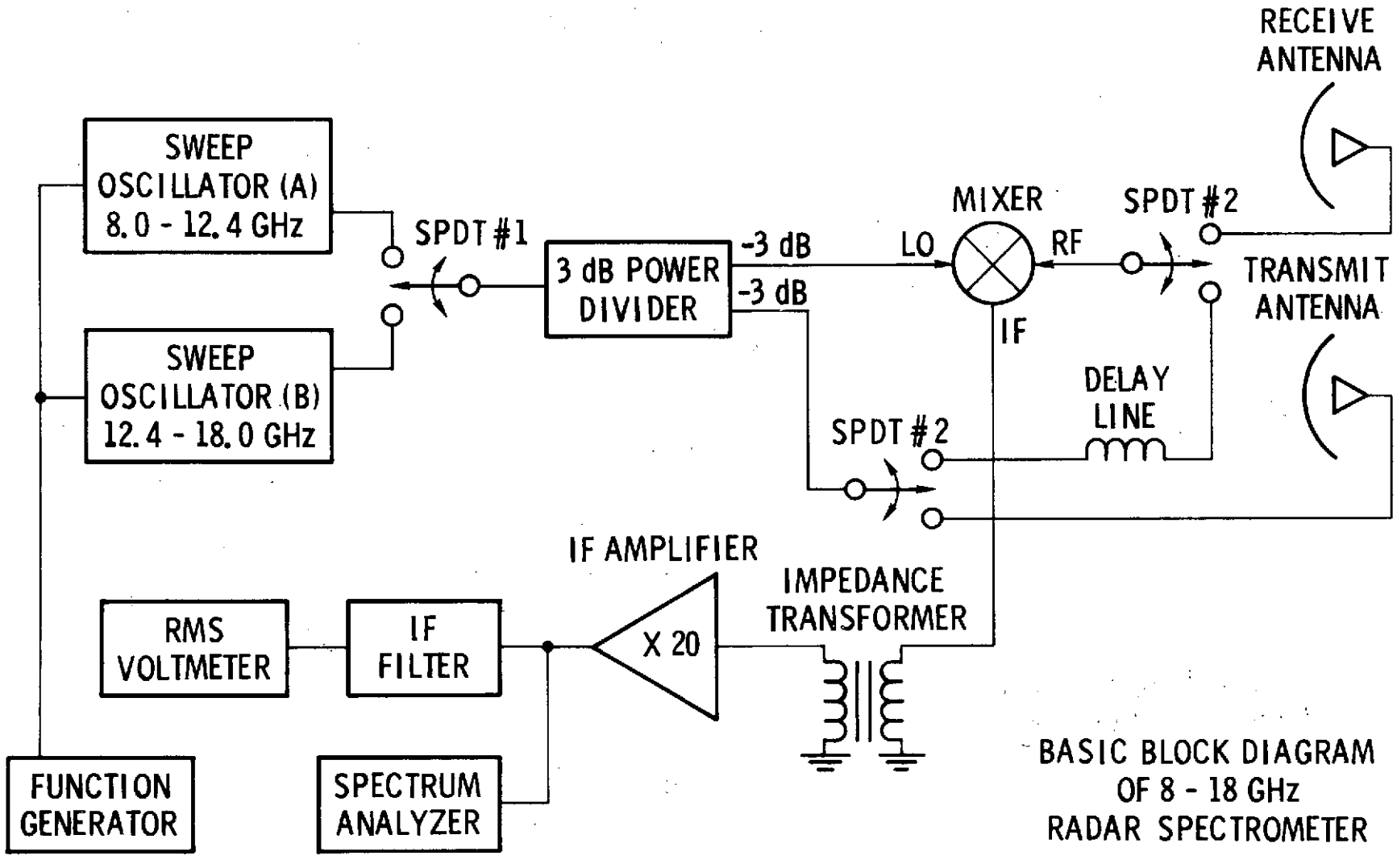
RECEIVE ANTENNA
SWEEP OSCILLATOR (A) 8.0 - 12.4 GHz
SWEEP OSCILLATOR (B) 12.4 - 18.0 GHz
SPDT #1
3 dB POWER DIVIDER
-3 dB
-3 dB
MIXER
LO
RF
IF
SPDT #2
TRANSMIT ANTENNA
DELAY LINE
SPDT #2
IF AMPLIFIER
X 20
IMPEDANCE TRANSFORMER
RMS VOLTMETER
IF FILTER
FUNCTION GENERATOR
SPECTRUM ANALYZER
BASIC BLOCK DIAGRAM OF 8 - 18 GHz RADAR SPECTROMETER

FIGURE 5.

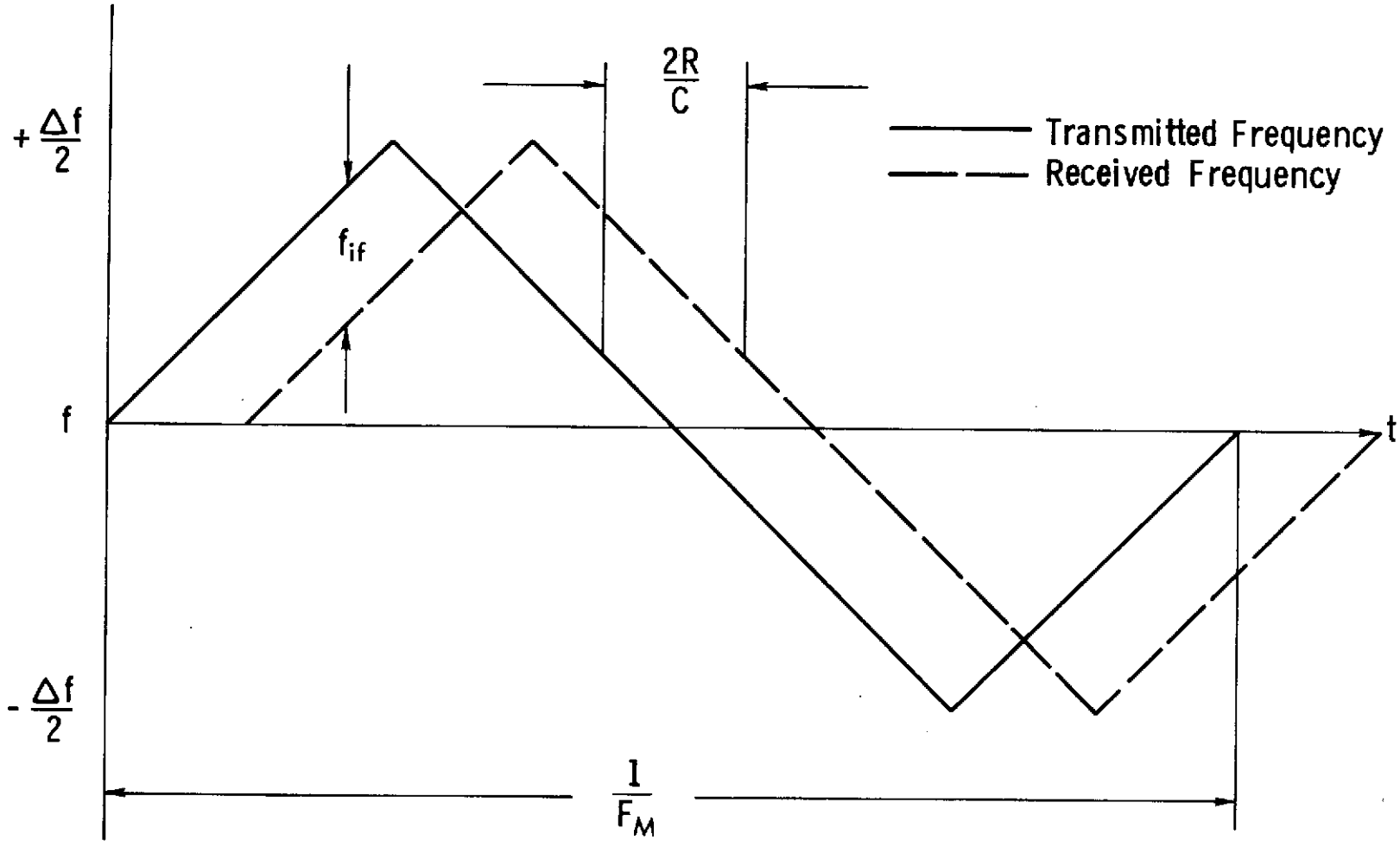

FIGURE 6. ILLUSTRATION SHOWING FREQUENCY RELATIONSHIP BETWEEN TRANSMITTED AND RECEIVED SIGNALS.

The power spectrum of both oscillators is shown in Figure 7. The fast undulations present in this spectrum contributed to the receiver noise significantly, as discussed in Section 6.5.

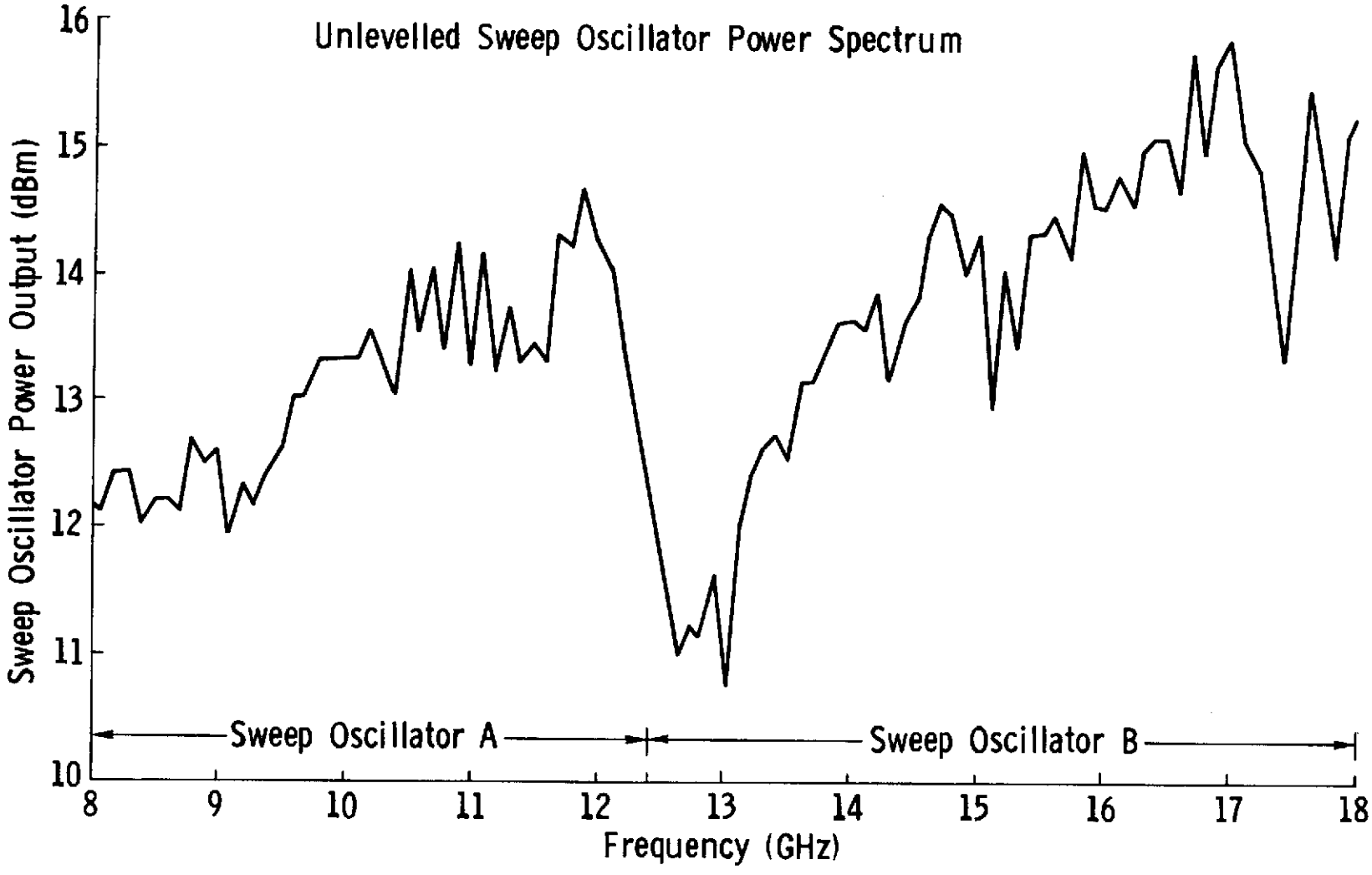
Unlevelled Sweep Oscillator Power Spectrum
Sweep Oscillator Power Output (dBm)
16
15
14
13
12
11
10
Sweep Oscillator A
Sweep Oscillator B
8
9
10
11
12
13
14
15
16
17
18
Frequency (GHz)

FIGURE 7.

6.0 RECEIVER

6.1 Mixer

The mixer used in the system is an extremely wide band device (1-18 GHz) manufactured by RHG Electronics Laboratory; Inc. Typically it requires +7 to +10 dBm local oscillator power and operates with a noise figure of 9.5 dB across the 8-18 GHz band. According to manufacturer's specifications, the LO-RF isolation is greater than 20 dB across the band.

6.2 Impedance Transformer and IF Amplifier

Following the mixer, the IF signal is fed into a Princeton Applied Research Model 211 amplifier via an impedance transformer with a 10:1 turns ratio. The IF amplifier is a low noise, single ended device providing 10 MΩ input impedance and flat frequency response from 1 Hz to 1 MHz. Calibrated gain settings on the front panel permit the selection of gains from 1 to 1000 in a 1-2-5 sequence.

It was discovered that a gain of 20 (26 dB) was the optimum gain setting. Two considerations lead to this choice: (a) maximum gain without amplifier saturation and (b) maximum gain without an increased signal-to-noise ratio. Consideration b was the overiding factor.

Testing showed that for a gain greater than 50, low frequency noise (see section 6.5) would saturate the amplifier under certain conditions. Not only did saturation occur but the saturation also caused the amplifier to oscillate which often caused an increase of 20 dB in the apparent signal-to-noise ratio. For a gain of 20 or less, no saturation or oscillation was seen to occur.

To improve the signal-to-noise ratio, an impedance transformer was used at the input of the amplifier. This configuration was suggested by the amplifier manufacturer who provided the noise figure contours shown in Figure 8. Note that the noise figure is a function of both frequency and source impedance. As shown, the contours predict a 35 dB noise figure when operating at 60 kHz with the IF port of the mixer (50 Ω impedance) connected directly to the amplifier. By using a 10:1 impedance transformer the effective source impedance is 5000 Ω which reduces the noise figure to approximately 8 dB.

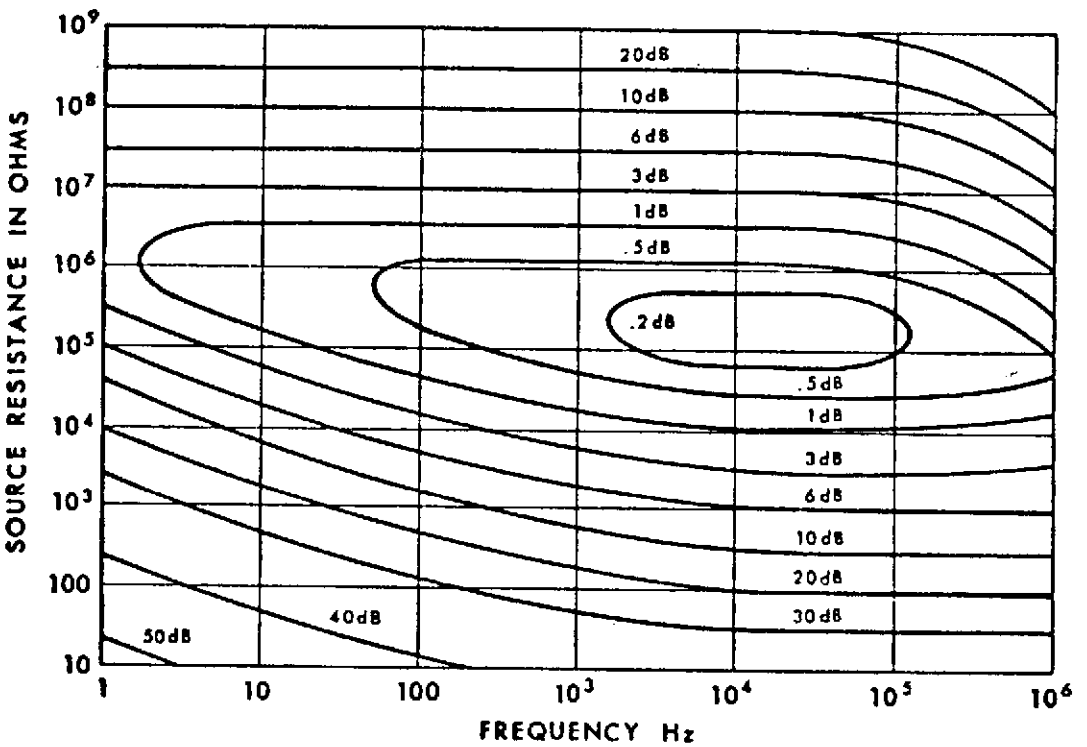

FIGURE 8. IF NOISE CONTOURS AS A FUNCTION OF FREQUENCY AND SOURCE IMPEDANCE.

6.3 IF Filter

As the look angle, θ, increases to values larger than about 40°, the illuminated area begins to increase drastically. To reduce the variability of the size of the illuminated cell the IF filter was designed to begin limiting the size of the cell at a look angle of 45°. Consider the case shown in Figure 9. For this case, a 3° beamwidth was assumed and an IF frequency of 60 kHz was chosen. ΔR_B is the range resolution afforded by the beam and from geometric considerations, $\Delta R_B = 1.92$ M.

From equation 5.0.2 it follows that

$$\Delta R_F = \frac{\Delta f_{if} c}{4 \Delta f F_M} \qquad 6\ 3.1$$

where ΔR_f is the range resolution afforded by the IF filter and $F_M = 312$ Hz for the range R = 36.75 m. Setting $\Delta R_F = \Delta R_B$ and solving for ΔF_{if} indicates an IF filter with a bandwidth, ΔF_{if}, of 3.2 kHz.

Thus, for $\theta < 45^{\circ}$, the range resolution is determined by the antenna beam while for $\theta > 45^{\circ}$, the IF filter is the limiting factor. The actual filter used had a bandwidth of 3.58 kHz (Figure 10) such that the filter began limiting at $\theta = 48^{\circ}$. The filter bandwidth was determined by integrating the area under the curve bounded by a -40 dB reference and then dividing by 10,000. All integration was done with a Hewlett-Packard 9125 B calculator-plotter.

It should be noted that the IF filter was also wide enough that the post-filtered signal was still representative of the actual received signal. That this is the case is shown in Figure 11 where a photo of the IF spectrum is shown for corn at $\theta = 0^{\circ}$. The vertical lines on the photo show the effective bandwidth of the IF filter. Note that the majority of the signal falls within the filter.

6.4 Signal Display

Following the IF filter, the signal was simultaneously fed into an RMS voltmeter and into a spectrum analyzer. The spectrum analyzer provided information as to the quality of the signal while the mean signal was read from the voltmeter.

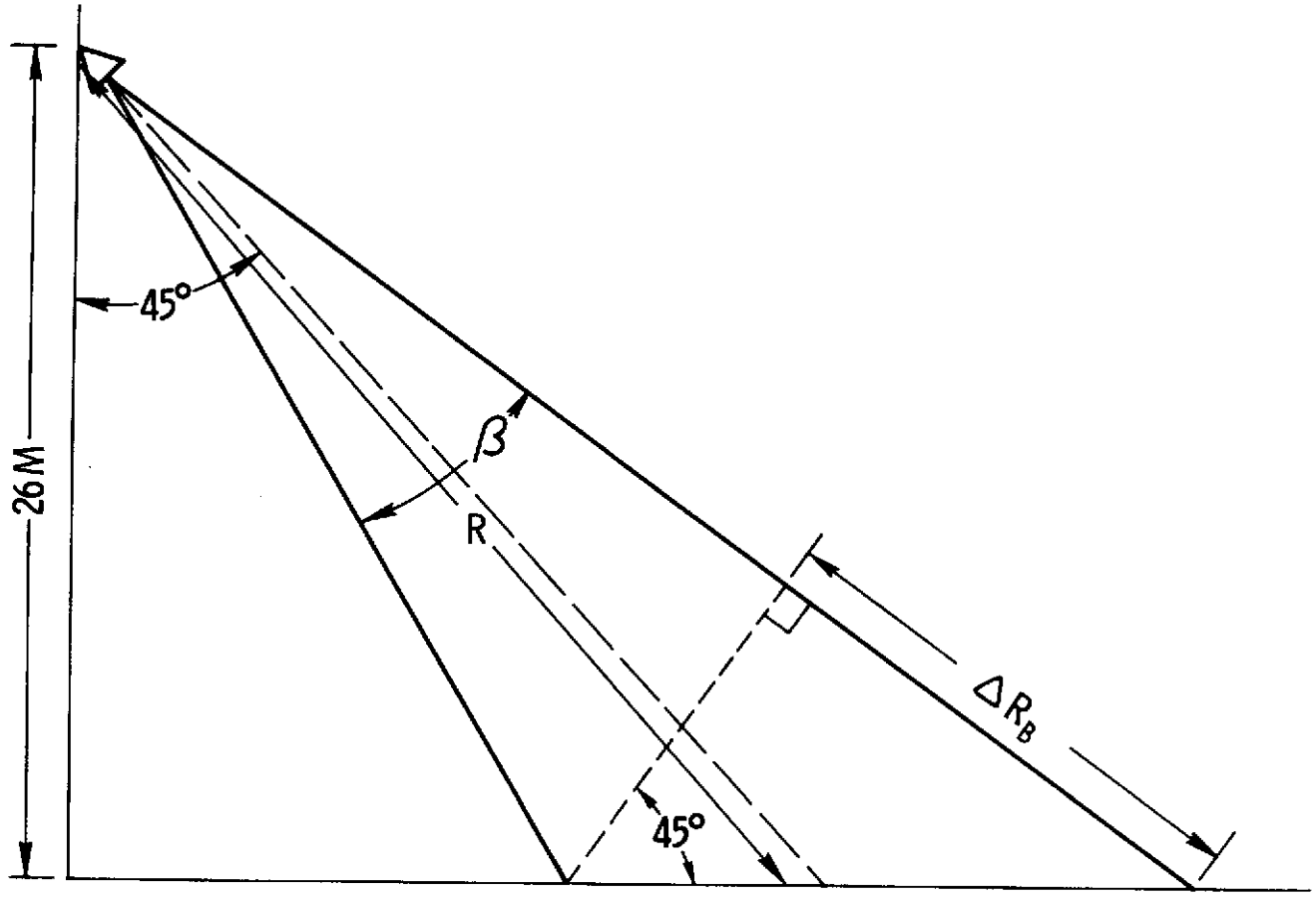

FIGURE 9. ILLUSTRATION REFINING R_B: THE RANGE RESOLUTION AFFORDED BY THE ANTENNA BEAM.

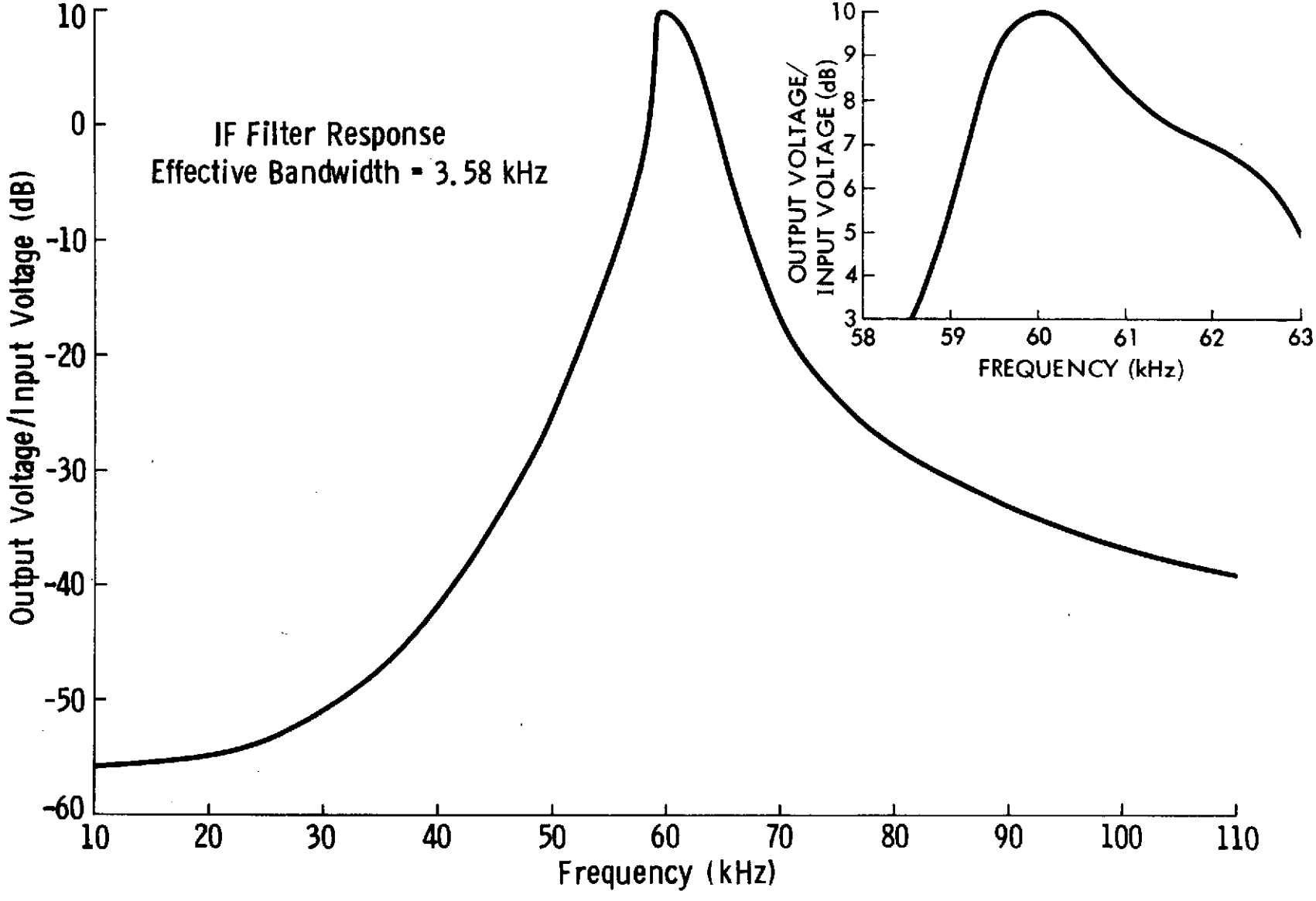

FIGURE 10. IF FILTER RESPONSE CHARACTERISTICS.

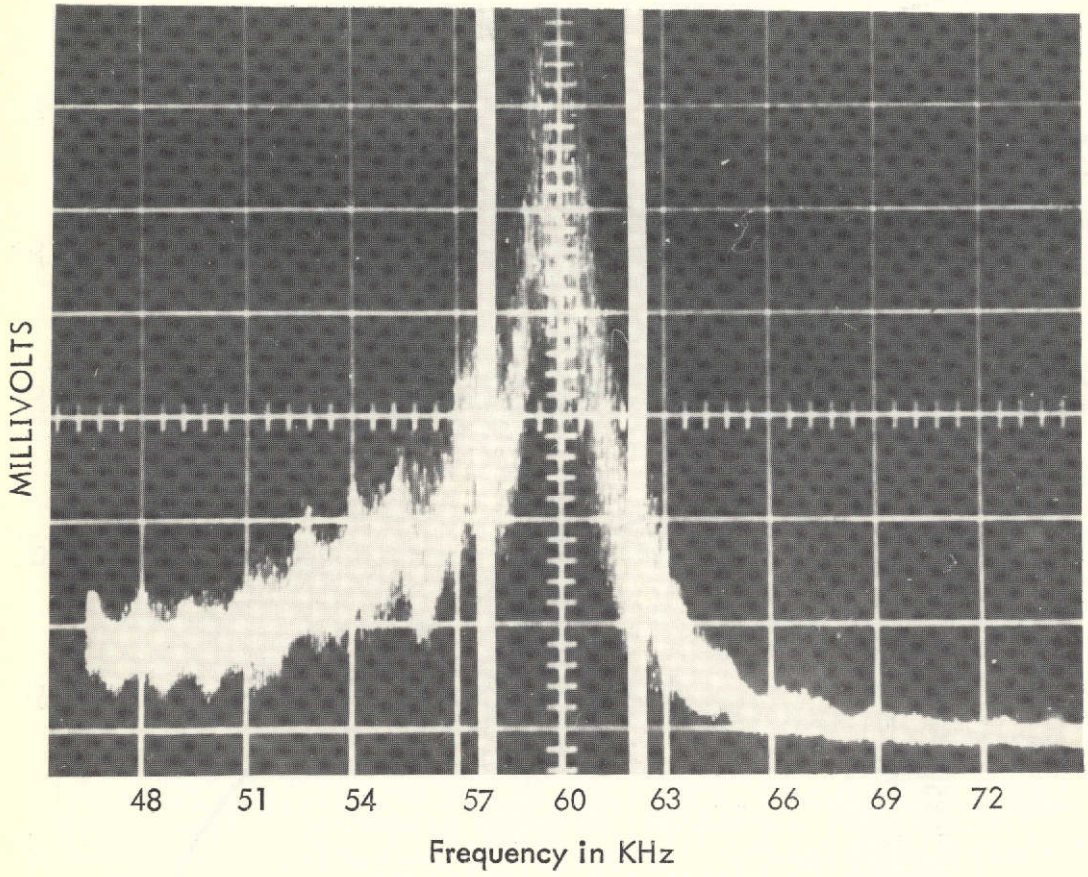

FIGURE 11. IF SPECTRUM FOR CORN AT A LOOK ANGLE OF ZERO DEGREES. NOTE THE MAJOR PORTION OF THE SPECTRUM FALLS WITHIN THE IF FILTER BAND AS INDICATED BY THE HEAVY WHITE LINES.

Vertical Scale = 50 mV/division

6.5 Receiver Noise

As for any receiver, noise was the factor limiting the sensitivity. This noise was not thermal noise, however, but rather it was the detected local oscillator signal. Figure 7 shows the sweep oscillator output power as a function of frequency. This power spectrum shows a trend of increasing power with frequency and also the smaller and faster undulations of the spectrum. Since this signal is frequency modulated about any point, the signal is thus also amplitude modulated. This "AM" signal is then detected by the mixer and thus becomes part of the IF signal.

Figure 12 shows the IF noise level for a number of modulation rates. As expected, the noise power increases with F_M. This is to be expected since increasing F_M merely increases the fundamental frequency of the AM signal causing the entire spectrum to shift toward higher frequencies, thus placing more noise power in the band of the IF filter.

This is perhaps shown in a better manner by Figure 13. These photos of the noise spectrum were taken for various values of F_M. All photos were taken with identical spectrum analyzer settings. Note that for F_M = 100 Hz practically no noise is present at the center frequency of the IF filter while for F_M = 700 Hz the spectrum has shifted to the right, placing a larger portion of the noise in the pass band of the filter.

In an attempt to alleviate this problem, a leveling loop was placed at the output of the sweep oscillator. It was hoped this would smooth the spectrum shown in Figure 7. The leveled spectrum is shown in Figure 14. It can be seen that the effect was to level the gross undulation of the spectrum while leaving the smaller, yet troublesome undulations present. Since the noise is a function of F_M it is also a function of range. Thus, although the noise increased as the range decreased, the signal also increased as R^4 so that the signal to noise ratio did not vary as much as might be predicted by Figure 12.

6.6 Dynamic Range and Tangential Sensitivity

In an attempt to estimate the minimum signal to be measured, the radar equation was used in the form

$$P_r = \frac{P_t G_t G_r \lambda^2 \sigma^o A_{ill}}{(4\pi)^3 R^4} \qquad 6\,6.1$$

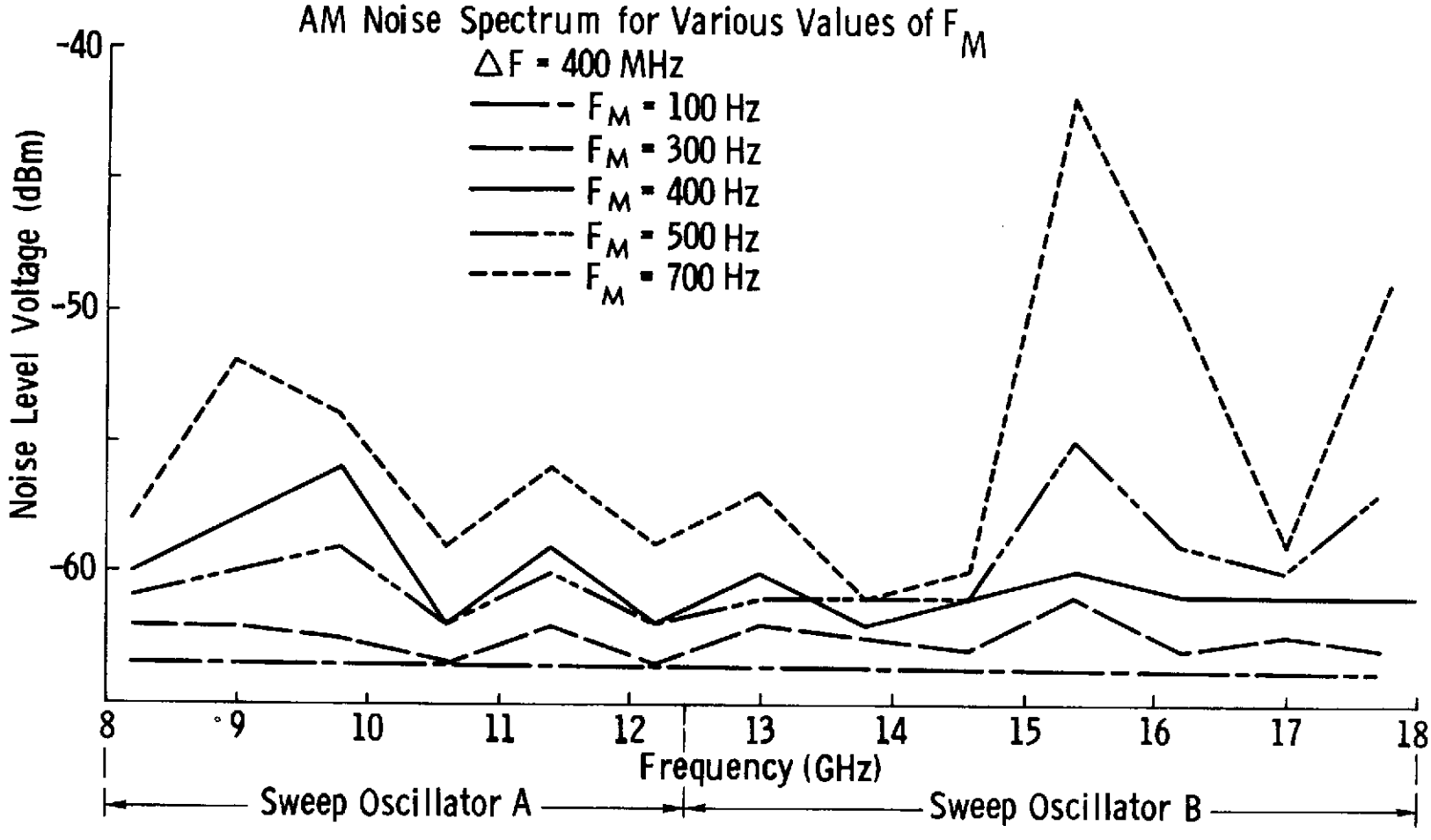

FIGURE 12. AM NOISE SPECTRUM FOR VARIOUS VALUES OF F_M. NOTE THE TREND OF INCREASING NOISE WITH INCREASING VALUES OF F_M.

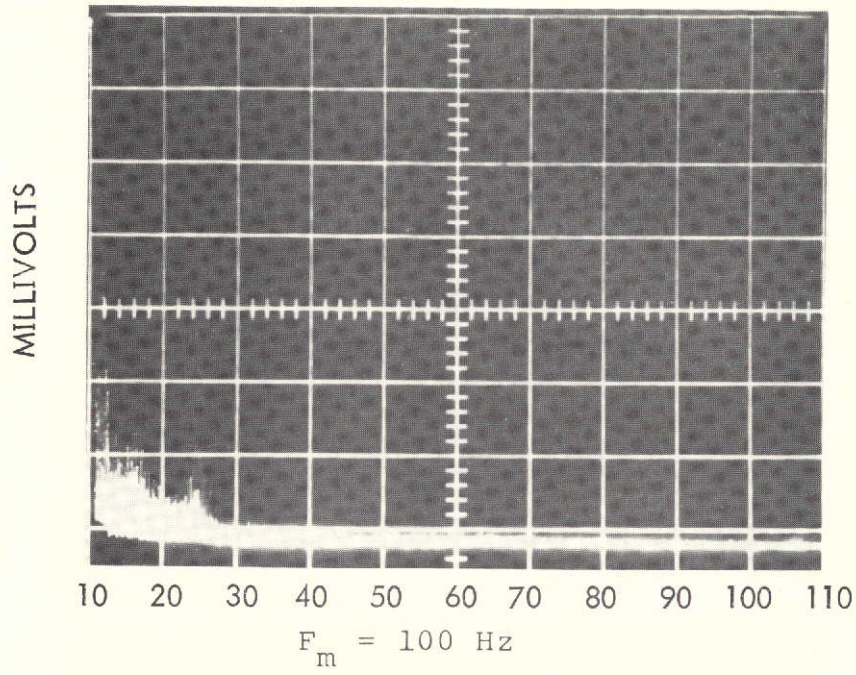

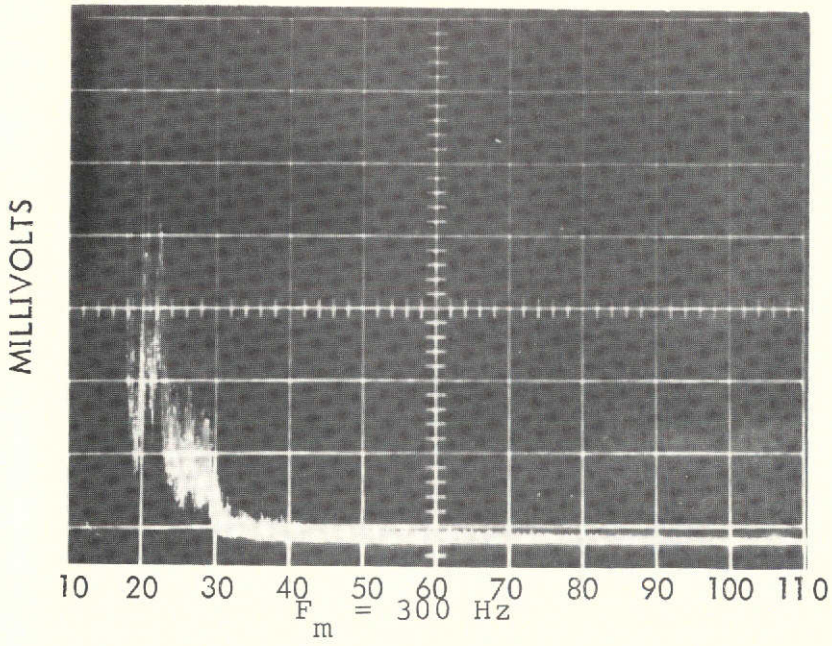

Photos showing the AM noise spectrum of the receiver for various values of F_m

Millivolts per division = 50

Hertz per division = 10 KHz

FIGURE 13.

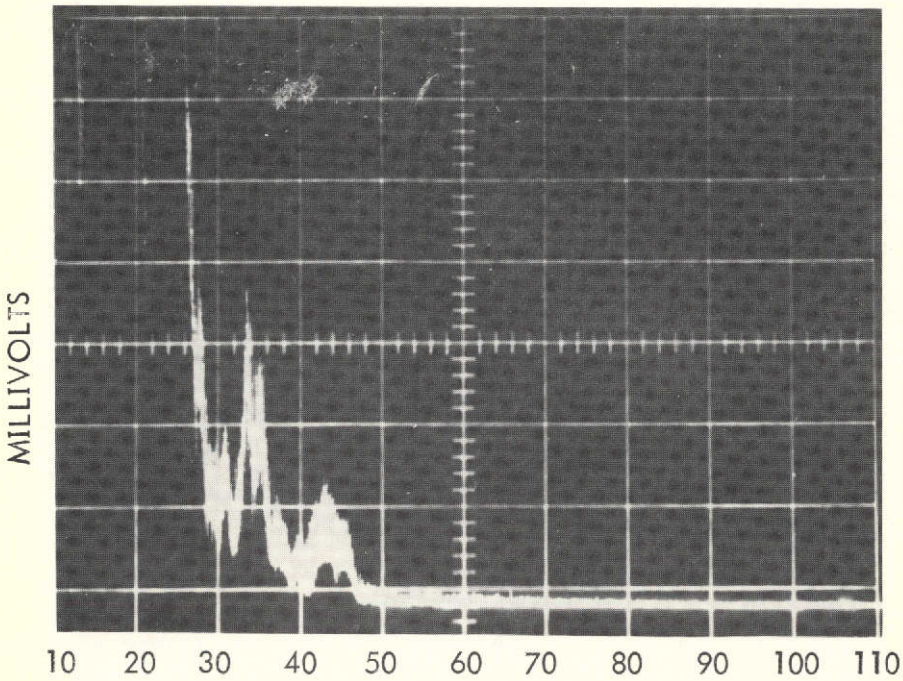

F_m = 500 Hz

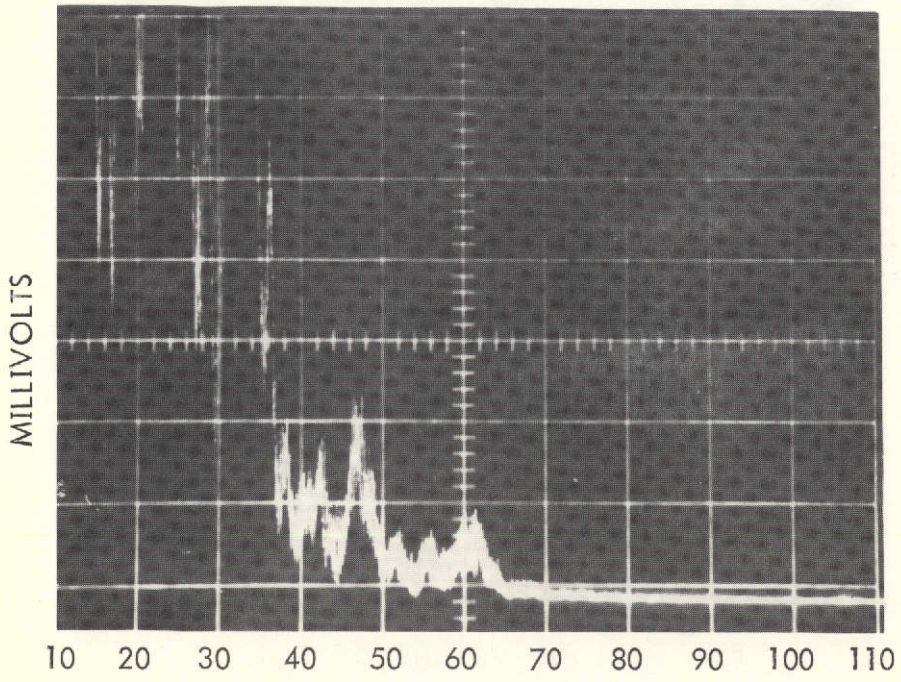

F_m = 700 Hz

FIGURE 13. (CONTINUED).

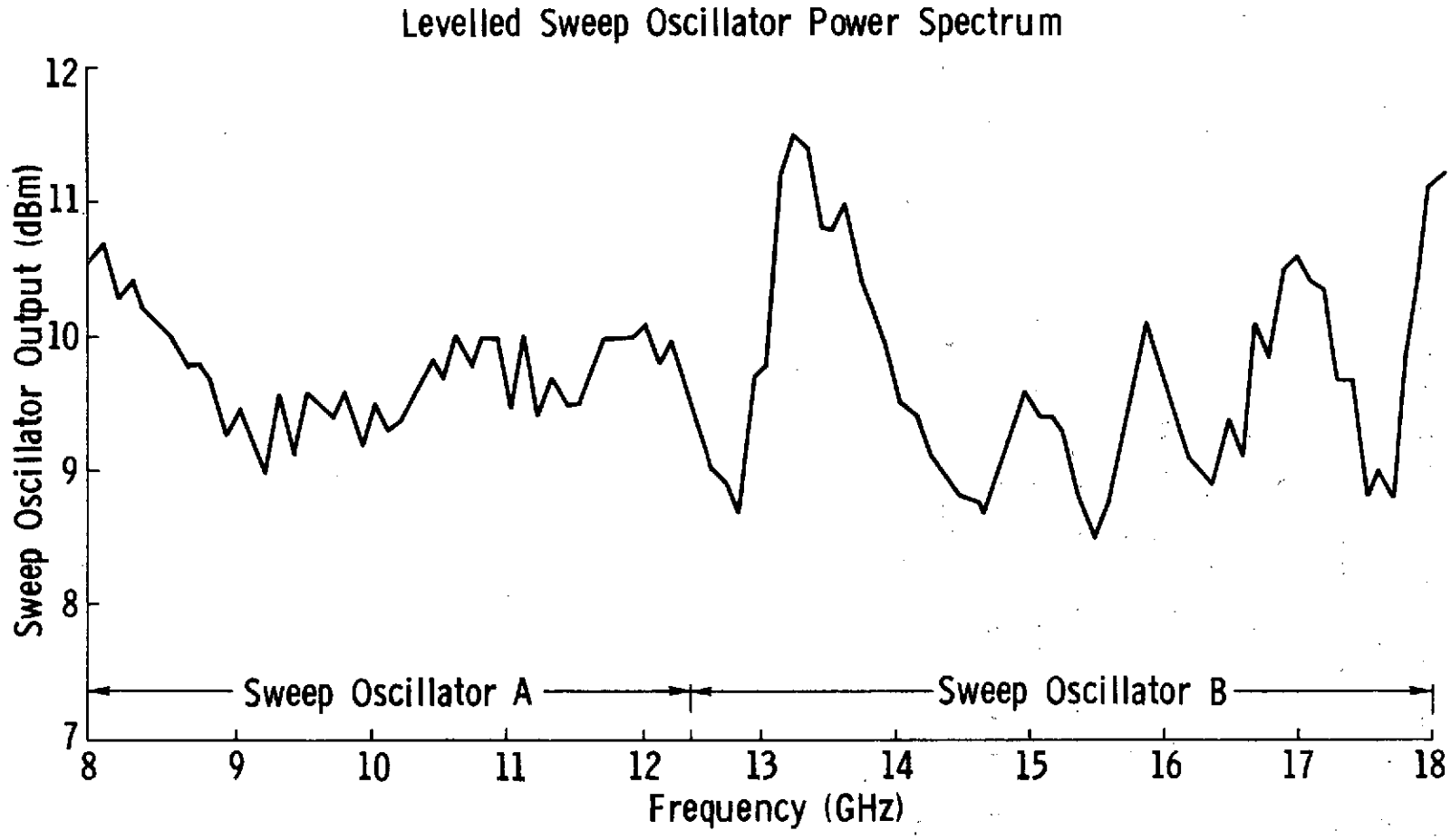

FIGURE 14. LEVELED SWEEP OSCILLATOR POWER SPECTRUM. NOTE THAT THE SPECTRUMS GROSS VARIATIONS ARE LEVELED WHILE THE MINOR UNDULATIONS PERSIST.

By referring to Figure 7, it can be seen that the transmitted power had an average value of 10 dBm. A worst case σ^{o} of -20 dB was chosen along with a worst case range of 76 m, that being the range at $\theta = 70^{o}$. At 70^{o}, the illuminated area contributing to the measured return would be 8 m^2, at 8 GHz, $G_t \cdot G_r = 66$ dB and $\lambda = .0375$ m. Substituting these values into the radar equation provides an estimate of the worst case return power. It turns out $P_r = -89$ dBm.

Figure 15 shows the tangential sensitivity of the receiver As defined by Taylor and Mattern (32), tangential sensitivity is the input signal which produces a unity signal to noise ratio at the receiver output. Thus, it is seen that the worst case estimate of the return signal falls as an average, 9 dB above the receiver tangential sensitivity except at 17 GHz where an anomalous dip occurs in tangential sensitivity. Care was taken in analyzing data taken at this frequency.

The dynamic range of the receiver as measured across the 8-18 GHz band was approximately 82 dB.

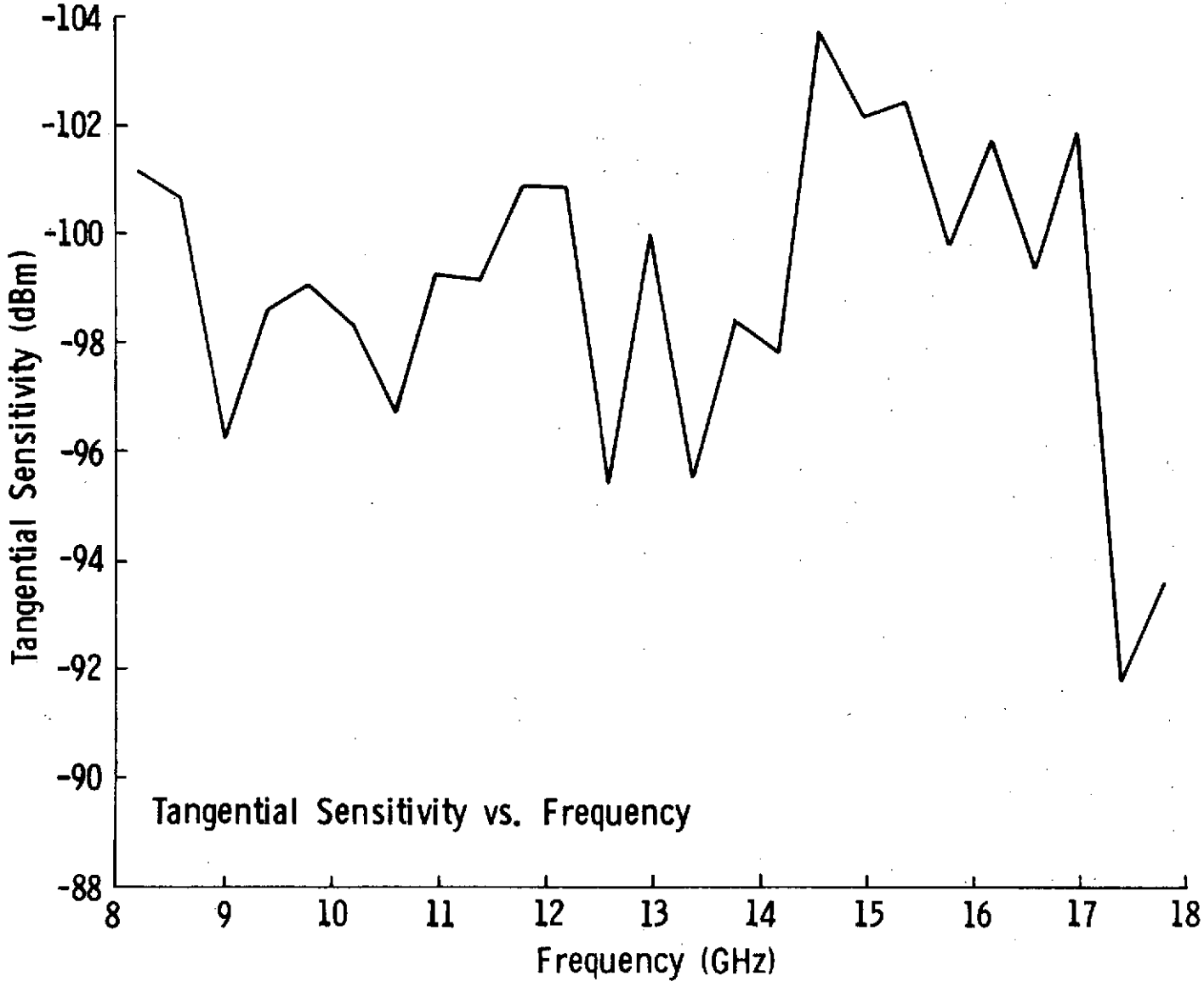

FIGURE 15. RECEIVER TANGENTIAL SENSITIVITY CURVES.

7.0 SYSTEM CONFIGURATION

Figure 16 is a schematic of the actual system configuration of the scatterometer. The upper section contains the various controls, indicators and the IF strip. These components are contained in an army topographic van as shown in Figure 17. Although the schematic is fairly self explanatory, two points should be discussed. The frequency controller is nothing but a resistive network which supplies a control voltage to the helix voltage generator in the sweep oscillator. More important than being a remote control device, it allows the operator to return to a given frequency time after time so that frequency inconsistency is not a problem. The look angle indicator is merely a voltmeter that has been calibrated in degrees. It operates in conjunction with a potentiometer whose position is controlled by a pendulum mounted on the shaft. All components shown inside of the dashed line are mounted on the boom as shown in Figure 18 with all of the RF components indicated by the heavy lines. It should be noted that the power divider, mixer and calibration switches are mounted directly behind the antenna feeds to minimize cable losses and reflections (see Figure 19). The following table presents, in a summarized manner, the major system specifications. Figure 20 shows the system with the boom fully extended.

TYPE		FM-CW
Modulating Waveform		Triangular
Frequency		8-18 GHz
FM sweep: Δf		400 MHz
Transmitter Power		10 dBm (10 mW)
Intermediate Frequency		60 kHz
IF Bandwidth		3.58 kHz
Antennas		
	Height above ground	26 m
	Reflector Diameter	61 cm
	Feeds	Cavity backed, log-periodic

Frequency (GHz)	Calculated Antenna Gain (dB)	Effective Beamwidths of Product Patterns (Degrees)	
		Az	El
8	31.2	2.94	3.43
10	33.0	3.07	3.24
12	34.6	2.42	2.38
14	35.9	2.35	2.34
16	37.1	1.65	1.46
18	38.1	2.02	3.20

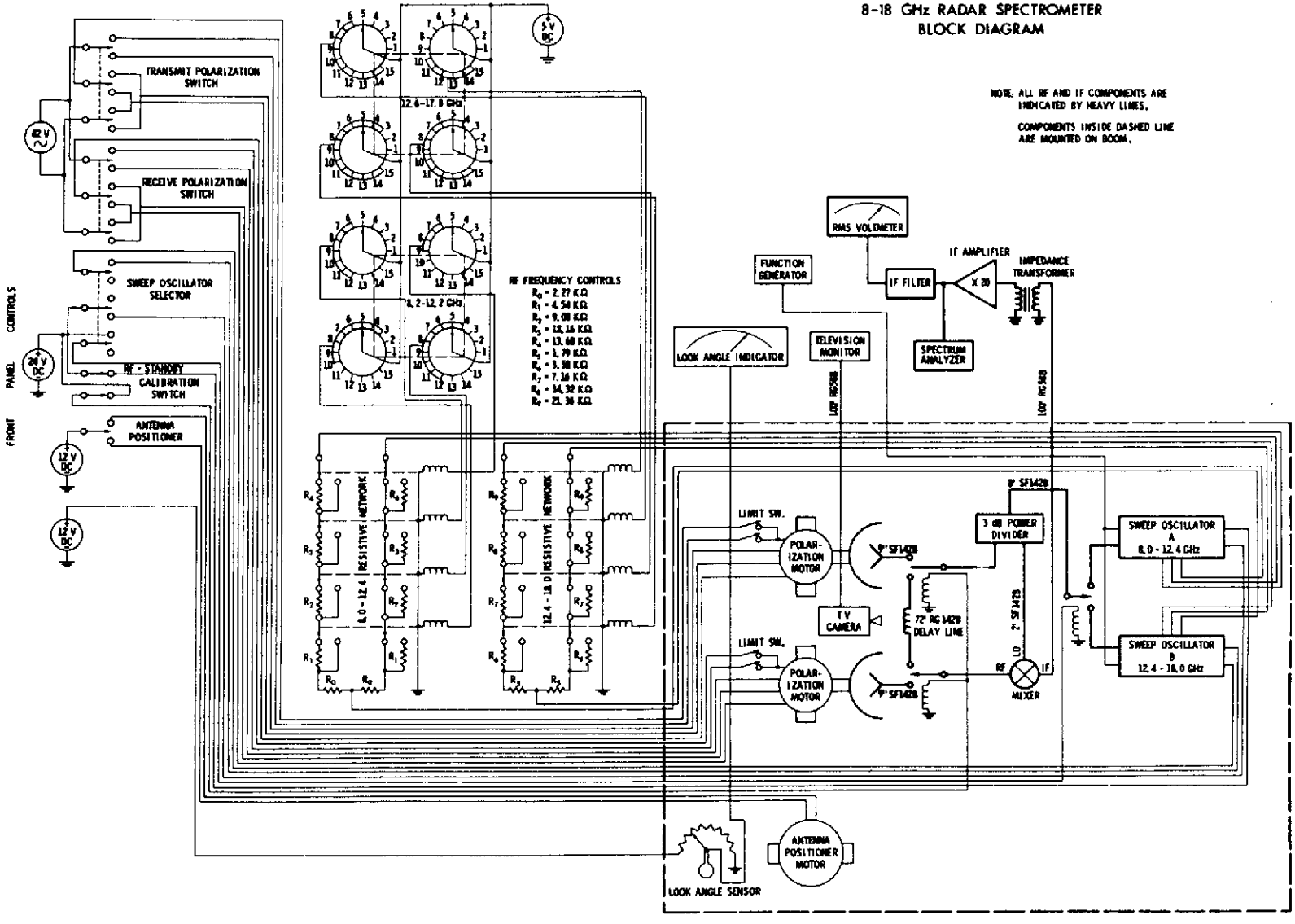
8-18 GHz RADAR SPECTROMETER
BLOCK DIAGRAM
NOTE: ALL RF AND IF COMPONENTS ARE INDICATED BY HEAVY LINES.
COMPONENTS INSIDE DASHED LINE ARE MOUNTED ON BOOM.
FRONT PANEL CONTROLS
TRANSMIT POLARIZATION SWITCH
RECEIVE POLARIZATION SWITCH
SWEEP OSCILLATOR SELECTOR
RF - STANDBY CALIBRATION SWITCH
ANTENNA POSITIONER
RF FREQUENCY CONTROLS
8.0 - 12.4 RESISTIVE NETWORK
12.4 - 18.0 RESISTIVE NETWORK
LOOK ANGLE INDICATOR
TELEVISION MONITOR
RMS VOLTMETER
FUNCTION GENERATOR
IF FILTER
IF AMPLIFIER
X 20
IMPEDANCE TRANSFORMER
SPECTRUM ANALYZER
LIMIT SW.
POLAR-IZATION MOTOR
3 dB POWER DIVIDER
SWEEP OSCILLATOR A
8.0 - 12.4 GHz
TV CAMERA
72" RG 142B DELAY LINE
SWEEP OSCILLATOR B
12.4 - 18.0 GHz
MIXER
LOOK ANGLE SENSOR
ANTENNA POSITIONER MOTOR

FIGURE 16.

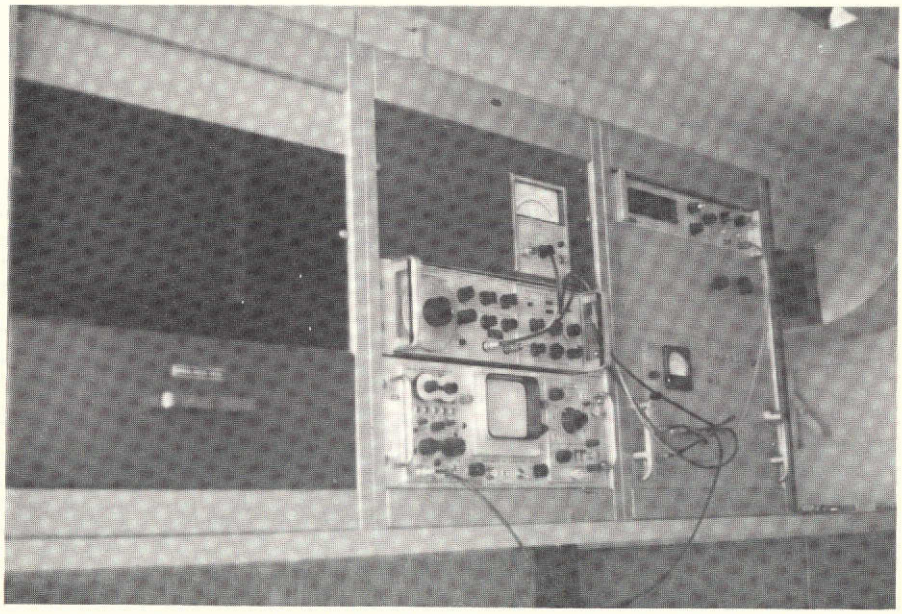

FIGURE 17. PHOTO SHOWING RADAR COMPONENTS LOCATED IN TOPOGRAPHIC VAN.

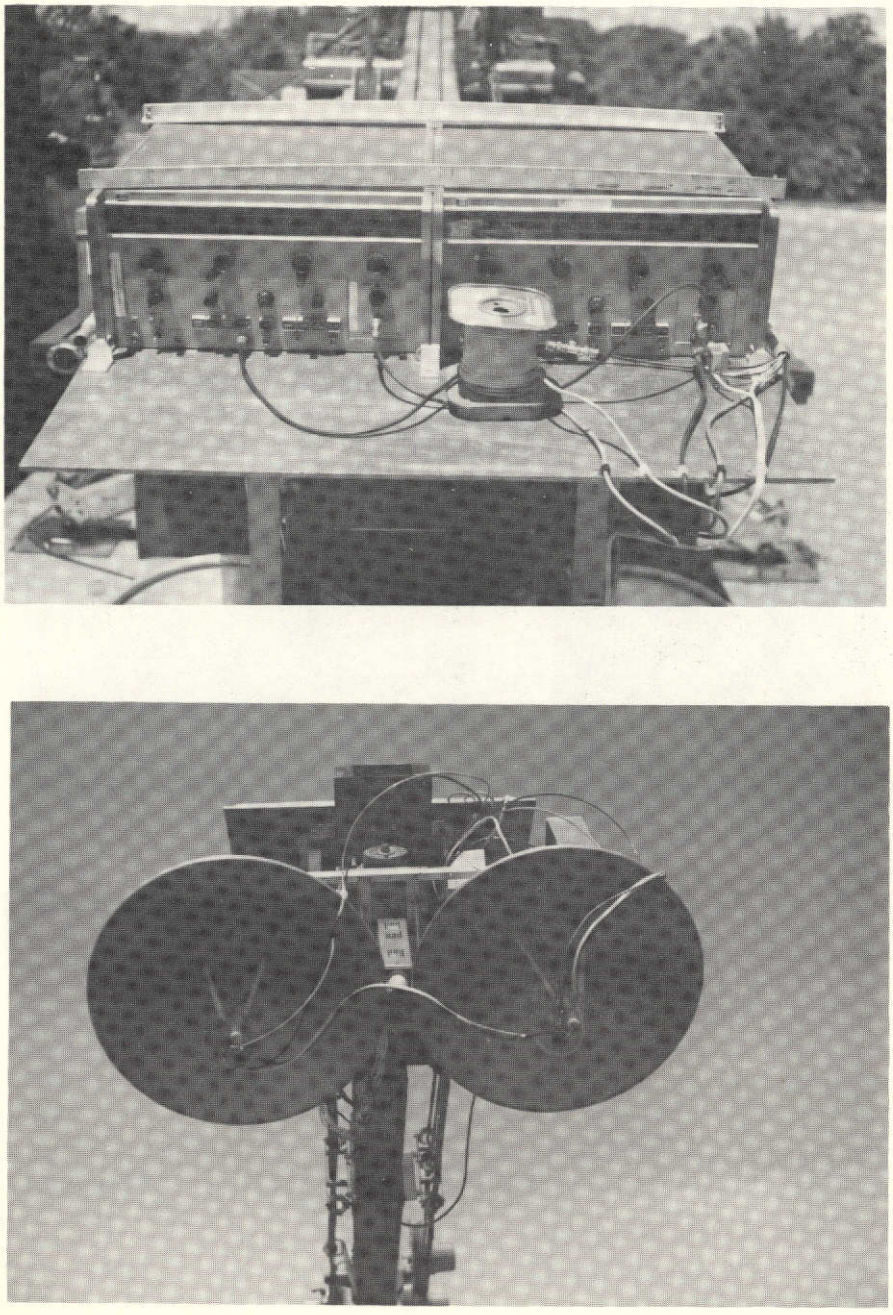

FIGURE 18. PHOTOS SHOWING THE PLACEMENT OF COMPONENTS ON BOOM.

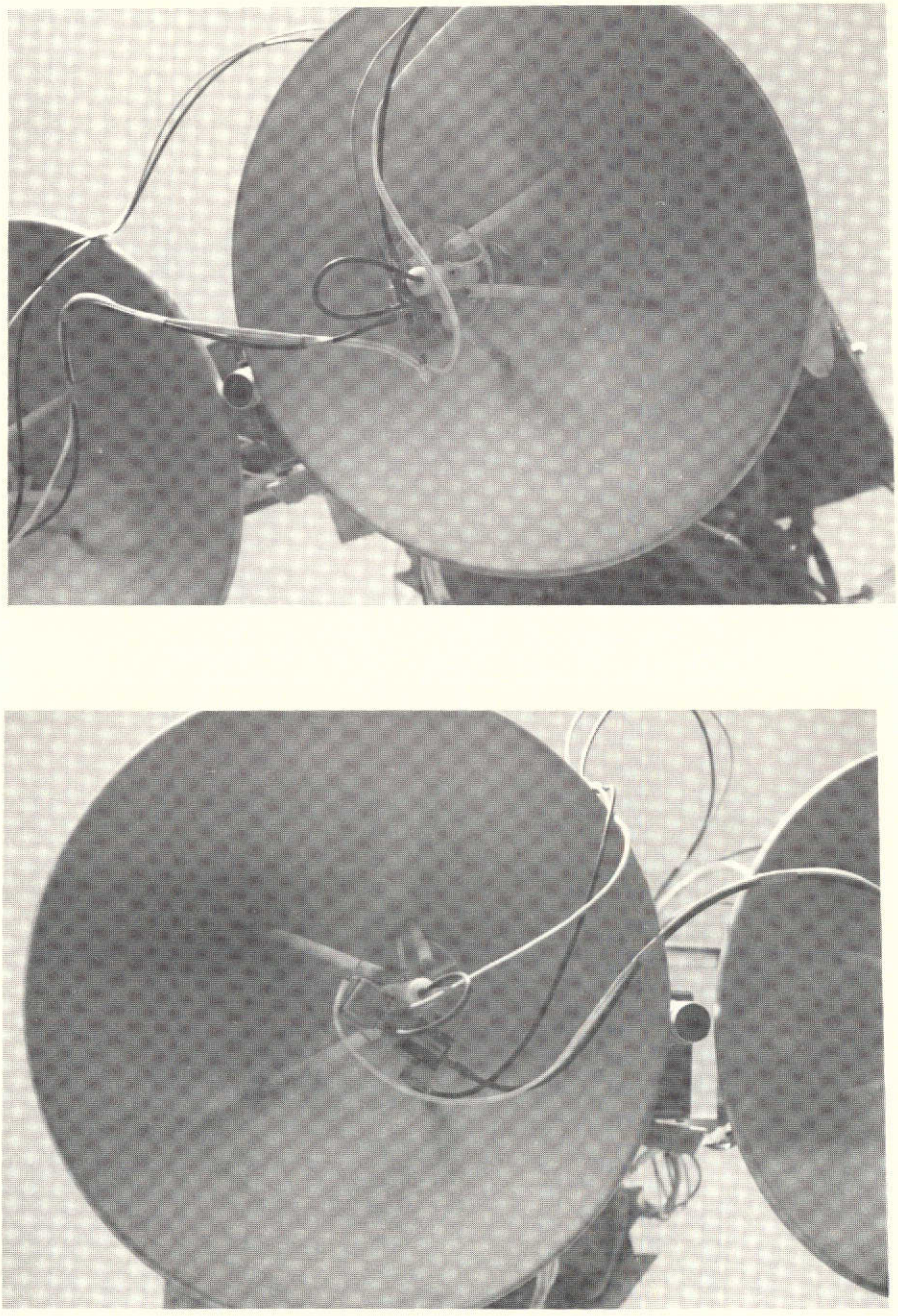

FIGURE 19. PHOTOS SHOWING PLACEMENT OF VARIOUS COMPONENTS BEHIND ANTENNA FEEDS.

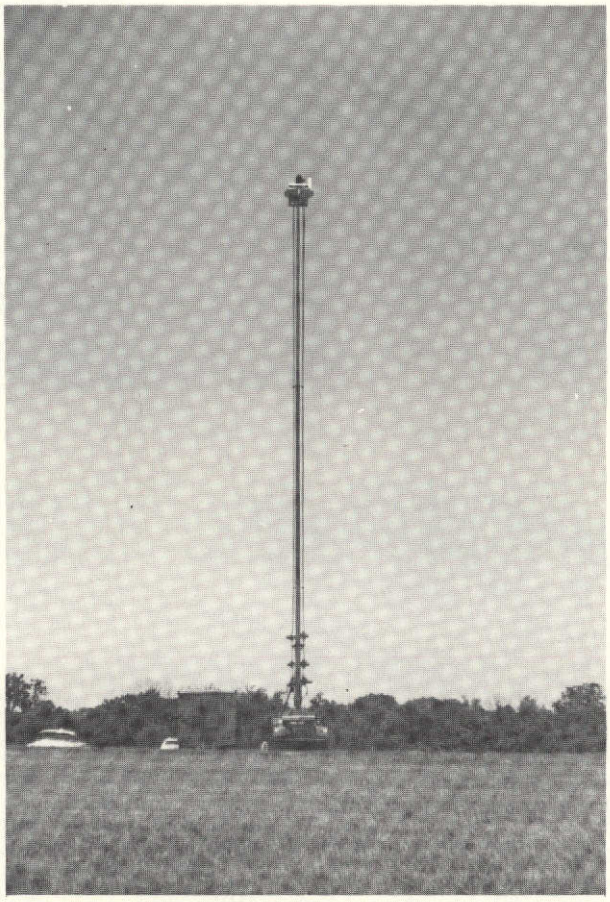

FIGURE 20. PHOTO SHOWING AN OVERALL VIEW OF THE SYSTEM WITH THE BOOM FULLY EXTENDED.

8.0 CALIBRATION

Two methods of calibration were employed in this system:

(1) Delay Line Calibration

To remove any slow system variations such as those that might be caused by ambient temperature variations, a delay line calibration was employed. This was accomplished by bypassing the antennas with a 21.6 m cable by means of RF switches at the feed of each antenna (see Figure 16). This provided a simulated signal which was used to perform a closed loop type of calibration.

(2) Luneberg Lens Calibration

In order to convert the data from relative to absolute values, an Emerson and Cumming, Inc., model 2B-109, Type 140 Luneberg lens was employed. This is a variable index of refraction, spherical lens having the property such that a wave incident on the lens is focused to a point on the opposite side of the sphere. A reflective cap placed over the back of the sphere reflects this energy so that the emerging signal travels in the same direction from which it entered.

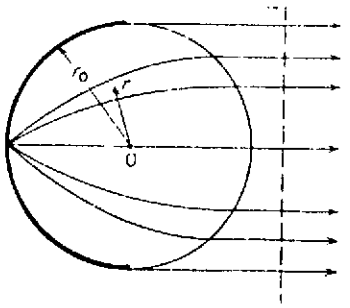

The index of refraction varies in a Luneberg lens of radius r_o as

$$\mu = \left[2 - \left(\frac{r}{r_o}\right)^2\right]^{1/2} \qquad 8.0.1$$

The Luneberg lens has advantages over both the reflective sphere and the corner reflector, both of which have been used as traditional calibration devices. Spheres have been widely used because of their geometric symmetry. That is, they appear the same when viewed from any direction. The disadvantage however is that a sphere has a very small scattering cross section. For a sphere,

$$\sigma_{sphere} = \pi r^2 \quad \text{for } \lambda^{-1} r > 2 \qquad 8.0.2$$

for the lens however,

$$\sigma_{lens} = \frac{(4\pi)^3 r^4}{\lambda^2} \qquad 8.0.3$$

A simple calculation shows that at 10 GHz, the cross section of a 23 cm lens is 26 dB higher (400 times) than a 23 cm metallic sphere.

The advantage of a lens over a trihedral corner reflector is that the lens is much more effective over a large solid angle. Experimental data shows a 61 cm corner reflector has approximately a 20° half power beamwidth at 24 GHz (33) while 23 cm Luneberg lens has a 140° beamwidth.

Figure 21 shows the lens hanging from a large wooden tripod which was used to support it during calibration.

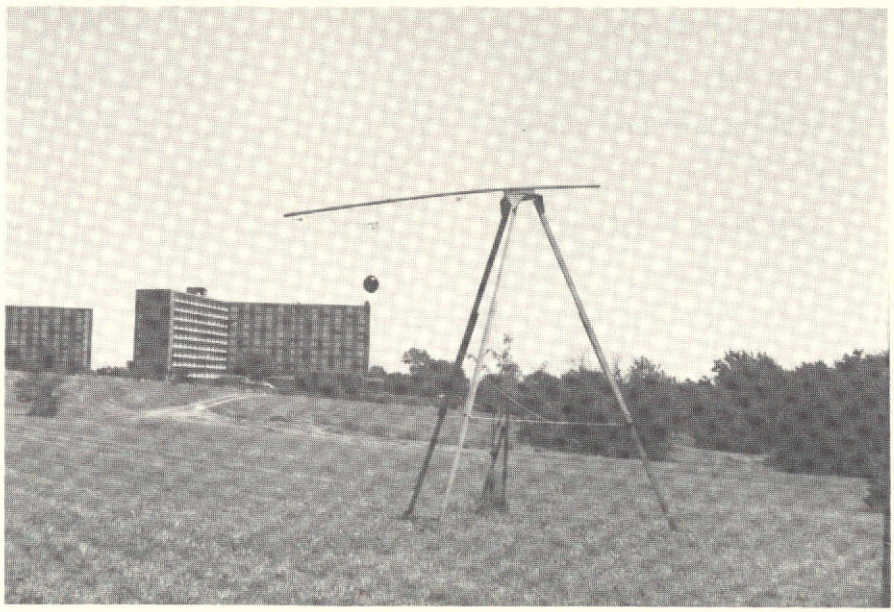

FIGURE 21. PHOTO SHOWING LENS AS USED DURING CALIBRATION.

9.0 CALCULATION OF σ^o

The power returned to the radar from an area extensive target is

$$P_r = \int_A \int \frac{P_t G_t G_r \lambda^2 \sigma^o \, dA}{(4\pi)^3 R_t^4} \qquad 9.0.1$$

where

P_r = Received power
P_t = Transmitted power
G_t = Transmit antenna gain
G_r = Receive antenna gain
λ = Wavelength
σ^o = Scattering coefficient
R_t = Target range
dA = Differential element of illuminated area

If the assumption is made that the parameters inside the integral are constant over the illuminated area the radar equation becomes:

$$P_r = \frac{P_t G_t G_r \lambda^2 \sigma^o A_{ill}}{(4\pi)^3 R_t^4} \qquad 9.0.2$$

Note that P_r represents the received power at the receive antenna terminal. If we introduce an unknown constant K to represent the effects of cable loss, mixer conversion loss etc., we can write

$$V = K \frac{P_t G_t G_r \lambda^2 \sigma^o A_{ill}}{(4\pi)^3 R_t^4} \qquad 9.0.3$$

where V = voltage at receiver output after square law detection. Thus we can write

$$V_L = K \frac{P_t G_t G_r \lambda^2 \sigma_L}{(4\pi)^3 R_L^4} \qquad 9.0.4$$

where the subscript "L" refers to the Luneberg lens. Since the delay line is switched into the circuit at the antenna ports we can also write

$$V_{dl} = K P_t L \qquad 9.0.5$$

where L = delay line attenuation.

With this background, it can be seen how σ^o is extracted from V. At the time of the lens calibration a delay line calibration is also made. We can thus write

$$V_L = K_1 \frac{P_t G_t G_r \lambda^2 \sigma_L}{(4\pi)^3 R_L^4} \qquad 9.0.6$$

If we assume K_1 remains constant during the calibration period (approximately 5 minutes) we can write for the delay line.

$$V_{dlL} = K_1 P_t L \qquad 9.0.7$$

Now consider the actual target data.

$$V_t = K_2 \frac{P_t G_t G_r \lambda^2 \sigma^o A_{ill}}{(4\pi)^3 R_t^4} \qquad 9.0.8$$

Again if we assume K_2 remains constant during the collection of data between delay line calibrations (40 minutes) we can write

$$V_{dlt} = K_2 P_t L \qquad 9.0.9$$

Taking the ratio of equations 9.0.8 and 9.0.6 we have

$$\frac{V_t}{V_L} = \frac{K_2 R_L^4 \sigma^o A_{ill}}{K_1 R_t^4 \sigma_2} \qquad 9.0.10$$

Taking the ratio of equations 9.0.9 and 9.0.7 we have

$$\frac{V_{dlt}}{V_{dlL}} = \frac{K_2}{K_1} \qquad 9.0.11$$

Combining equations 9.0.10 and 9.0.11 and solving for σ^o we obtain

$$\sigma^o = \frac{V_t V_{dlL} R_t^4 \sigma_L}{V_L V_{ldt} R_L^4 A_{ill}}$$

It is important to note that the above equation is independent of K_1 or K_2. Thus, the delay line is an effective means of removing any system parameter variations.

Knowing the frequency of modulation, R_t and R_L can be calculated according to equation 5.0.2. The range information then allows the calculation of the illuminated area as discussed in section 4.5.

10.0 MEASUREMENT ACCURACY

Because of the relative phases of signals which have been reflected from individual scatterers within a resolution cell, any radar return will be subject to fading. In the case of the 8-18 GHz radar spectrometer presently under discussion, the fading is particularly pronounced as can be seen from Figure 22. This figure was derived from data taken in the following manner.

For look angles at 0°, 10°, 20°, 30°, 50° and 70°, the radar return was recorded as a function of boom position. After each measurement was taken, the boom was moved in the azimuth plane approximately 2°. Each measured return was processed to produce a value of σ° which is plotted versus azimuth angle.

Although this figure was drawn only for look angles of 0°, 30° and 70°, it points out an important fact; that being that the fading is drastically reduced as look angles increase. The reason for this reduction, of course, is that more independent samples are available for averaging at large look angles. According to Waite, the frequency spacing between independent samples is given by 3.2.1.1.

$$\Delta F_s = \frac{150}{D} \text{ MHz} \qquad 10.0.1$$

For corn, the target height always exceeds the range resolution of the system so that if we assume that the return (prior to I. F. filtering) includes contributions from the entire height of the plant, D can be replaced by the range resolution of the system (see section 3.2.1).

$$\Delta R = \frac{R \Delta f_{if}}{f_{if}} \qquad 10.0.2$$

In this case, $\Delta f_{if} = 3.58$ KHz and $f_{if} = 60$ KHz so that

$$\Delta R = .059R \qquad 10.0.3$$

Since, in this case, $D = \Delta R$ we can write

$$\Delta F_s = \frac{150}{.059R} \text{ MHz} = \frac{2542}{R} \text{ MHz} \qquad 10.0.4$$

Now, since $\Delta f = 400$ MHz, and since the number of independent samples provided per measurement is

$$N = \frac{\Delta f}{\Delta F_s} \qquad 10.0.5$$

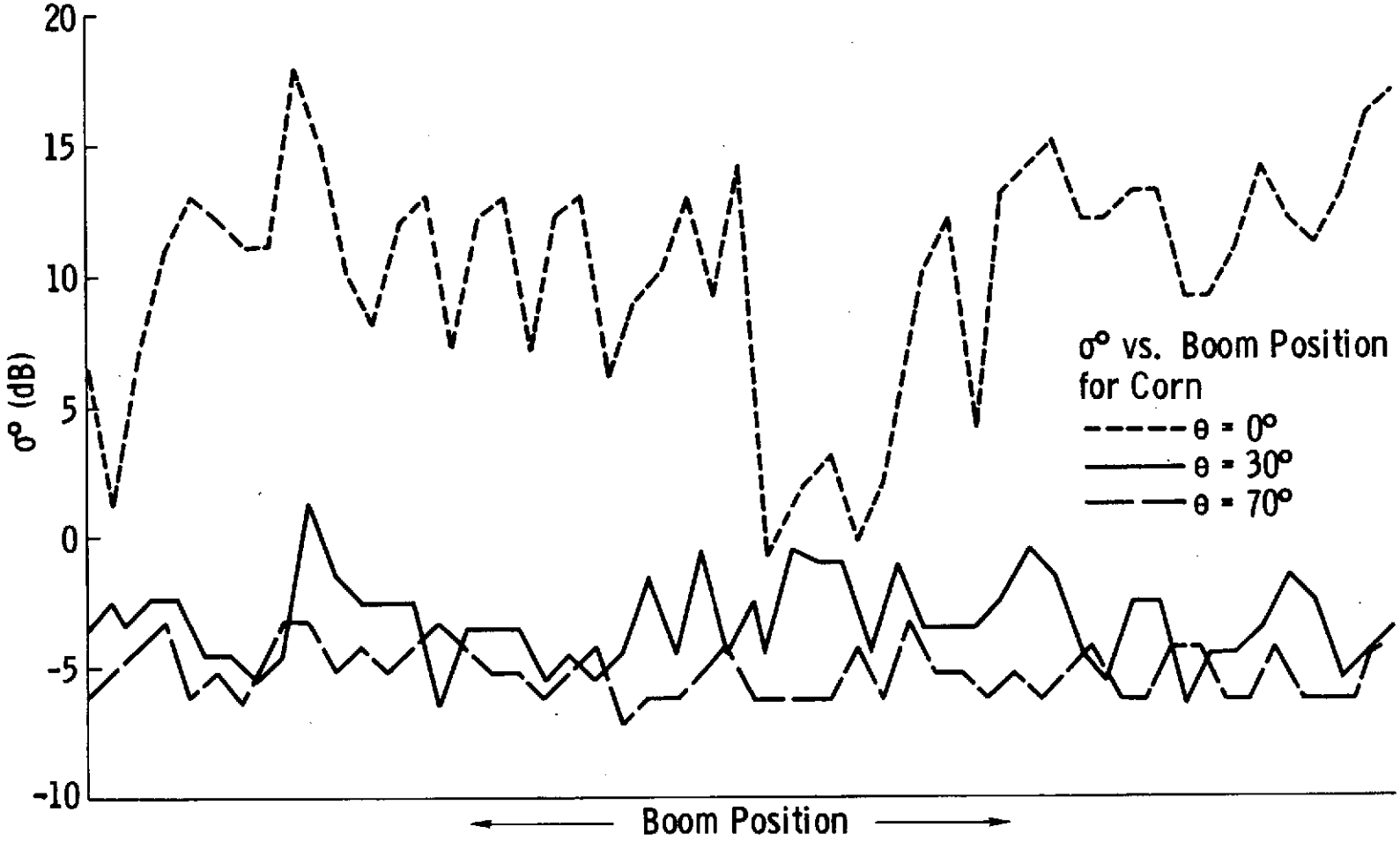

FIGURE 22. CURVES DEPICTING THE FADING OF THE RETURN SIGNAL AS THE BOOM WAS MOVED IN THE AZIMUTH PLANE. NOTE THE REDUCTION IN THE FADING AS θ, THE INCIDENCE ANGLE, INCREASES.

we obtain

$$N = 0.1573R \qquad 10.0.6$$

Thus, we can theoretically write the number of independent samples, N, provided at each angle.

Shown in Figure 23 are histograms of the fading distributions for corn at 9 GHz for look angles of 0°, 30° and 70°. Although each has the shape of a Chi-square distribution, it definitely appears that n, the number of degrees of freedom, increases with θ, the look angle. This increase in n suggests that we are indeed averaging more and more independent samples as θ, and thus R increases. This is consistent with equation 3.2.1.1.

To determine how many independent samples are indeed being averaged, an empirical approach was taken. First, it will be assumed that the radar return distribution is exponential, often known as a chi-square distribution with two degrees of freedom. Since we are averaging the return, which involves the addition of random variables, we can say the return will be described by a chi-square distribution with 2N degrees of freedom. This is justifiable by the additive property of the chi-square distribution which says that the sum of independent chi-square distributions is a chi-square distribution with the number of degrees of freedom equal to the sum of the number of degrees of freedom in each individual distribution (43).

For a chi-square distribution, the mean and the variance are given by:

$$\mu = n\sigma_c^2 \qquad \sigma^2 = 2n\sigma_c^4 \qquad 10.0.7$$

where

n = number of degrees of freedom

σ_c = variance of population from which the samples were taken (40)

Combining the above expressions for the mean and the variance provides

$$\frac{\sigma^2}{\mu^2} = \frac{2}{n} = \frac{1}{N} \qquad 10.0.8$$

or

$$N = \frac{\mu^2}{\sigma^2} \qquad 10.0.9$$

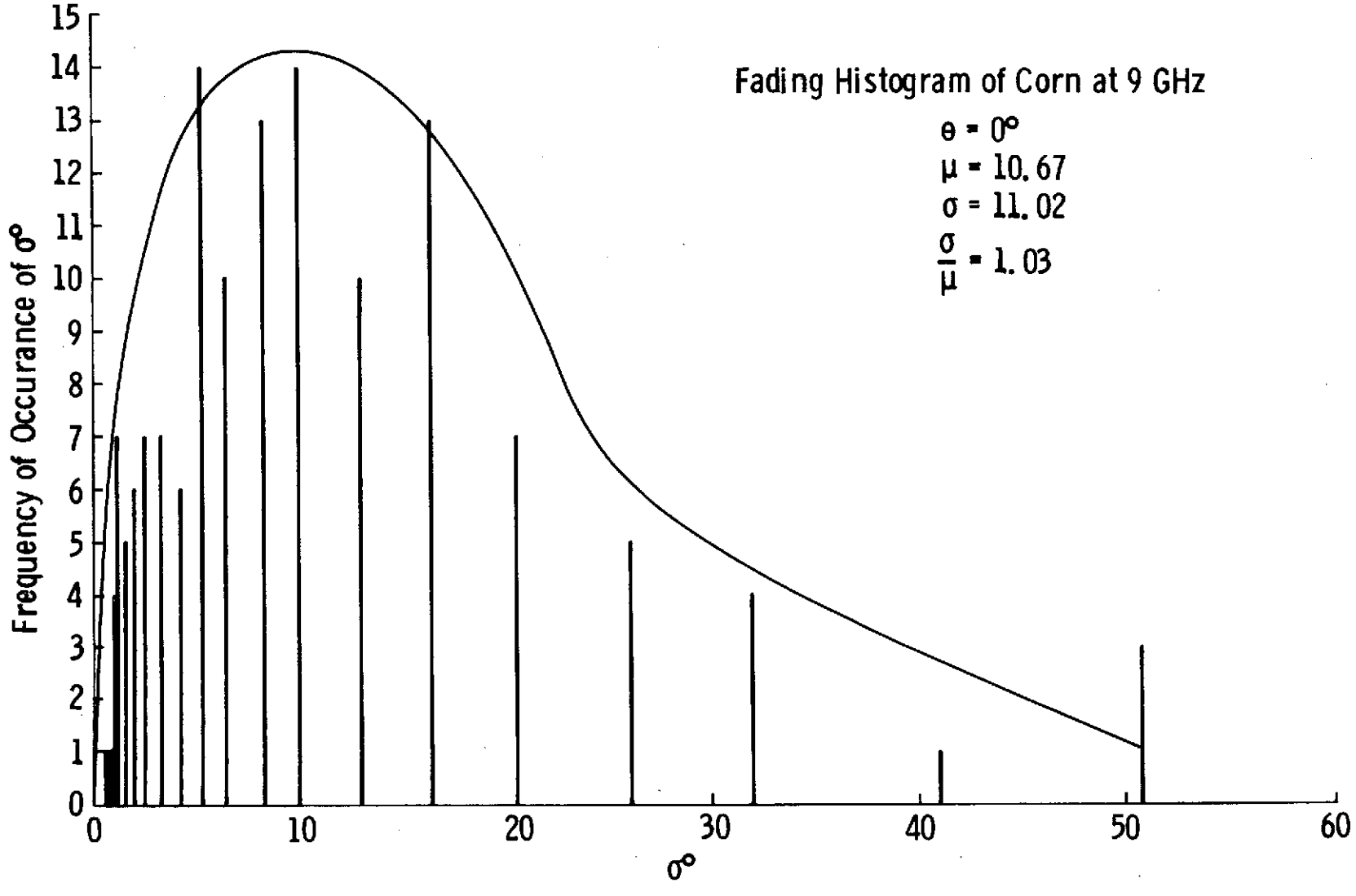

FIGURE 23. FADING HISTOGRAM OF CORN AT 9 GHz.
a) $\theta = 0^{\circ}$, b) $\theta = 30^{\circ}$, and c) $\theta = 70^{\circ}$.

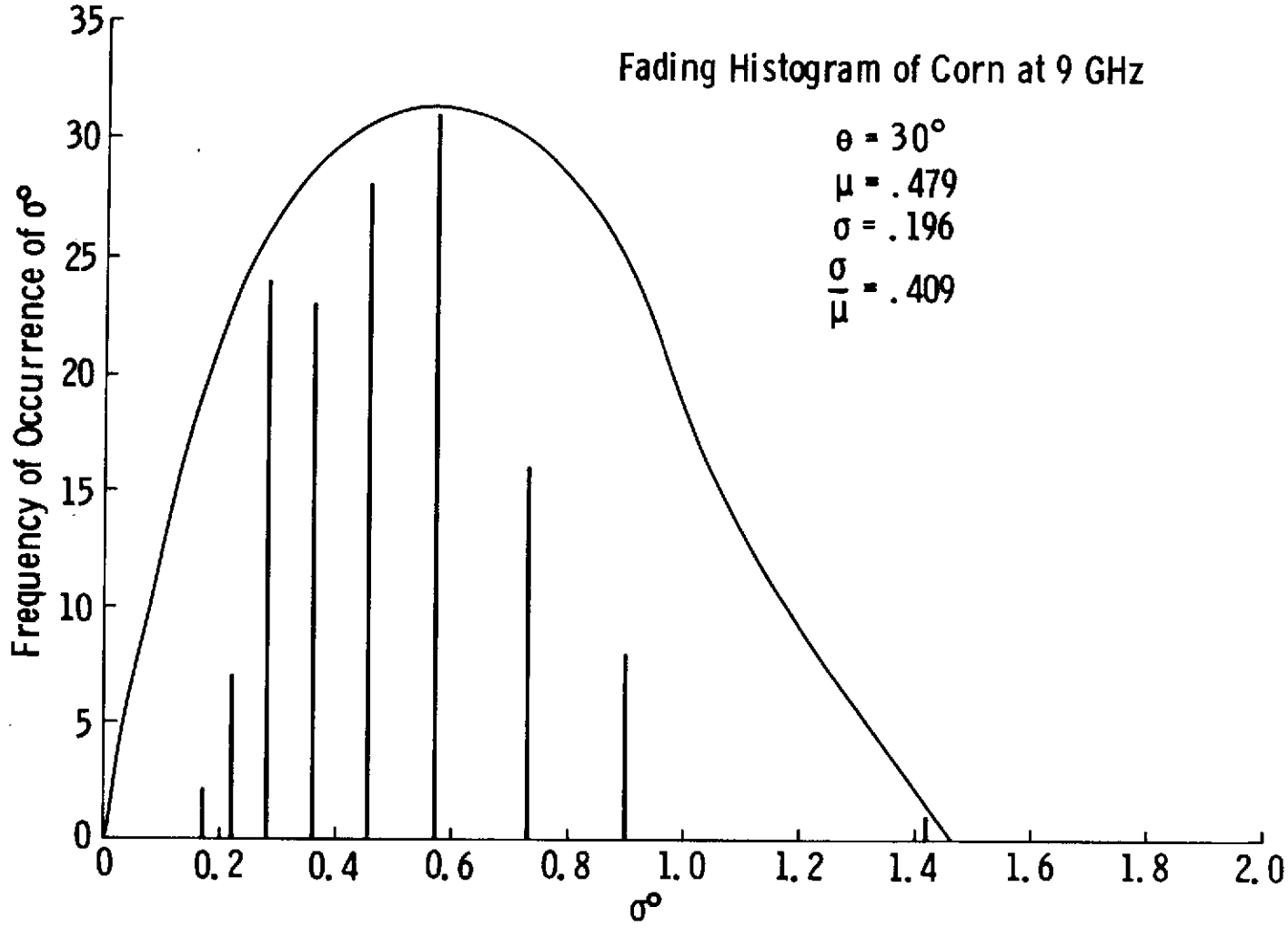
Fading Histogram of Corn at 9 GHz
θ = 30°
μ = .479
σ = .196
σ/μ = .409
Frequency of Occurrence of σ°
σ°
0
5
10
15
20
25
30
35
0
0.2
0.4
0.6
0.8
1.0
1.2
1.4
1.6
1.8
2.0

FIGURE 23b.

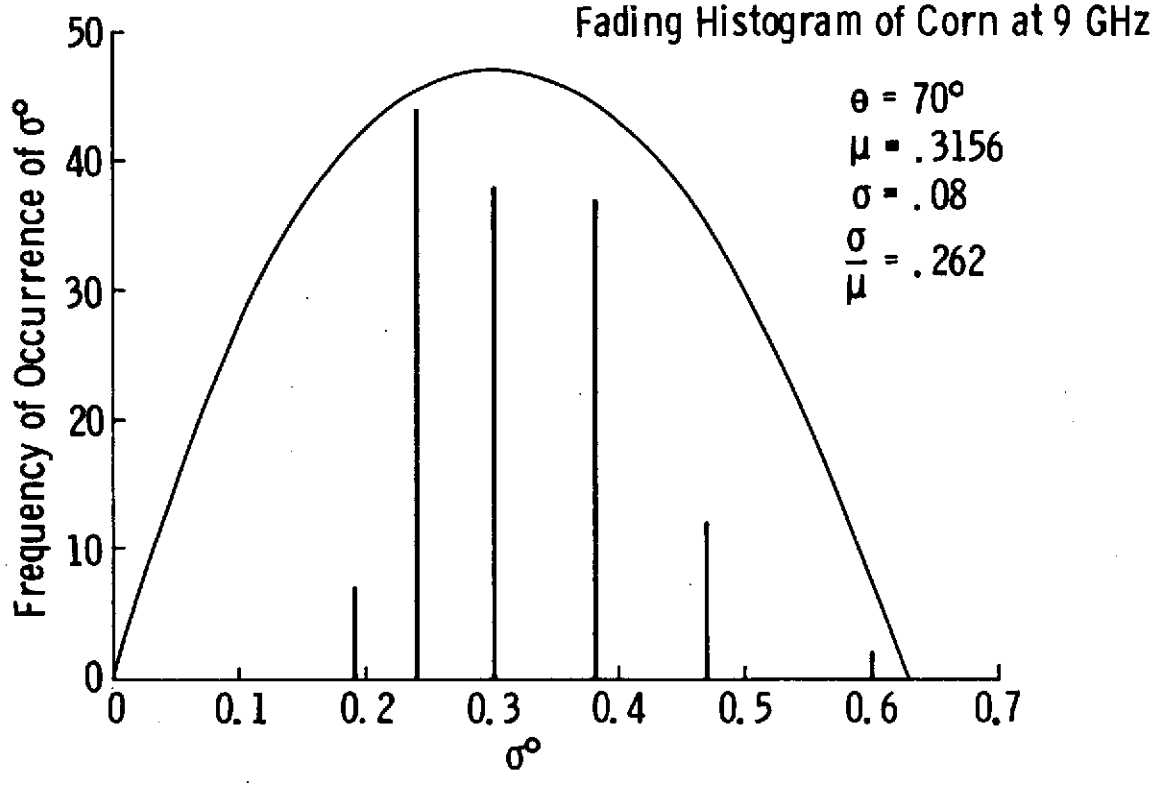
Fading Histogram of Corn at 9 GHz
θ = 70°
μ = .3156
σ = .08
σ/μ = .262
Frequency of Occurrence of σ°
50
40
30
20
10
0
0
0.1
0.2
0.3
0.4
0.5
0.6
0.7
σ°

FIGURE 23c.

Thus, if the mean and standard deviation of the radar return are known, N, the number of independent samples provided can be calculated.

The data needed to calculate μ and σ was collected, as mentioned earlier. Although only 50 points are shown in Figure 22, 140 points were actually gathered for each of the targets of interest at the look angles mentioned at a frequency of 9 GHz. From this data, the mean, standard deviation and consequently N, were calculated. These values of N, σ and μ are presented below for corn along with N_p, the number of independent samples predicted by equation 10.0.6. Note that one must assume that the measured σ and μ are extremely good estimates of the actual values of σ and μ.

Look Angle	μ	σ	N	N_p
0°	10.6	11.0	1	4
10°	2.83	2.6	2	4
20°	0.552	0.308	4	4
30°	0.479	0.196	6	5
50°	0.171	0.059	9	6
70°	0.315	0.08	16	12

Obviously, averaging is necessary to obtain a representative value of σ° at each angle. As can be seen, more averaging is definitely necessary at the lower angles. This brings up the question: How many independent samples must be averaged to predict that the mean value of σ° will fall within a specified range with a specified probability? As an example we might consider σ° for corn at a look angle of 0°. We see that the mean value of σ° is 10.6; this, however, is an average of 140 independent samples. We might now wish to know how many samples must we average in order to say that this average will fall in a symmetric interval about the mean, from 9 to 12,95 per cent of the time.

This question does not have an obvious answer for an asymmetric distribution such as the chi-square. For a Gaussian distribution it becomes much easier. This arises from the fact that the mean and the median have the same value.

If we want to construct a symmetrical, 90 per cent confidence interval around the mean of a Gaussian distribution we pick the end points, x_1 and x_2, of the interval such that

$$.05 = \int_o^{x_1} p_x \, dx \quad \text{and} \quad .95 = \int_o^{x_2} P_x \, dx \qquad 10.0.10$$

This is possible since by definition

$$0.5 = \int_o^{\mu} p_x \, dx \qquad 10.0.11$$

Consider now a chi-square distribution with 2 degrees of freedom. For this particular distribution it turns out that

$$.633 = \int_o^{\mu} p_{\chi^2} \, d\chi^2 \quad \text{or} \quad .337 = \int_{\mu}^{\infty} p_{\chi^2} \, d\chi^2 \qquad 10.0.12$$

Thus, although it is impossible to construct a symmetrical 90 per cent confidence interval around the mean, it is possible to construct a 90 per cent confidence interval around the median M, since

$$0.5 = \int_o^{M} p_{\chi^2} \, d\chi^2 \qquad 10.0.13$$

Having found χ_1^2 and χ_2^2 such that,

$$.05 = \int_o^{\chi_1^2} p_{\chi^2} \, d\chi^2, \quad .05 = \int_{\chi_2}^{\infty} p_{\chi^2} \, d\chi^2 \qquad 10.0.14$$

the points $M-\chi_1^2$ and $M+\chi_1^2$ were plotted versus N. This was done for 90 per cent, 80 per cent and 50 per cent confidence intervals as shown in Figure 24.

Now

$$\lim_{n \to \infty} \mu - M = 0 \qquad 10.0.15$$

as can be seen from Figure 25 where μ and M have been plotted versus n. Note that μ and M have been normalized to $\mu=1$. For $n > 10$, $\mu - M < .06$ so we can say

$$\mu \simeq M \qquad n > 10 \qquad 10.0.16$$

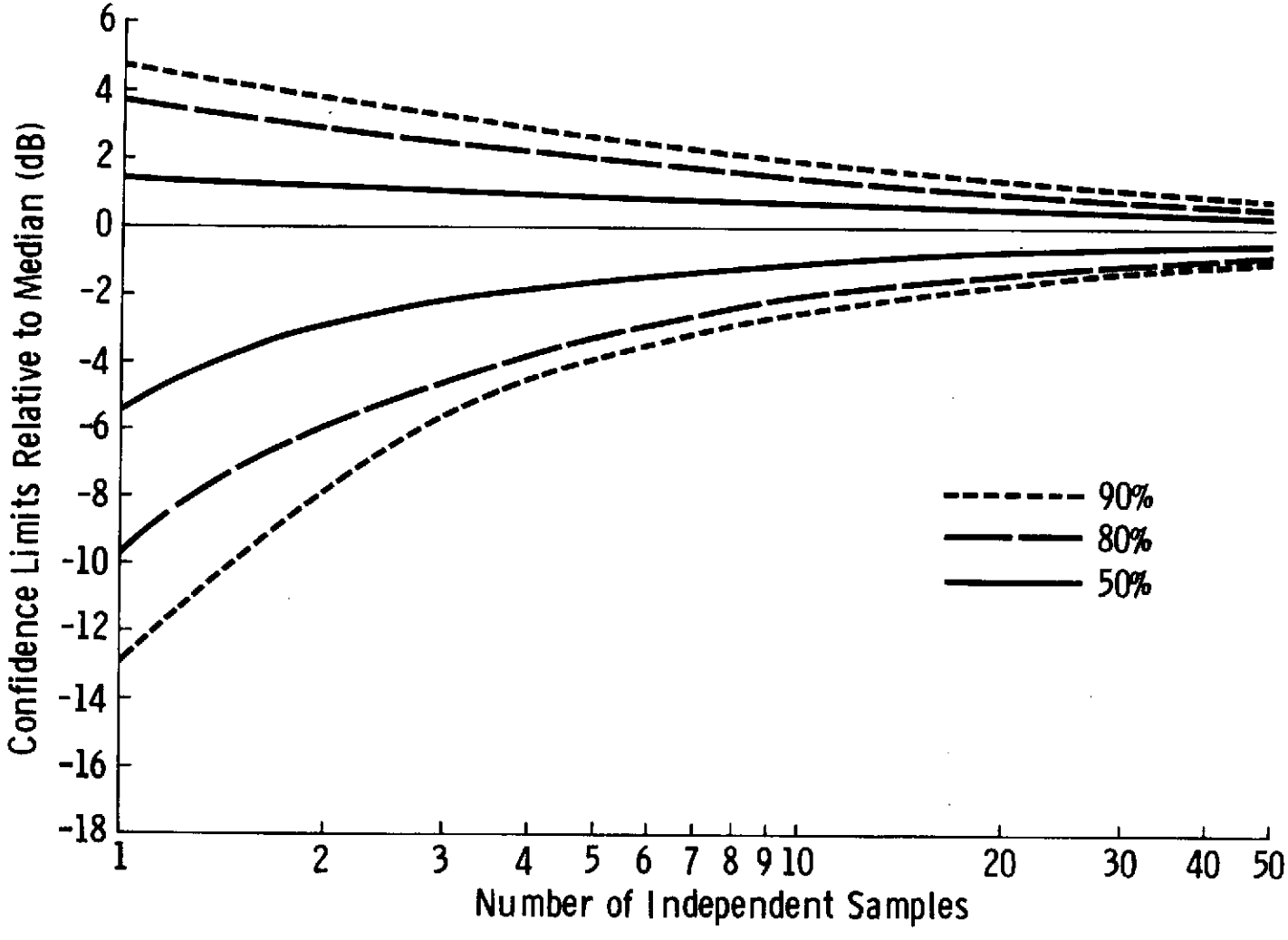

FIGURE 24. 90, 80, AND 50 PER CENT CONFIDENCE INTERVALS AS A FUNCTION OF NUMBER OF INDEPENDENT SAMPLES.

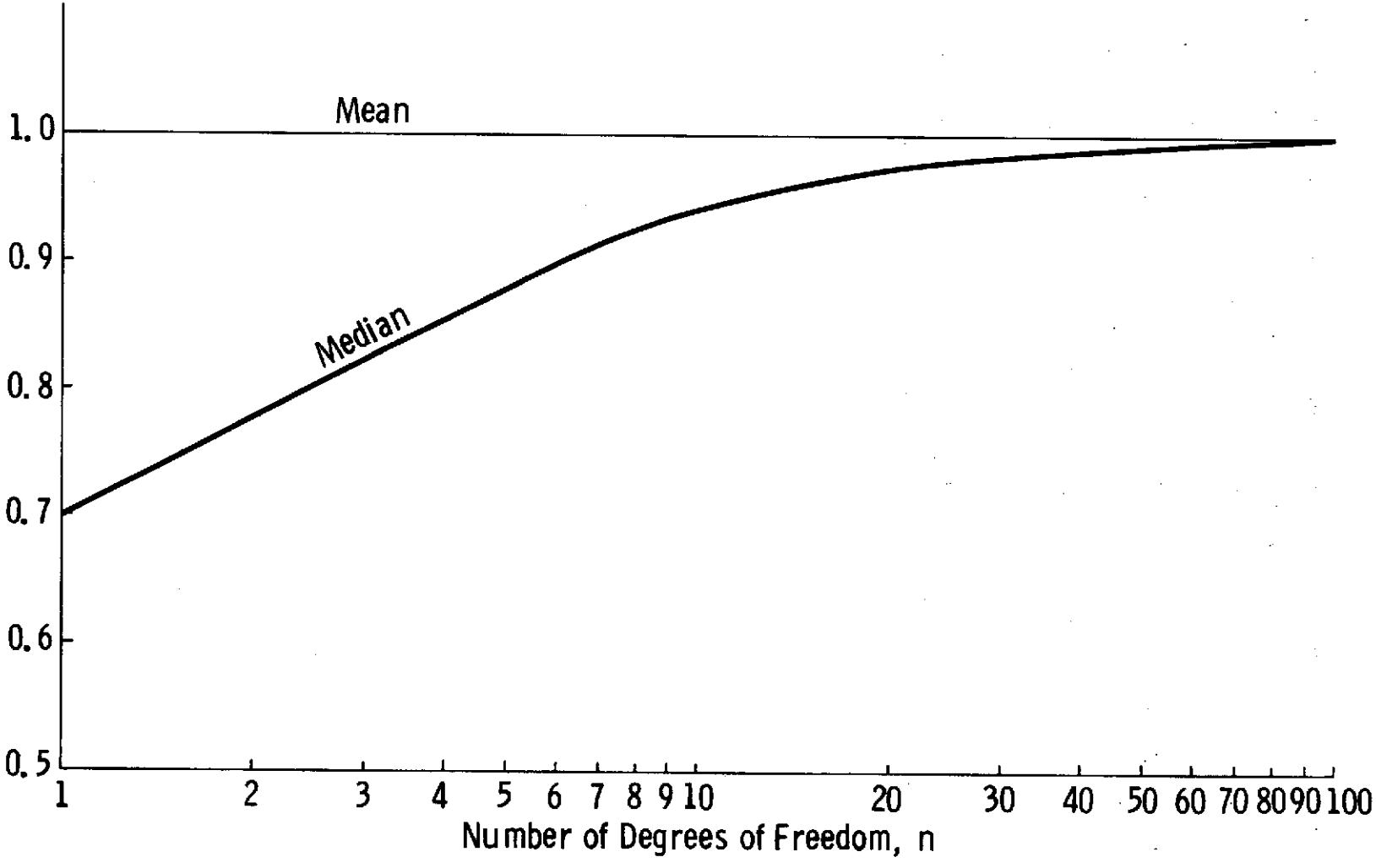

FIGURE 25. CURVES OF THE MEAN AND MEDIAN AS A FUNCTION OF NUMBER OF DEGREES OF FREEDOM. NOTE THE MEDIAN RAPIDLY APPROACHES THE MEAN AS N INCREASES.

Thus, for more than 5 independent samples we have a fairly good approximation of a symmetric confidence interval around the mean. Data was taken to exploit the fact that more individual samples are averaged at larger look angles. Thus, at zero degrees, when only one independent sample is available per observation, it was necessary to make nine observations. At seventy degrees, however, when 16 independent samples per observation were available, it was only necessary to make four observations to provide sixty four independent samples.

Look Angle	Number of Measurements made	Effective Number of Independent Samples
0^{o}	9	9
10^{o}	8	16
20^{o}	7	28
30^{o}	6	36
40^{o}	5	40
50^{o}	4	36
60^{o}	4	48
70^{o}	4	64

11.0 CONCLUSION

Because of the inadequate amount of scattering data on naturally occurring targets, the 8–18 GHz radar spectrometer was determined to be an important tool for the field of remote sensing. The basic parameters of such a system have been presented along with its performance characteristics. Not only did it provide useful scattering data for the determination of σ^{o}, but it also provided useful data on the fading distribution of signals returned from agricultural targets.

Approximately 75,000 data points were collected with this system for use in determining the scattering coefficients of selected agricultural targets. Extensive ground truth was taken simultaneously with the scattering data. There is, however, a need for much more data to answer the questions raised during this initial study. Plans are being made to build a more sophisticated spectrometer capable of making cross polarized measurements (along with HH and VV) at a faster rate than is presently possible.

APPENDIX A

ANTENNA FEED PRINCIPAL PLANE POWER PATTERNS

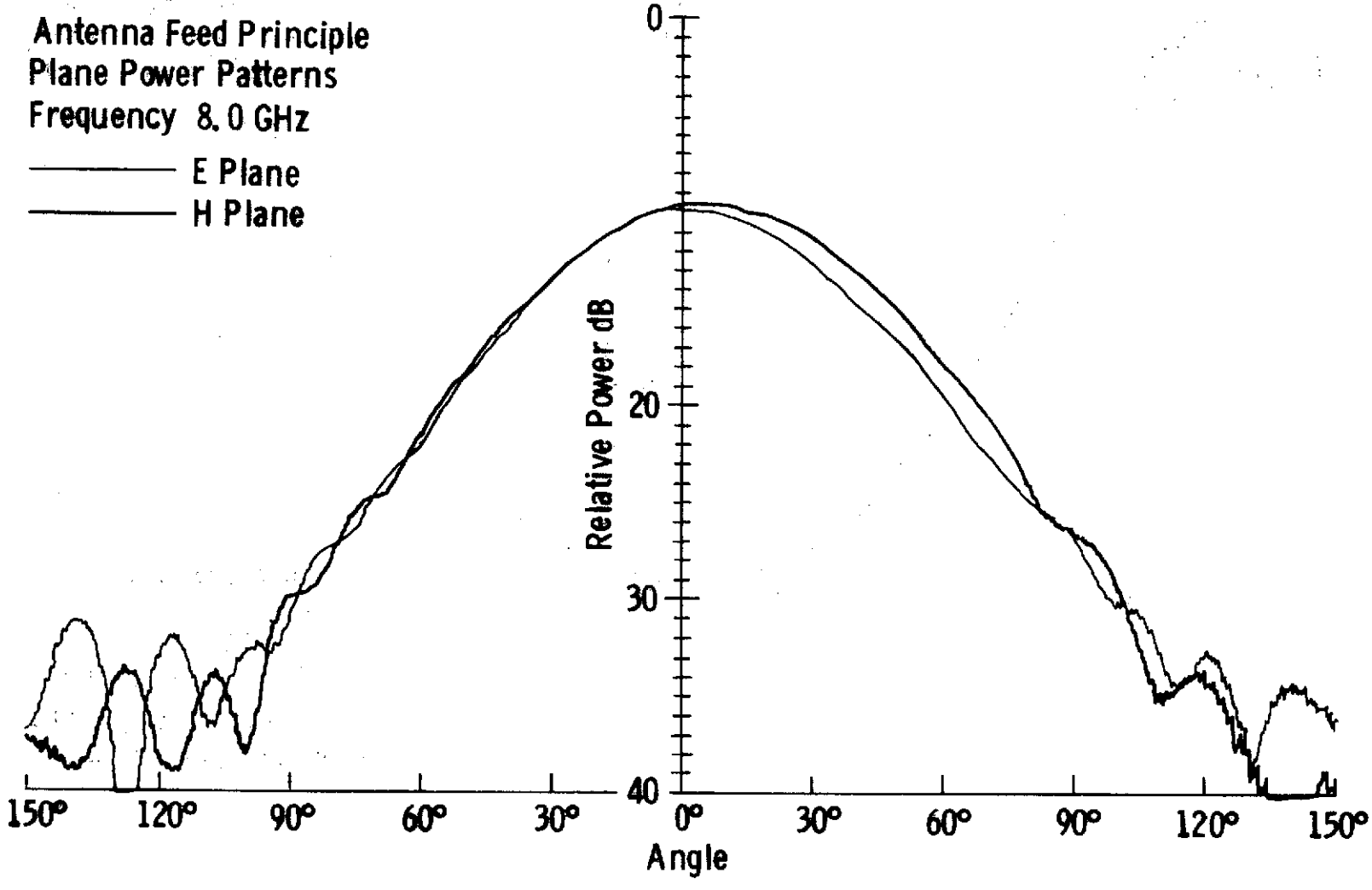
Antenna Feed Principle
Plane Power Patterns
Frequency 8.0 GHz
E Plane
H Plane
Relative Power dB
0
20
30
40
150°
120°
90°
60°
30°
0°
30°
60°
90°
120°
150°
Angle

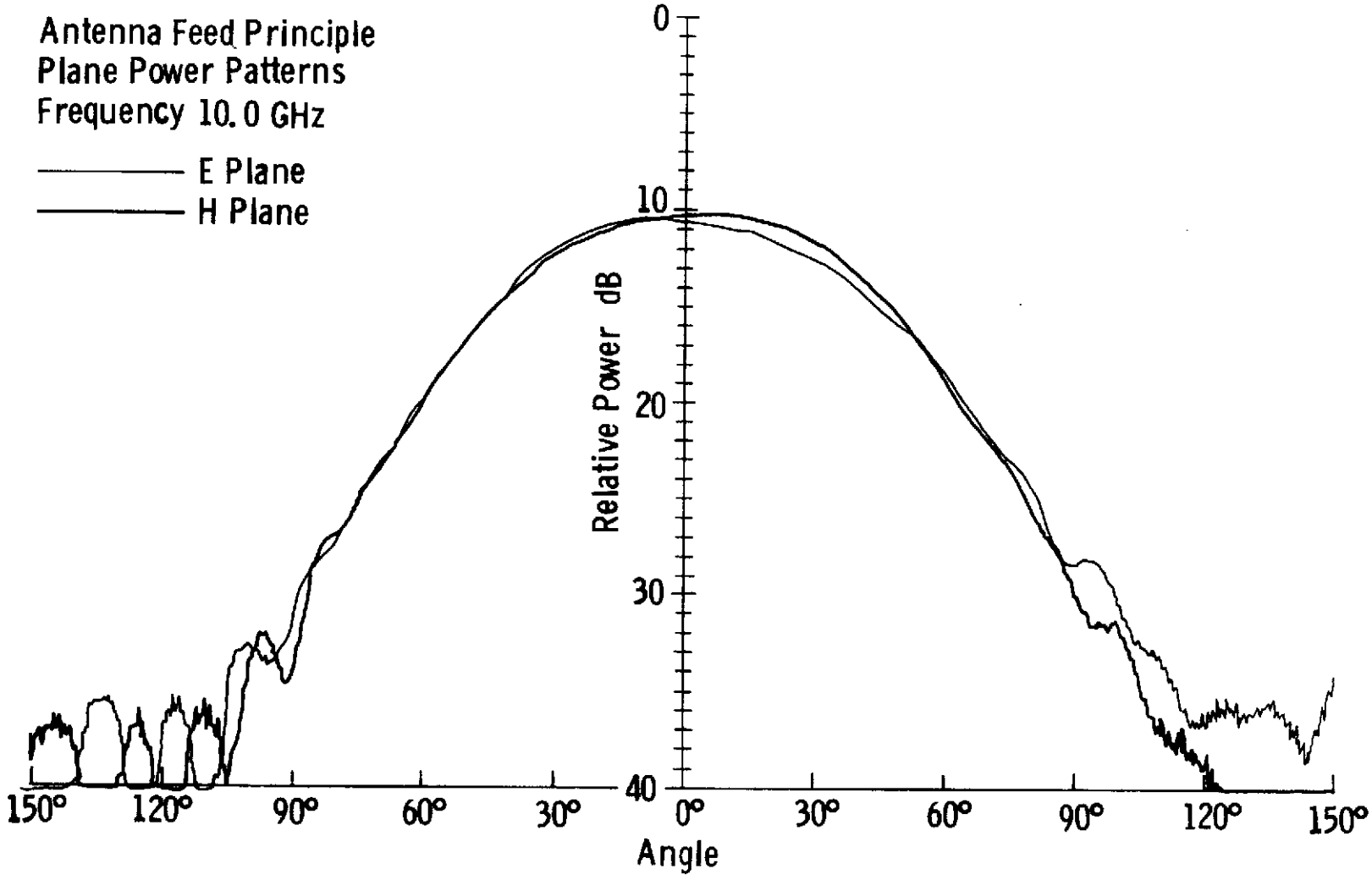
Antenna Feed Principle
Plane Power Patterns
Frequency 10.0 GHz
E Plane
H Plane
Relative Power dB
0
10
20
30
40
150°
120°
90°
60°
30°
0°
30°
60°
90°
120°
150°
Angle

A2

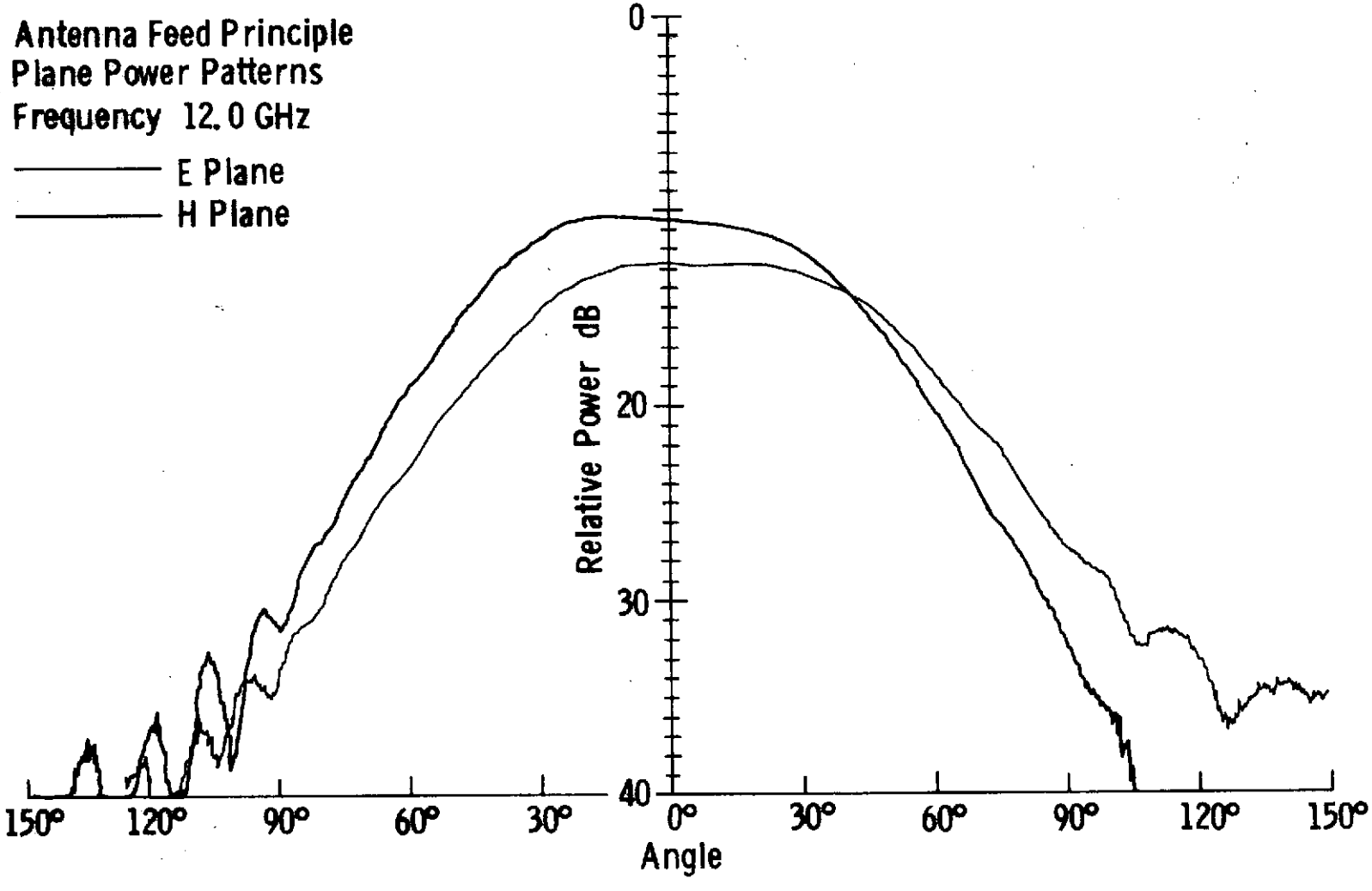
Antenna Feed Principle
Plane Power Patterns
Frequency 12.0 GHz
E Plane
H Plane
Relative Power dB
0
20
30
40
150°
120°
90°
60°
30°
0°
30°
60°
90°
120°
150°
Angle

A3

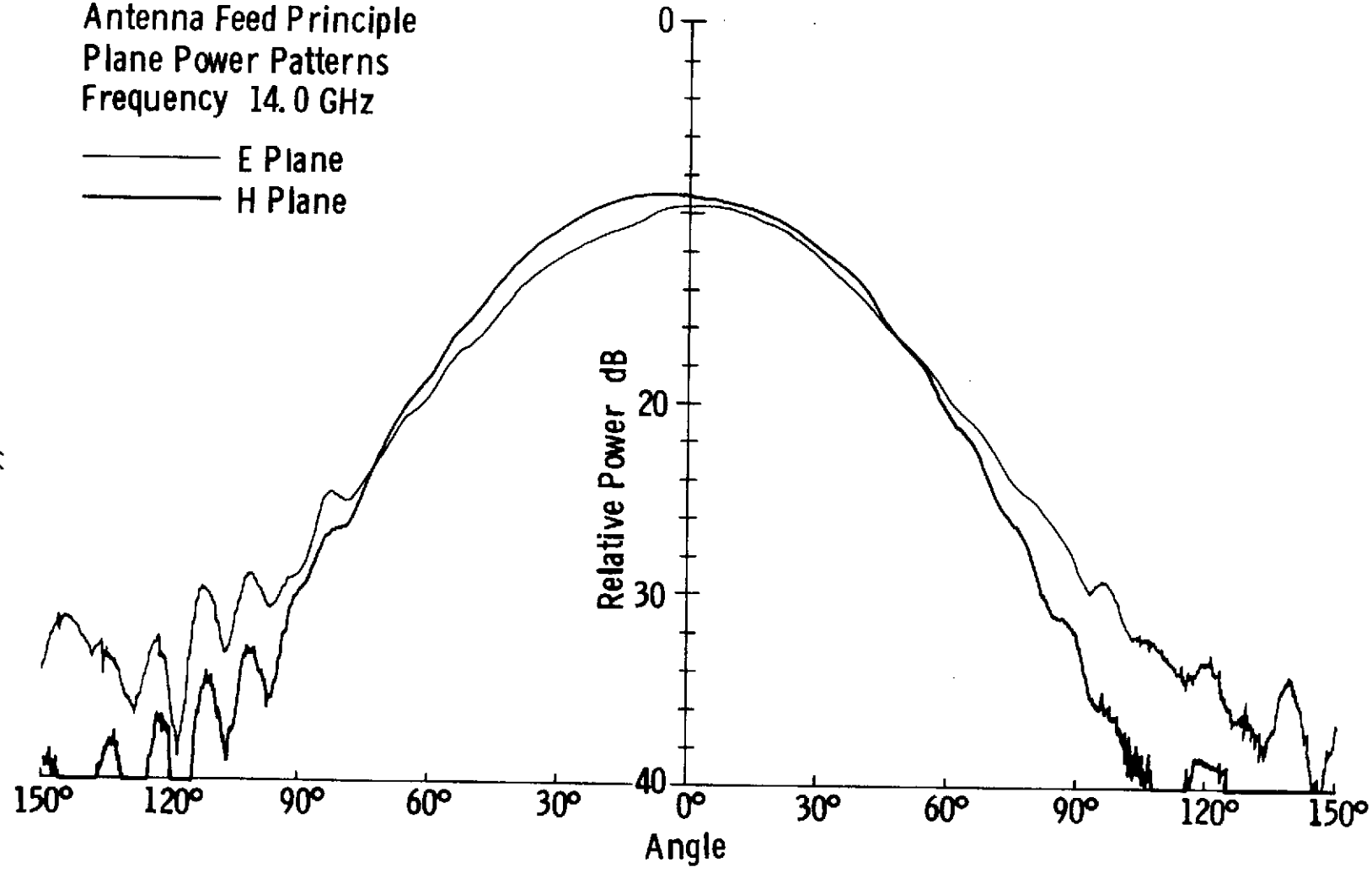
Antenna Feed Principle
Plane Power Patterns
Frequency 14.0 GHz
E Plane
H Plane
Relative Power dB
0
20
30
40
150°
120°
90°
60°
30°
0°
30°
60°
90°
120°
150°
Angle

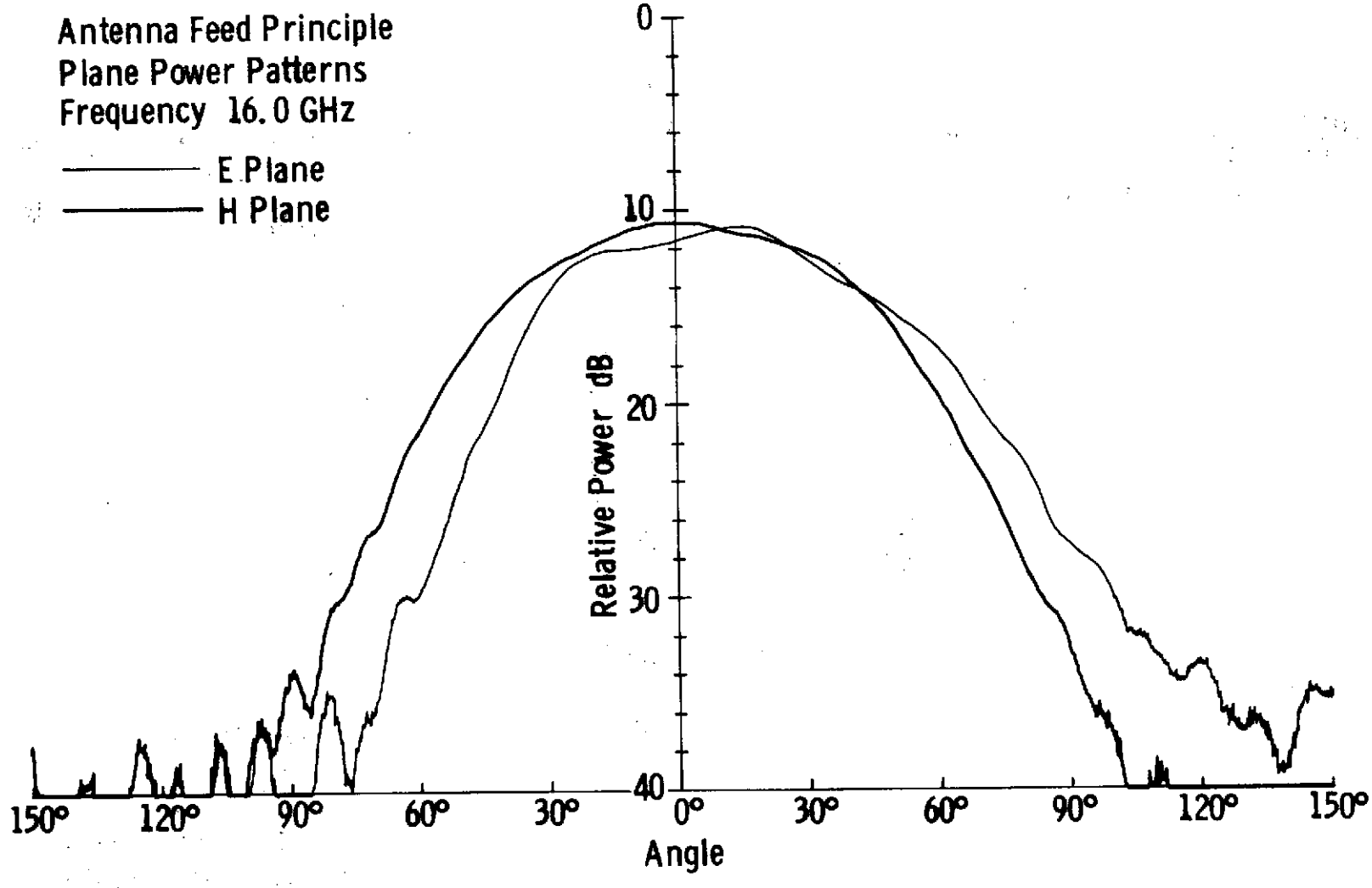
Antenna Feed Principle
Plane Power Patterns
Frequency 16.0 GHz
E Plane
H Plane
0
10
20
30
40
Relative Power dB
150°
120°
90°
60°
30°
0°
30°
60°
90°
120°
150°
Angle

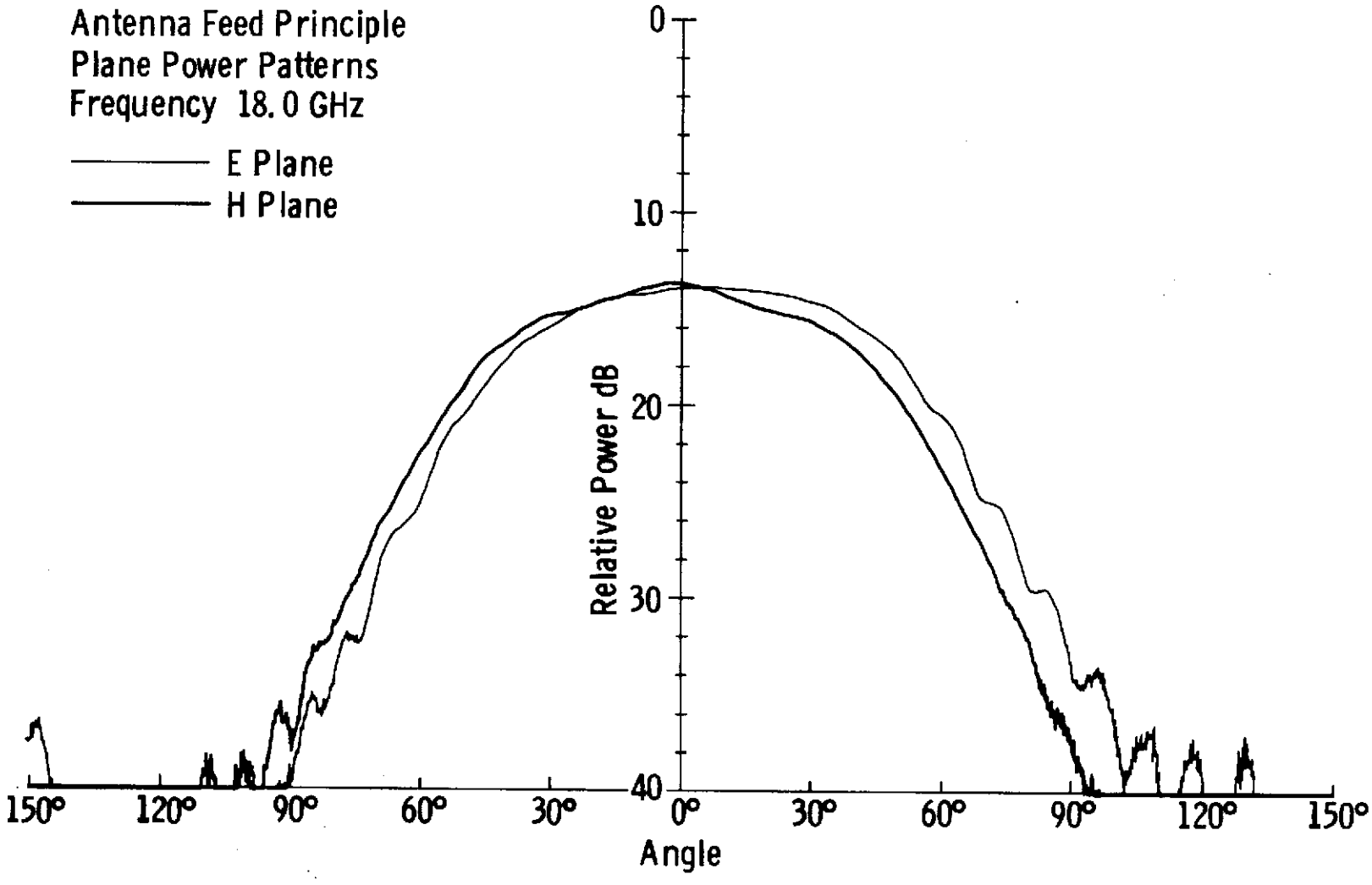
Antenna Feed Principle
Plane Power Patterns
Frequency 18.0 GHz
E Plane
H Plane
0
10
20
30
40
Relative Power dB
150°
120°
90°
60°
30°
0°
30°
60°
90°
120°
150°
Angle

A6

APPENDIX B

ANTENNA FEED BEAMWIDTH, VSWR, GAIN, AND ISOLATION CURVES

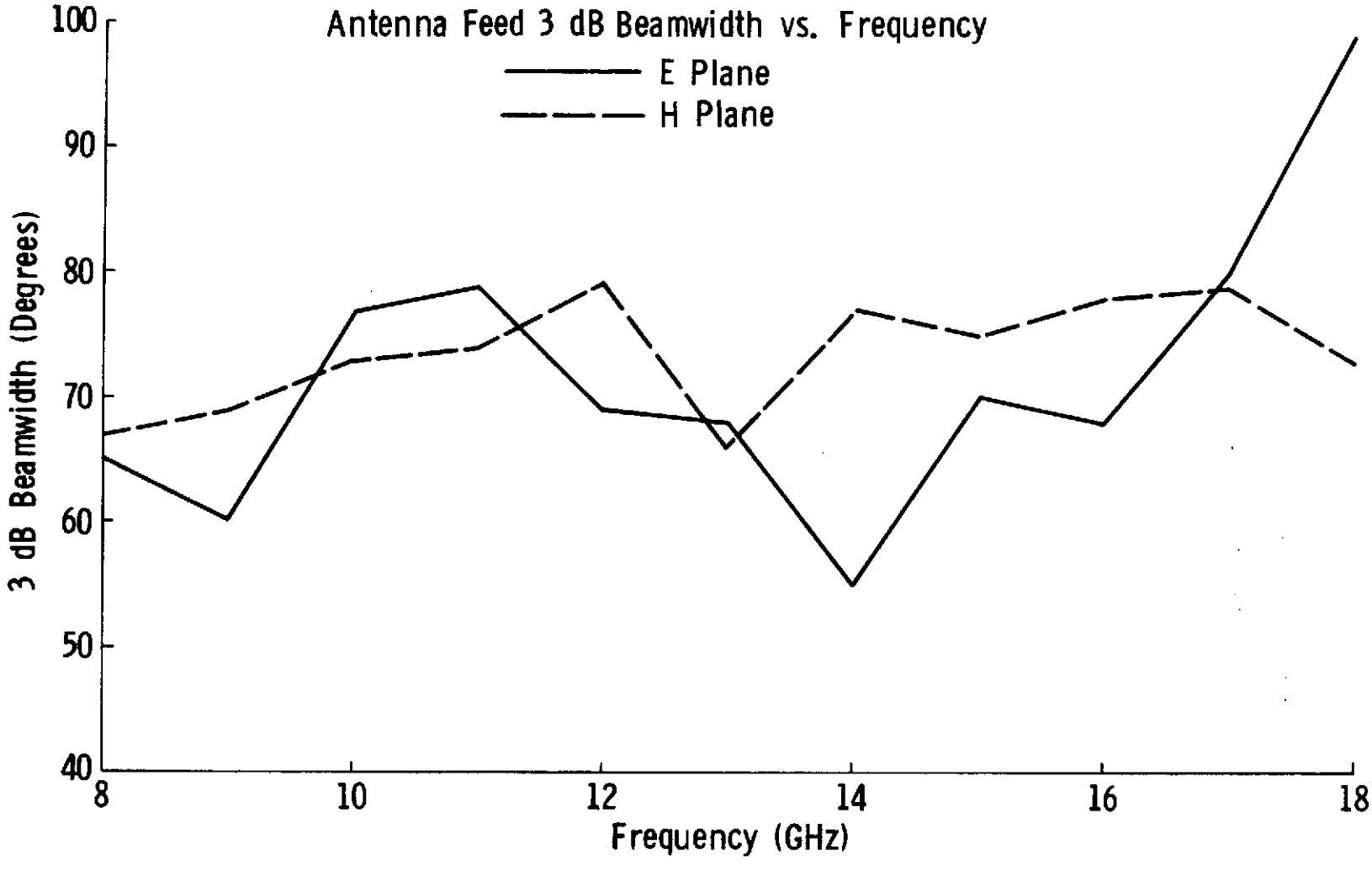
Antenna Feed 3 dB Beamwidth vs. Frequency
E Plane
H Plane
3 dB Beamwidth (Degrees)
100
90
80
70
60
50
40
8
10
12
14
16
18
Frequency (GHz)

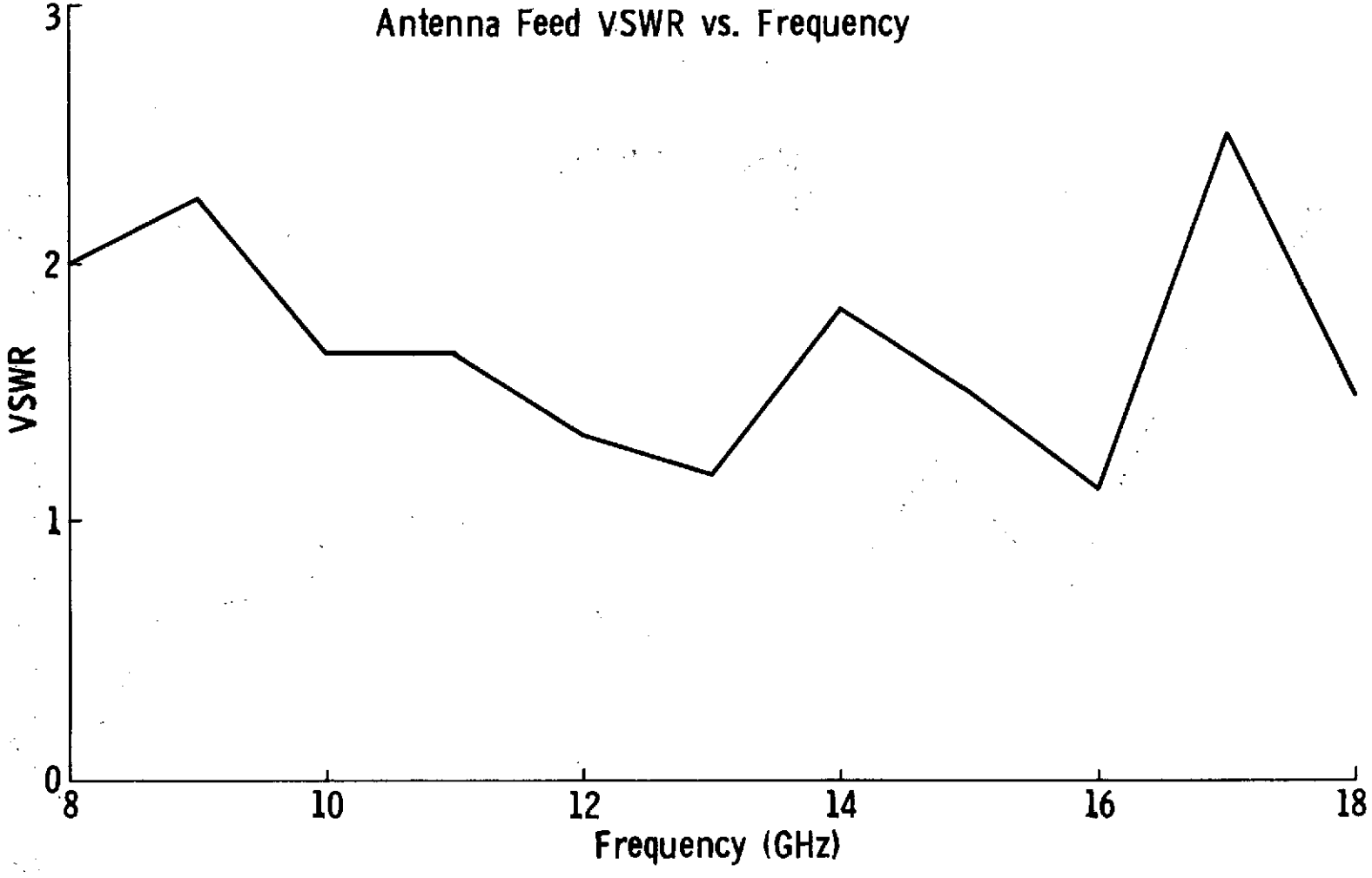
Antenna Feed VSWR vs. Frequency
VSWR
3
2
1
0
8
10
12
14
16
18
Frequency (GHz)

B2

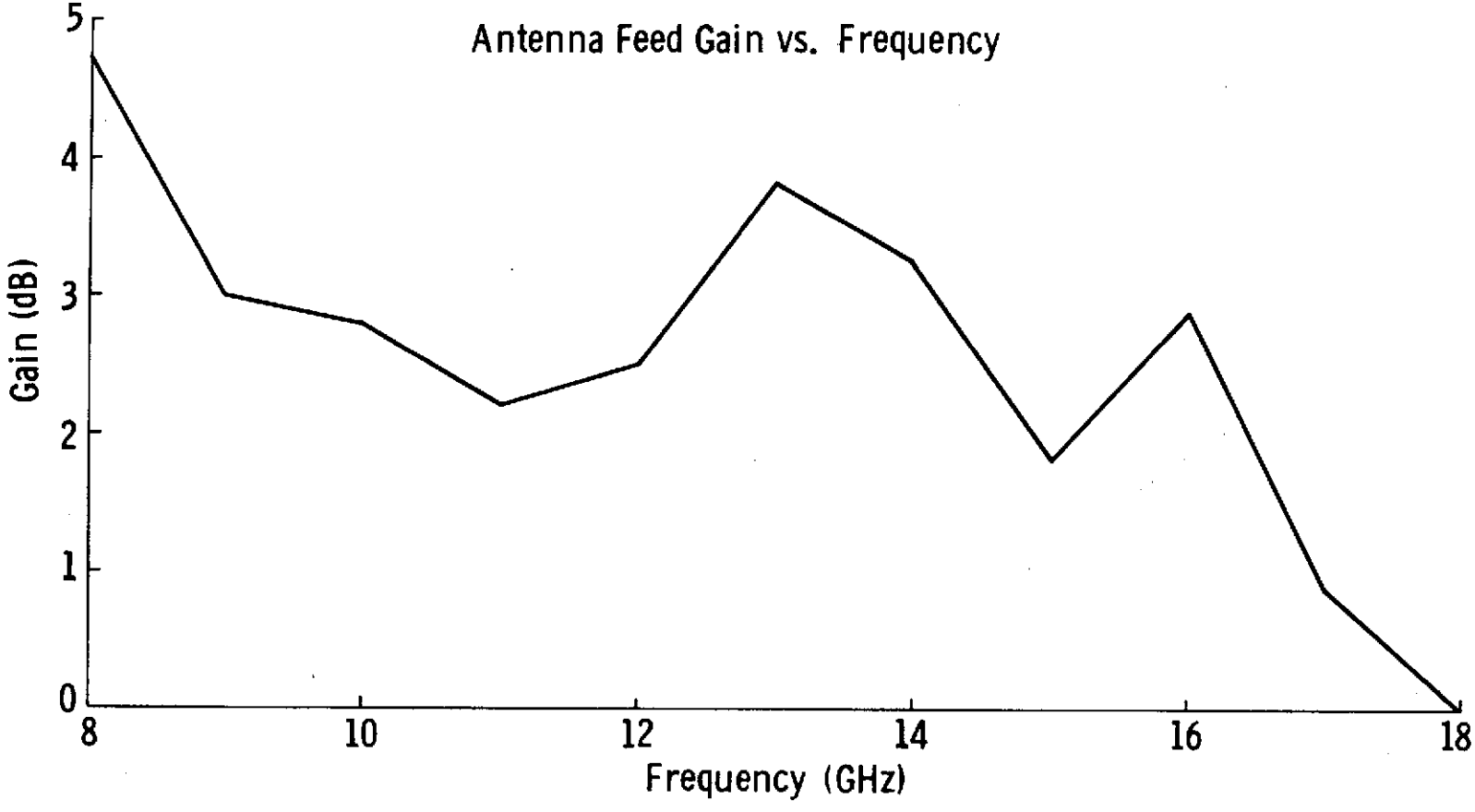
Antenna Feed Gain vs. Frequency
Gain (dB)
0
1
2
3
4
5
8
10
12
14
16
18
Frequency (GHz)

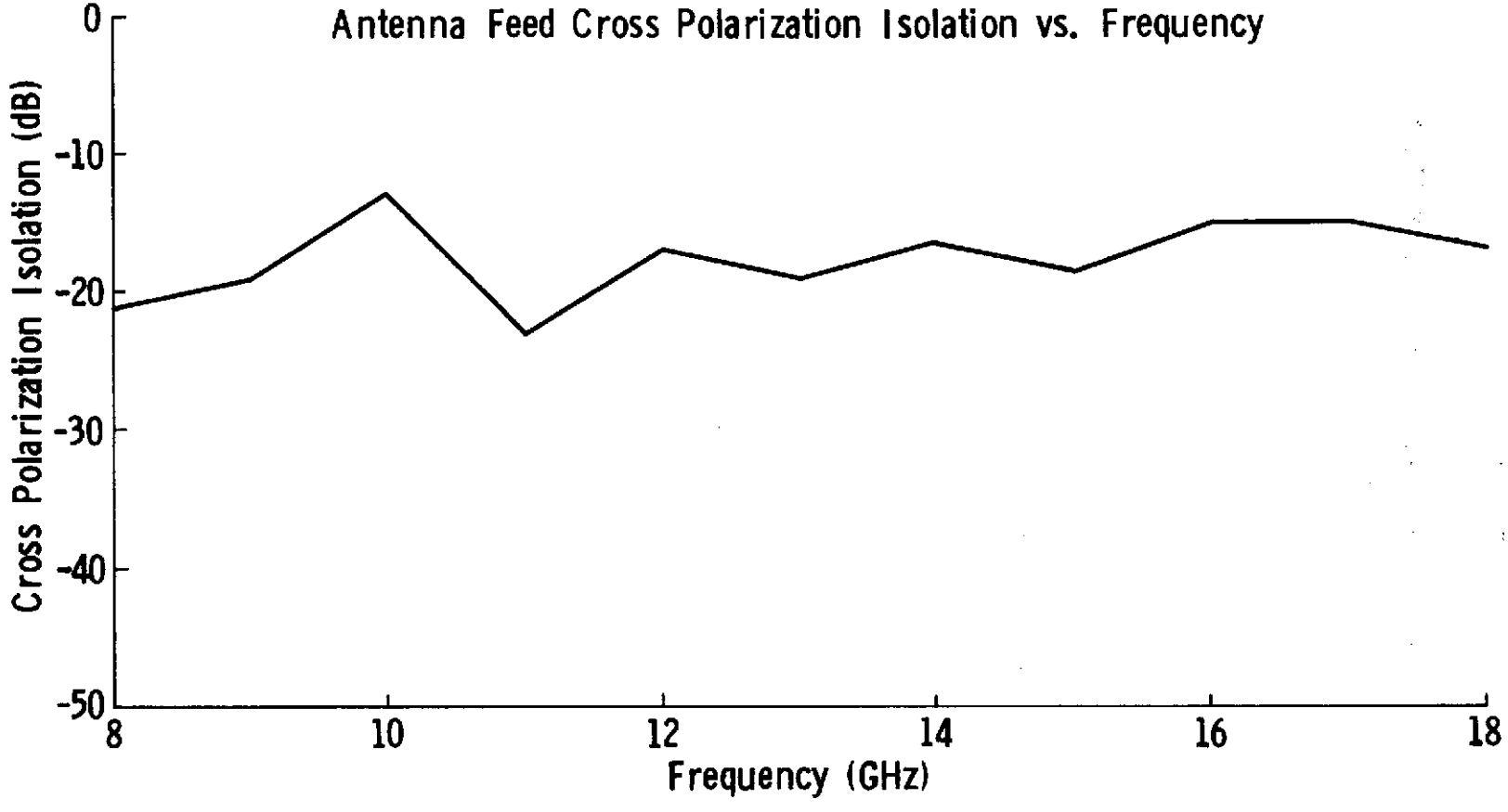
Antenna Feed Cross Polarization Isolation vs. Frequency
Cross Polarization Isolation (dB)
0
-10
-20
-30
-40
-50
8
10
12
14
16
18
Frequency (GHz)

APPENDIX C

TRANSMIT ANTENNA PRINCIPAL PLANE POWER PATTERNS

4 div. = 3 dB

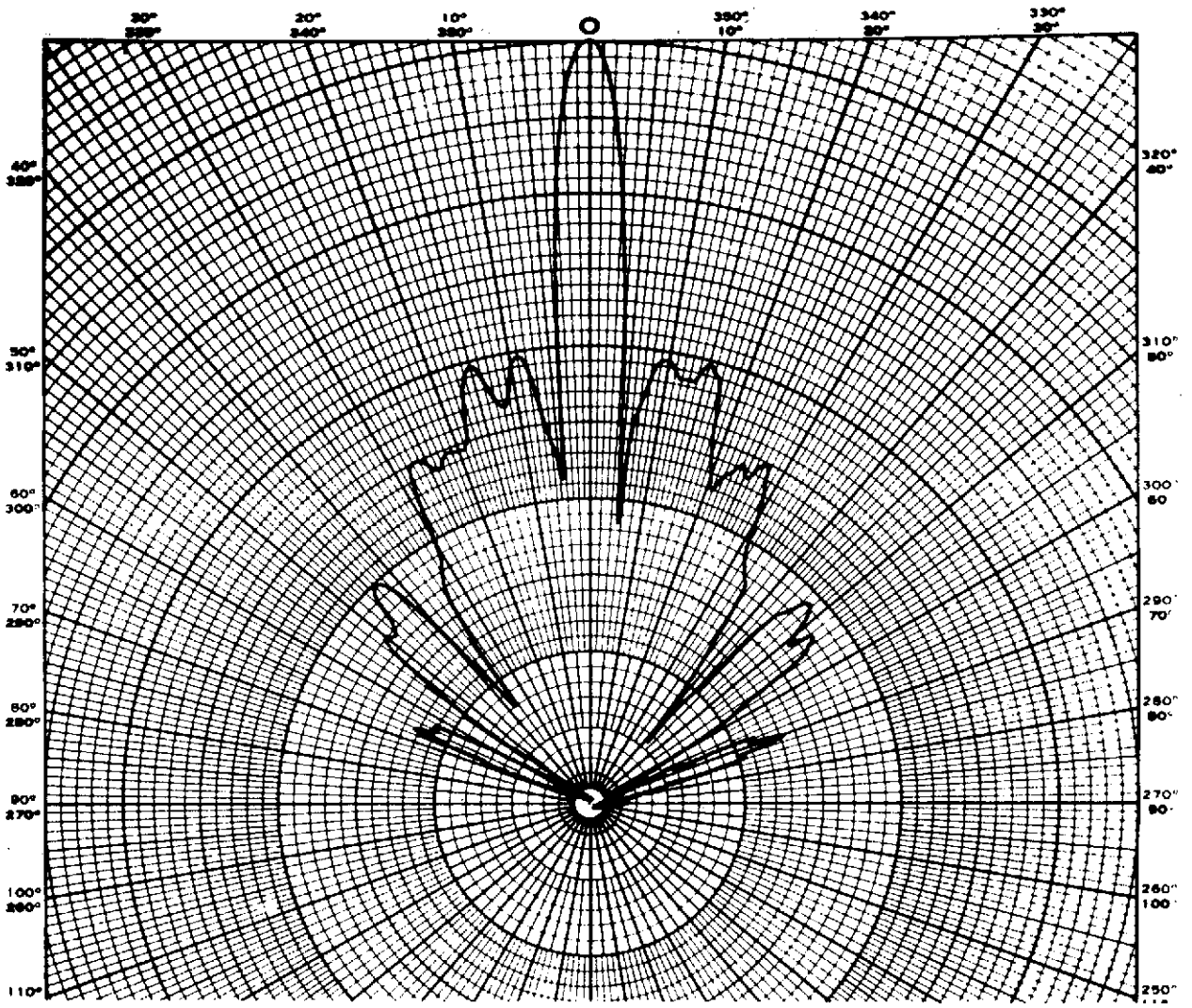

TRANSMIT ANTENNA
FREQUENCY = 8 GHz
AZIMUTH PATTERN

C1

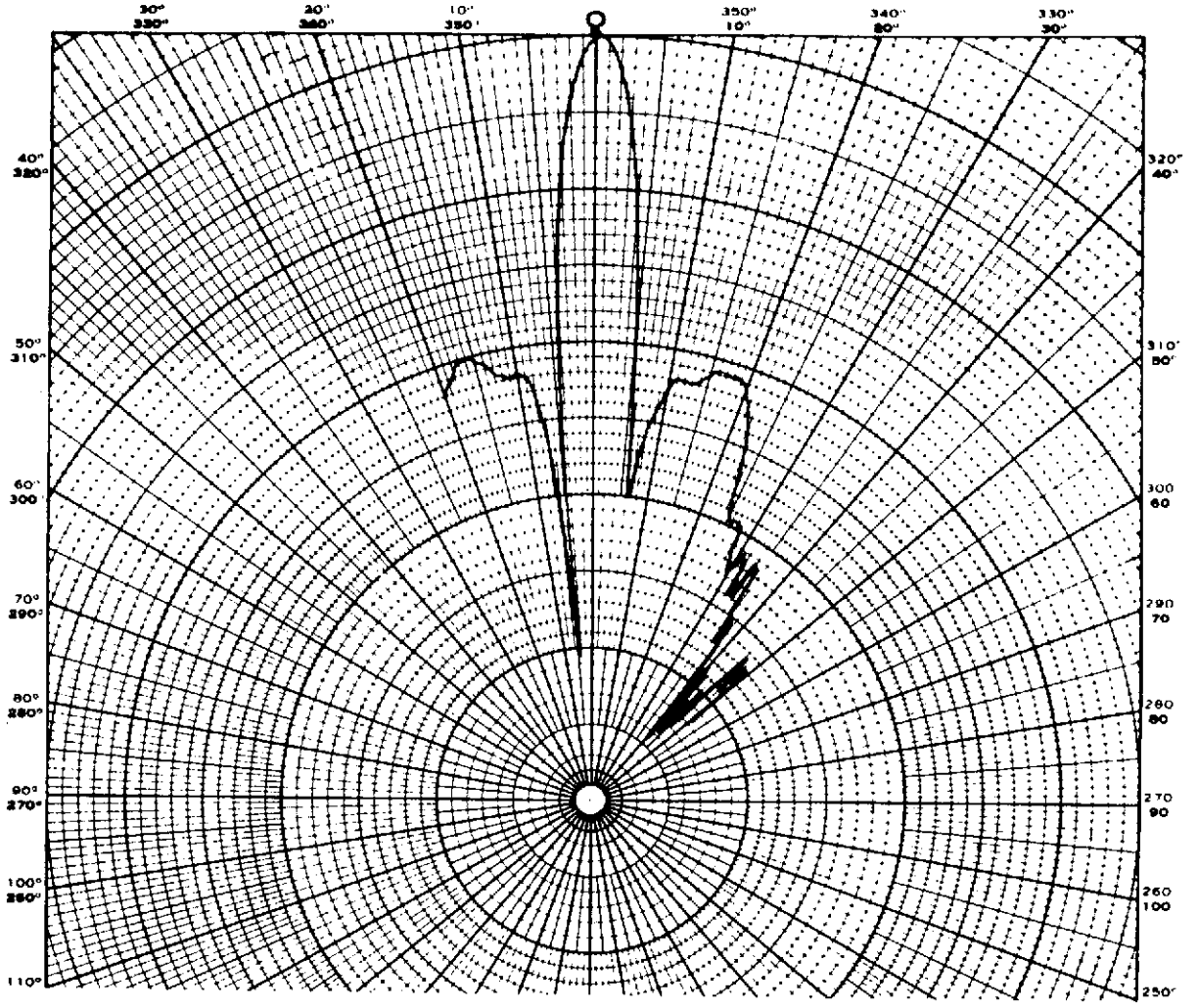

TRANSMIT ANTENNA
FREQUENCY = 8 GHz
ELEVATION PATTERN

C2

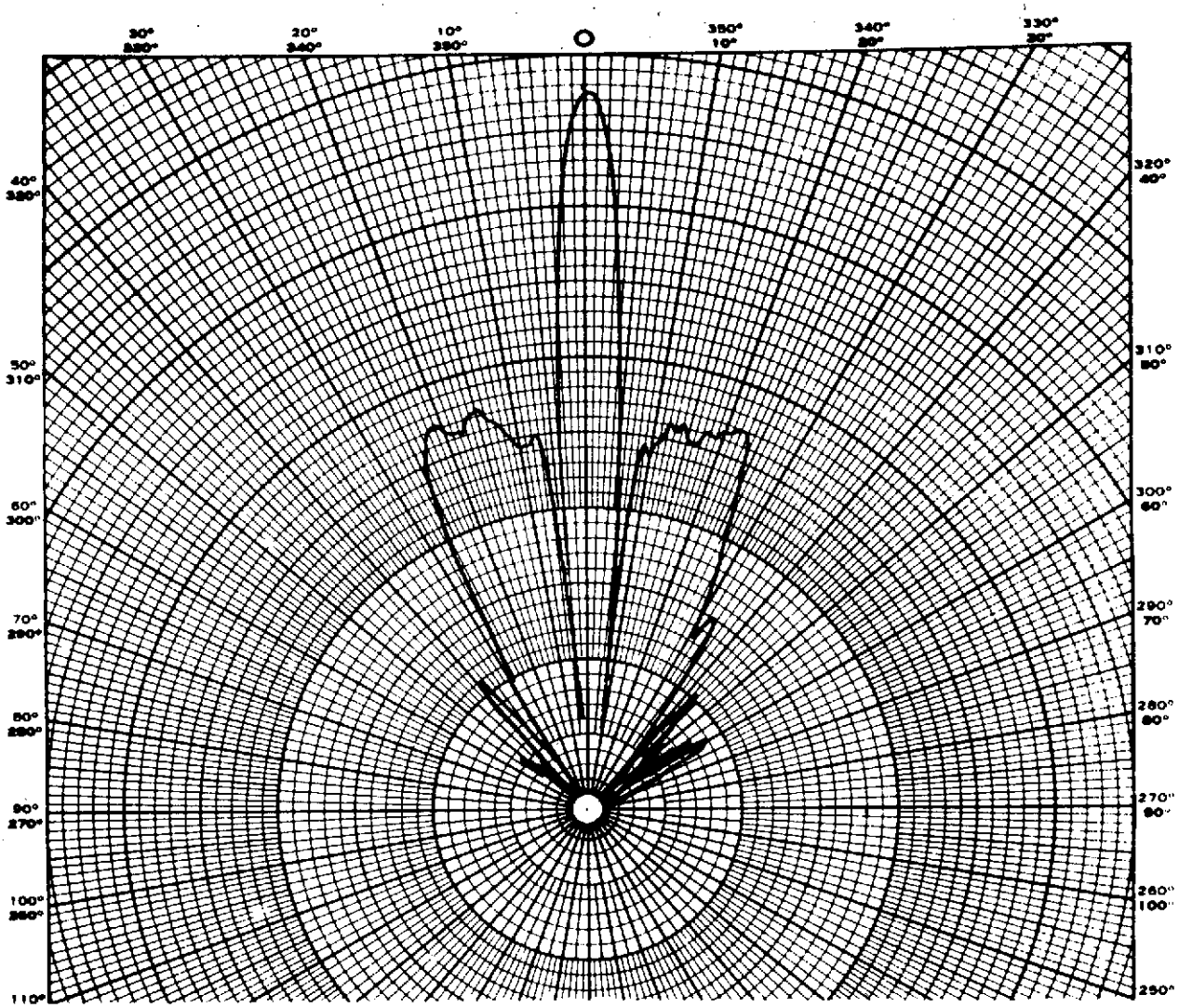

TRANSMIT ANTENNA
FREQUENCY = 10 GHz
AZIMUTH PATTERN

C3

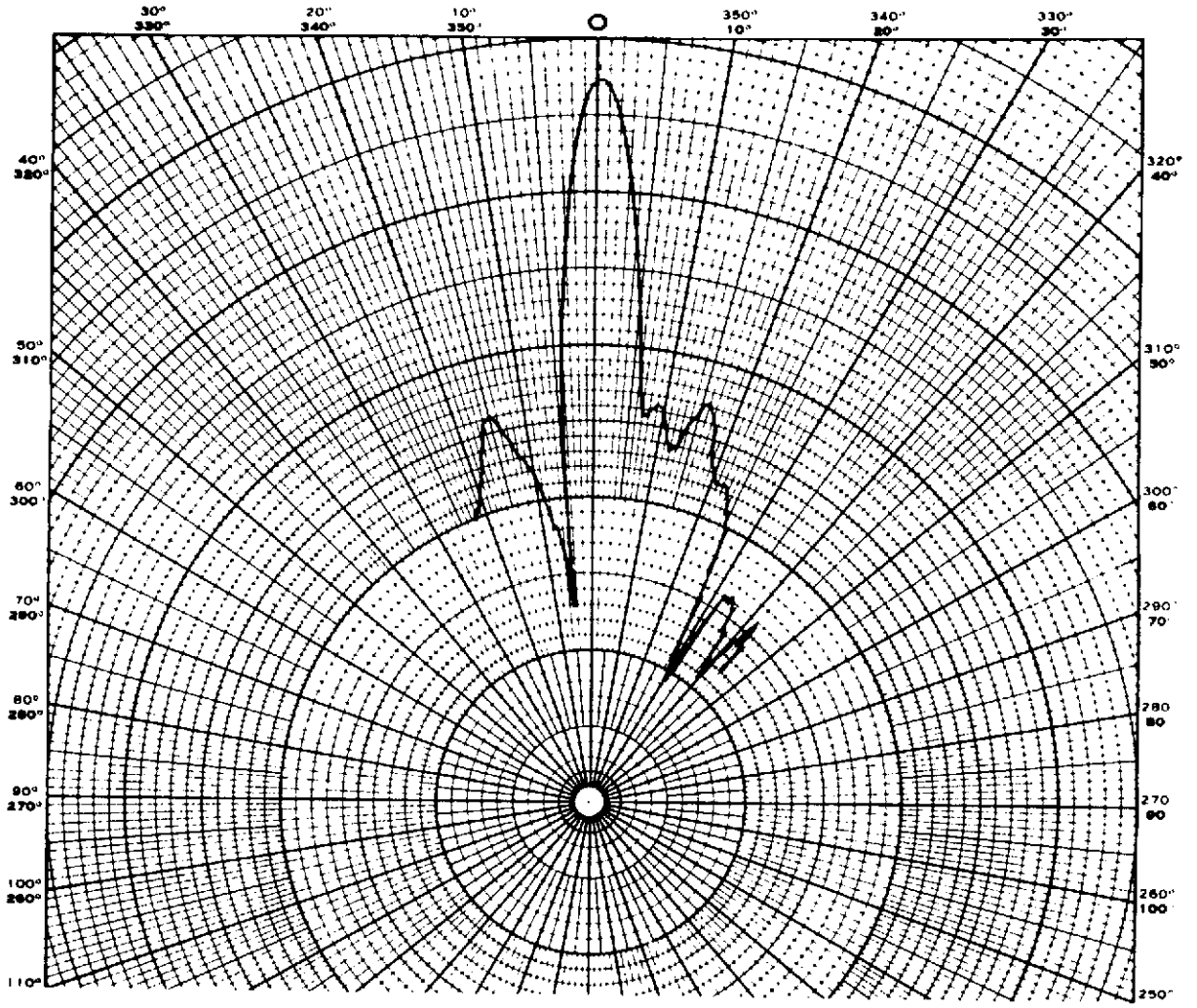

TRANSMIT ANTENNA
FREQUENCY = 10 GHz
ELEVATION PATTERN

C4

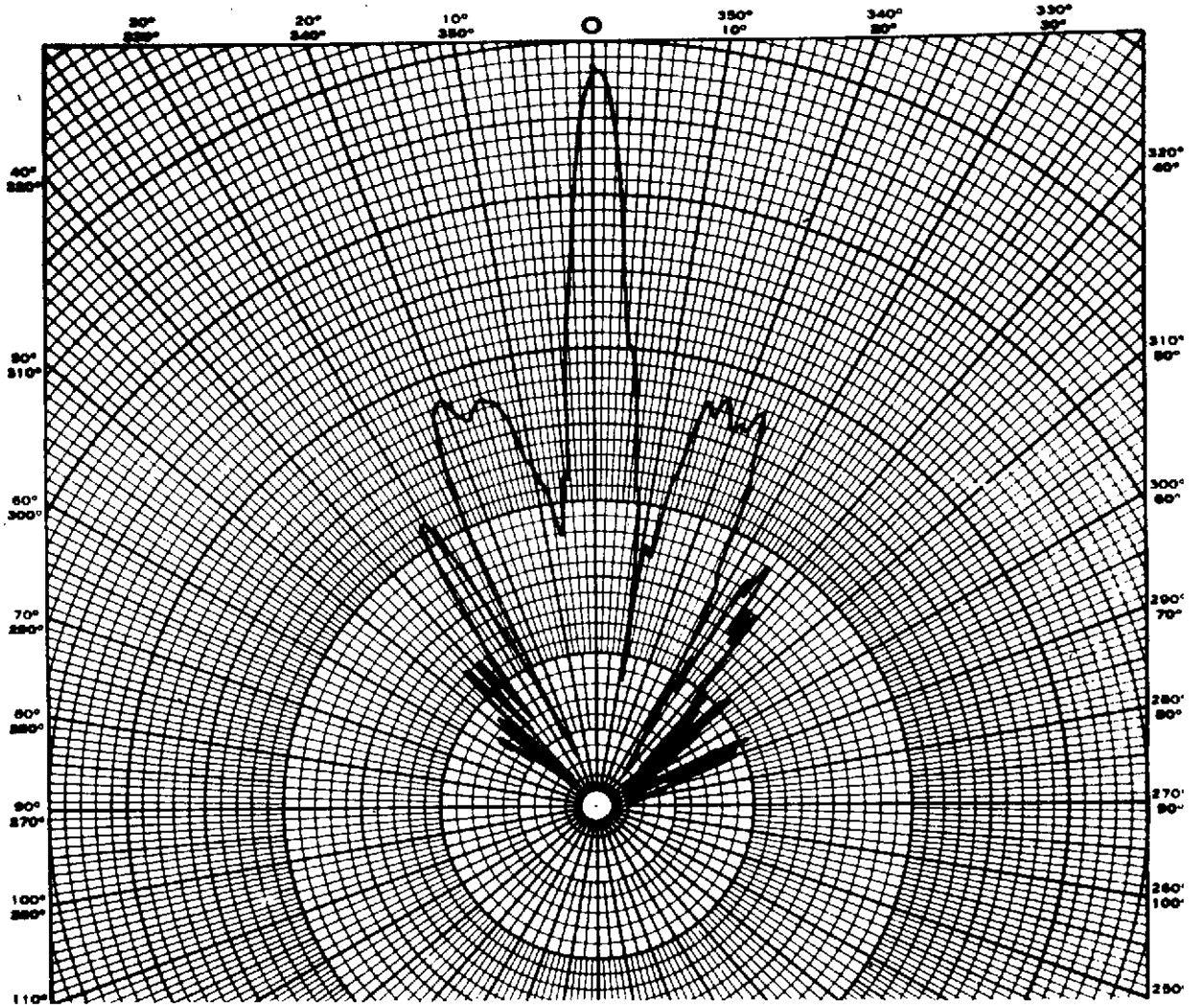

TRANSMIT ANTENNA
FREQUENCY = 12 GHz
AZIMUTH PATTERN

C5

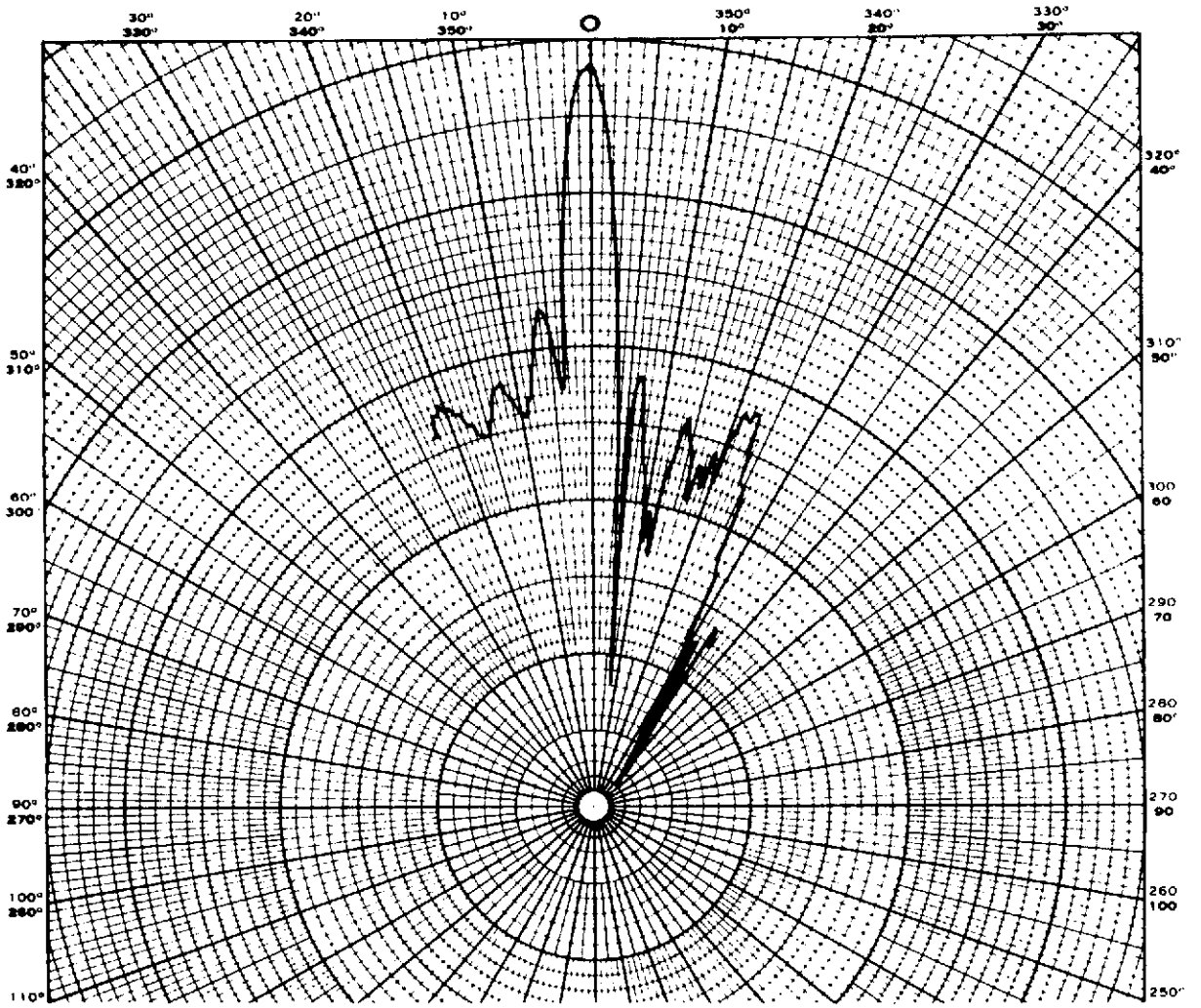

TRANSMIT ANTENNA
FREQUENCY = 12 GHz
ELEVATION PATTERN

C6

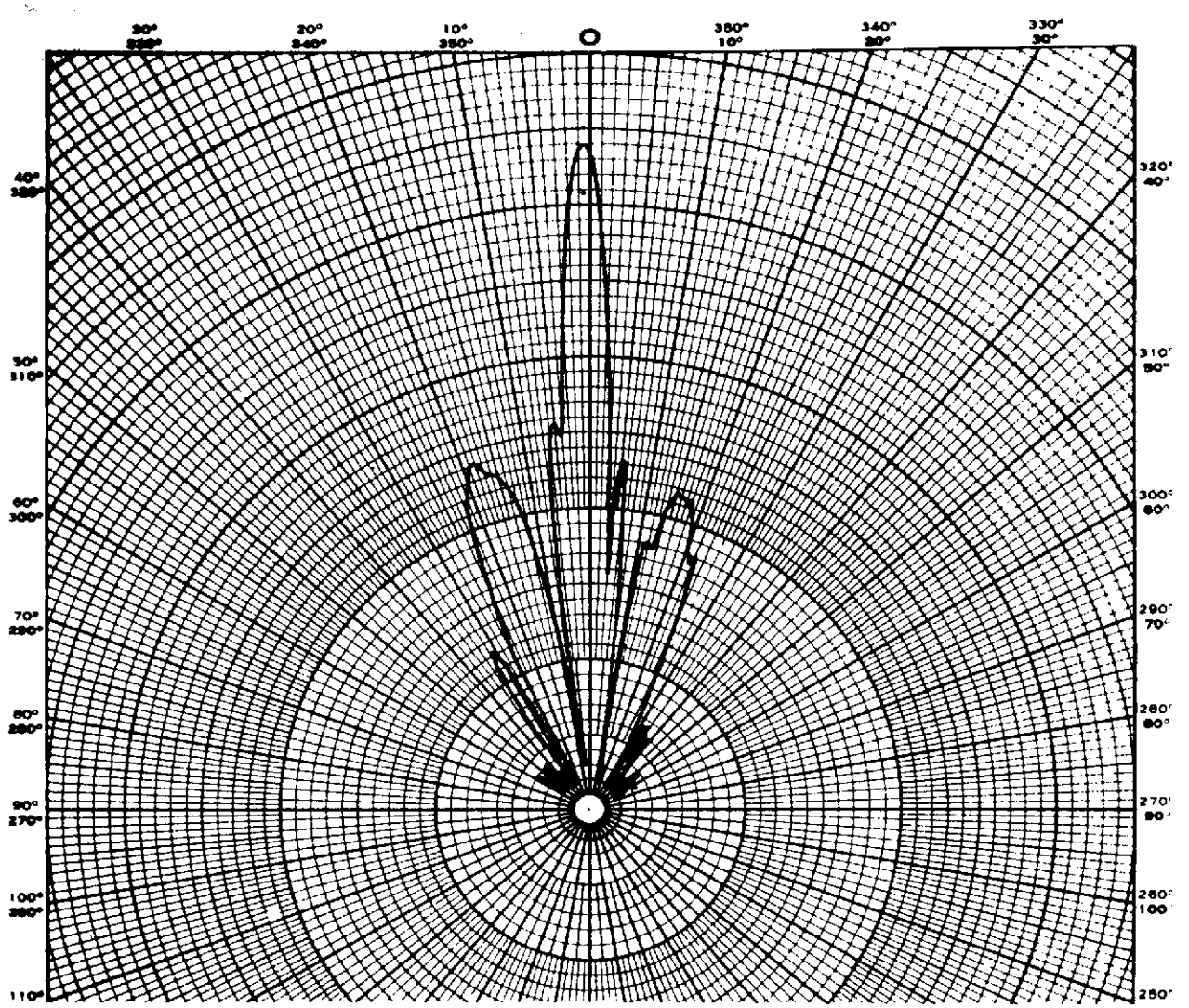

TRANSMIT ANTENNA
FREQUENCY = 14 GHz
AZIMUTH PATTERN

C7

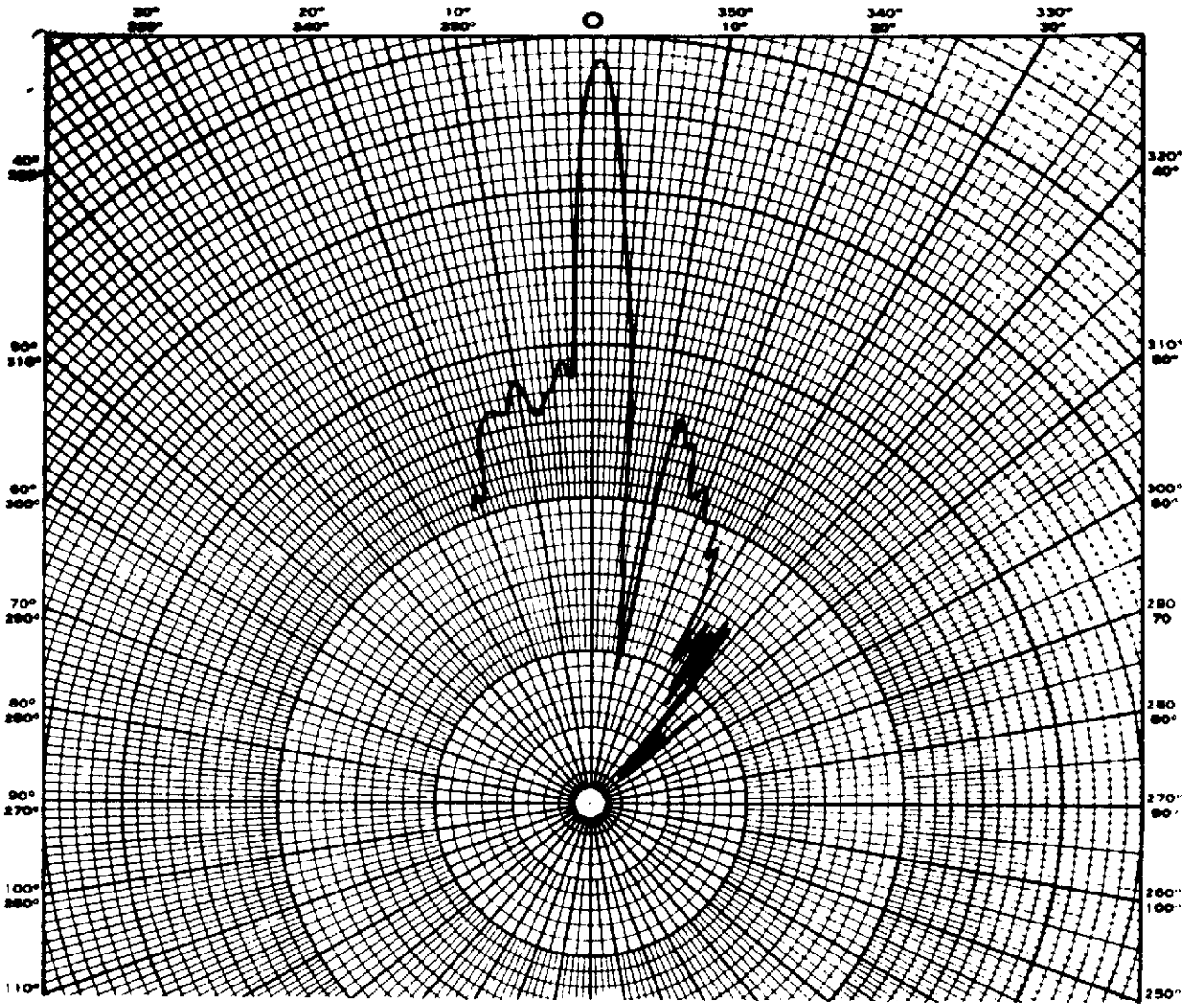

TRANSMIT ANTENNA
FREQUENCY = 14 GHz
ELEVATION PATTERN

C8

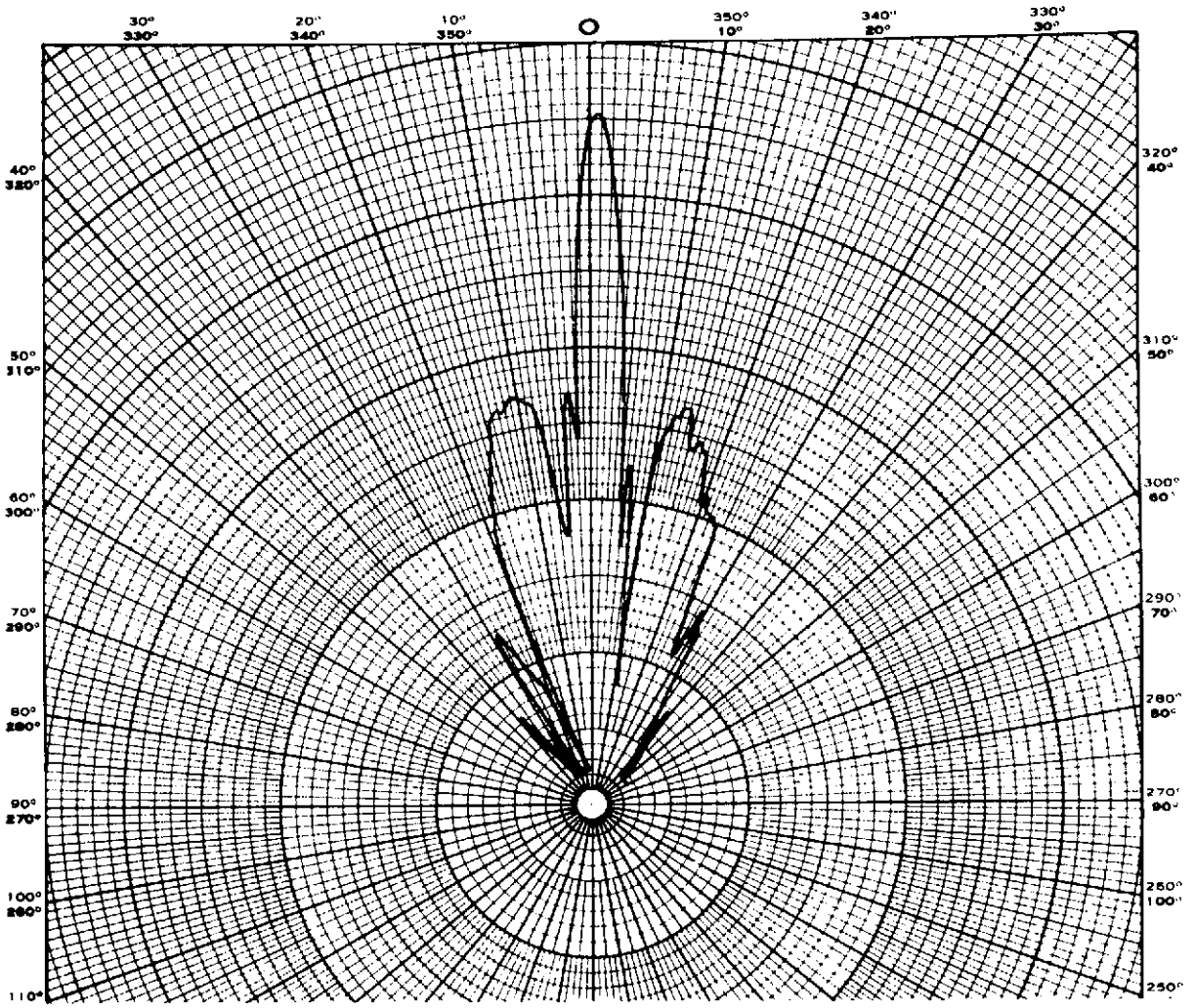

TRANSMIT ANTENNA
FREQUENCY = 16 GHz
AZIMUTH PATTERN

C9

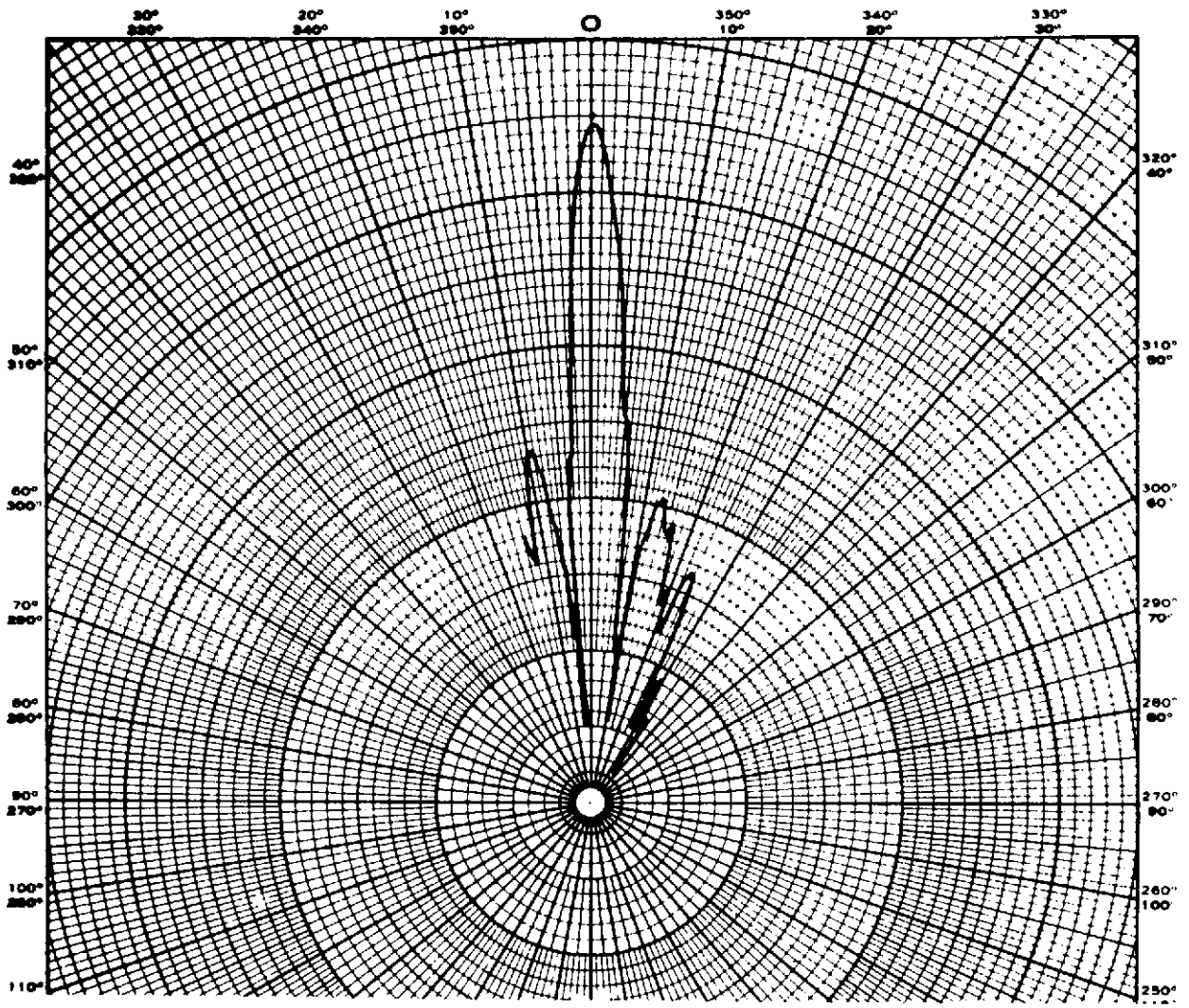

TRANSMIT ANTENNA
FREQUENCY = 16 GHz
ELEVATION PATTERN

C10

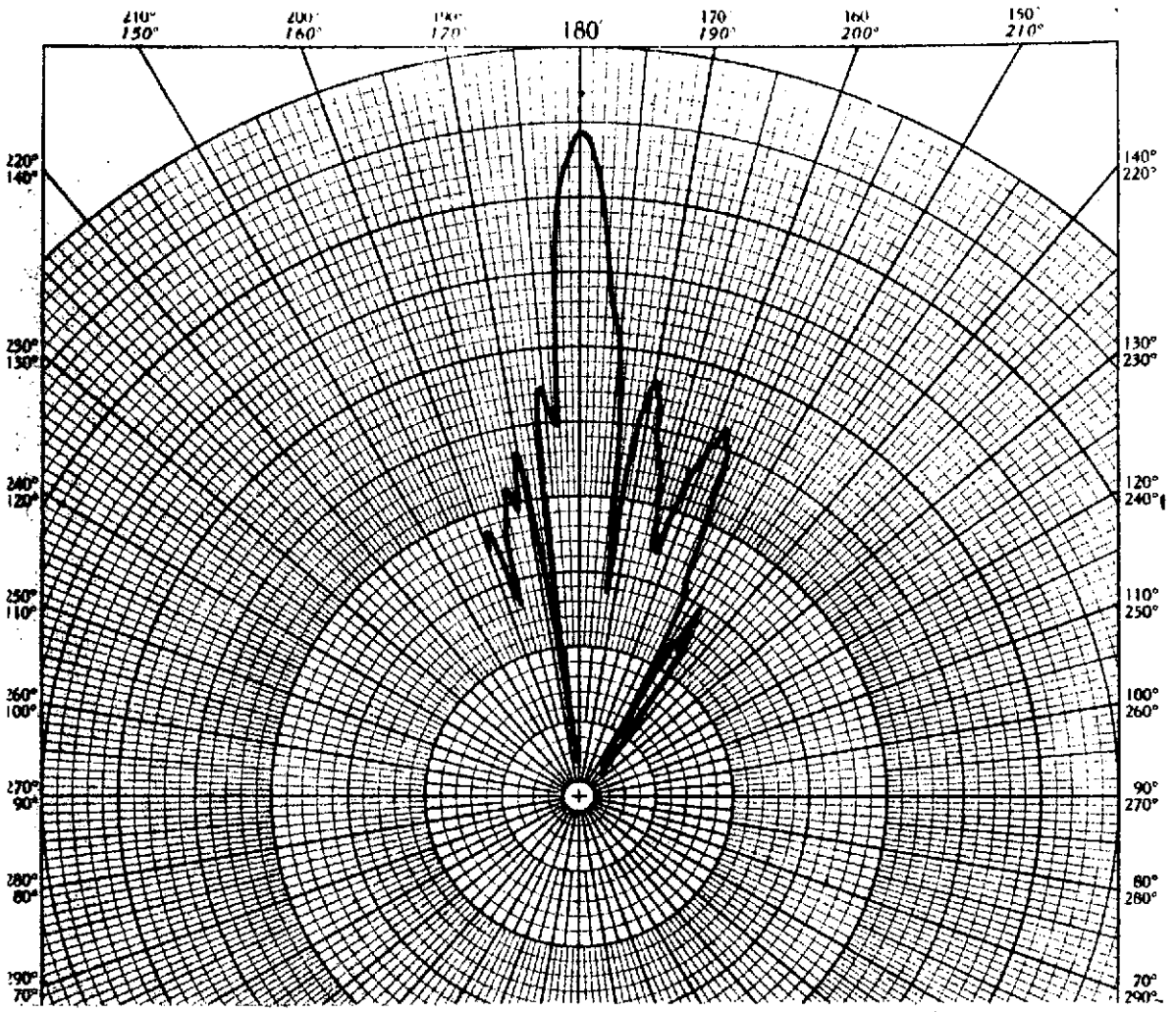

TRANSMIT ANTENNA
FREQUENCY = 18 GHz
ELEVATION PATTERN

C11

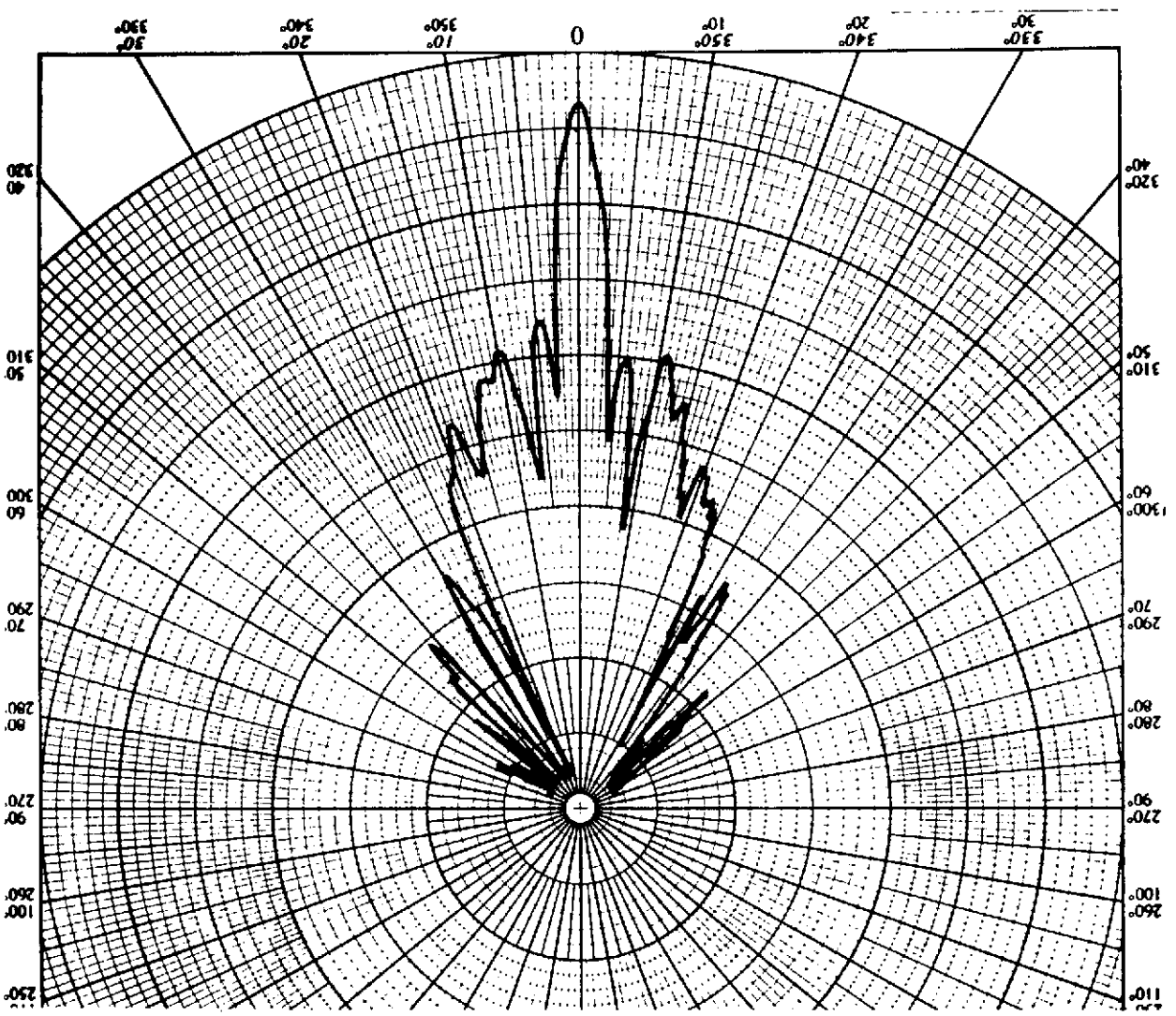

TRANSMIT ANTENNA
FREQUENCY = 18 GHz
AZIMUTH PATTERN

C12

APPENDIX D

RECEIVE ANTENNA PRINCIPAL PLANE POWER PATTERNS

4 div. = 3 dB

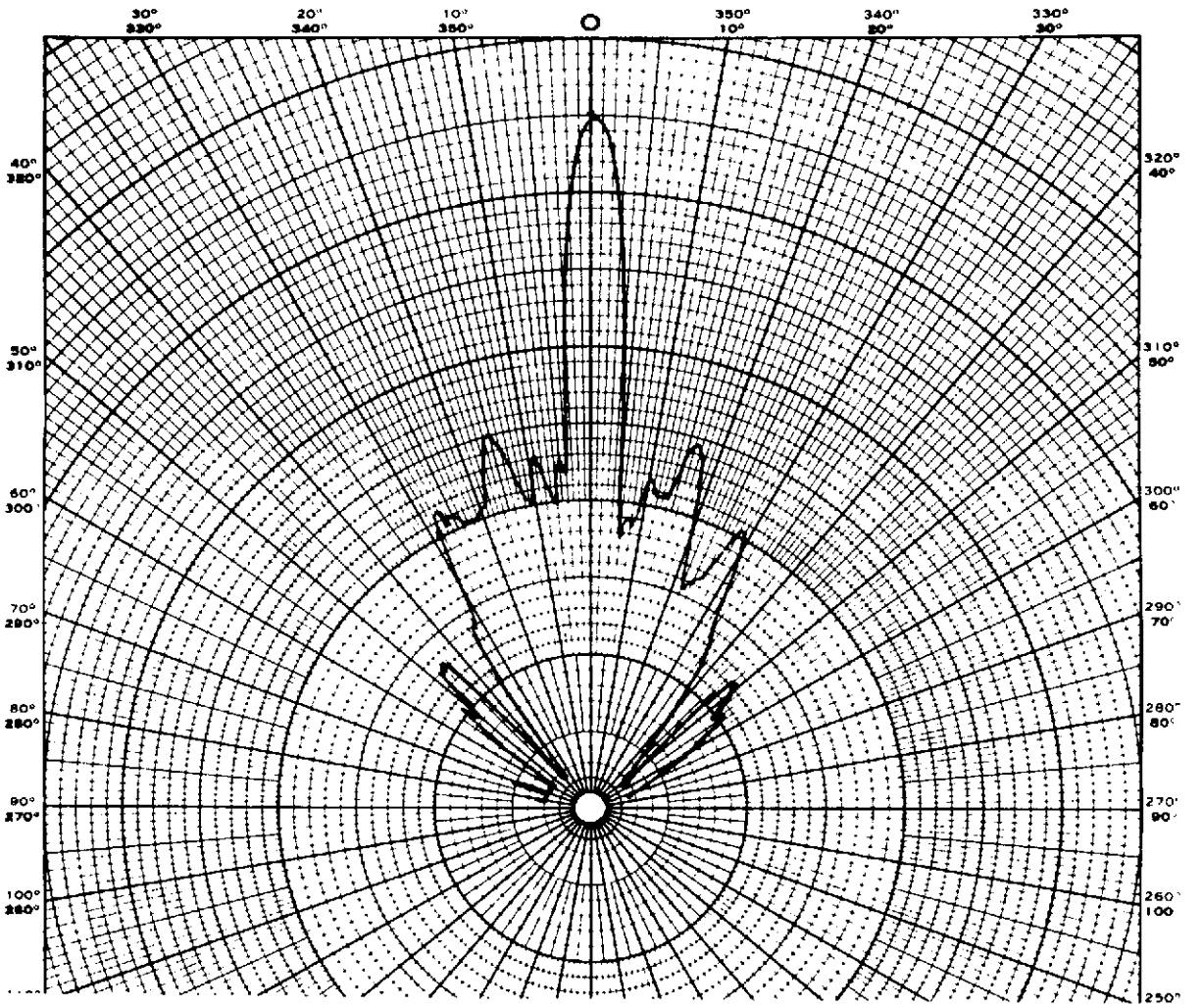

RECEIVE ANTENNA
FREQUENCY = 8 GHz
AZIMUTH PATTERN

D1

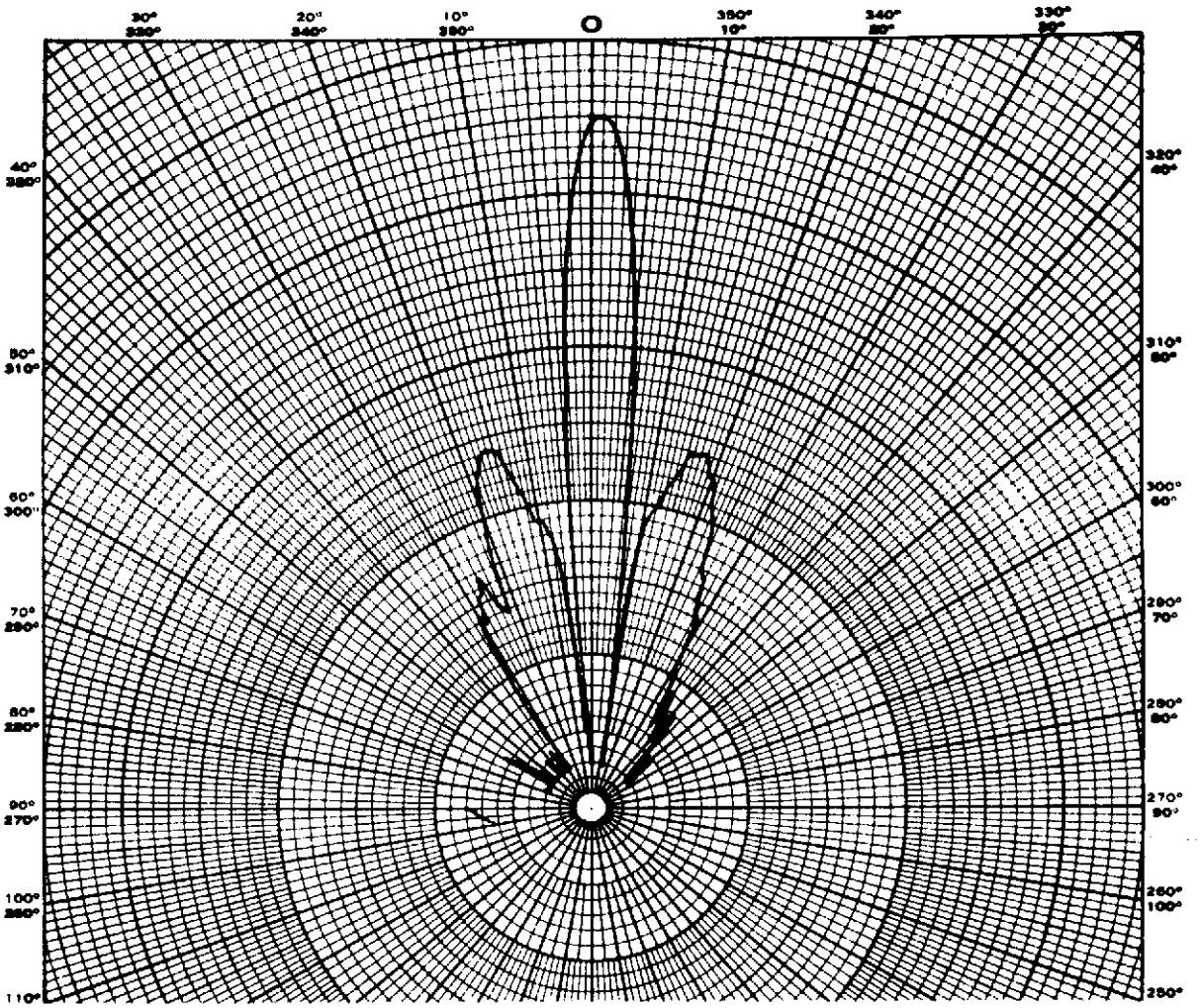

RECEIVE ANTENNA
FREQUENCY = 8 GHz
ELEVATION PATTERN

D2

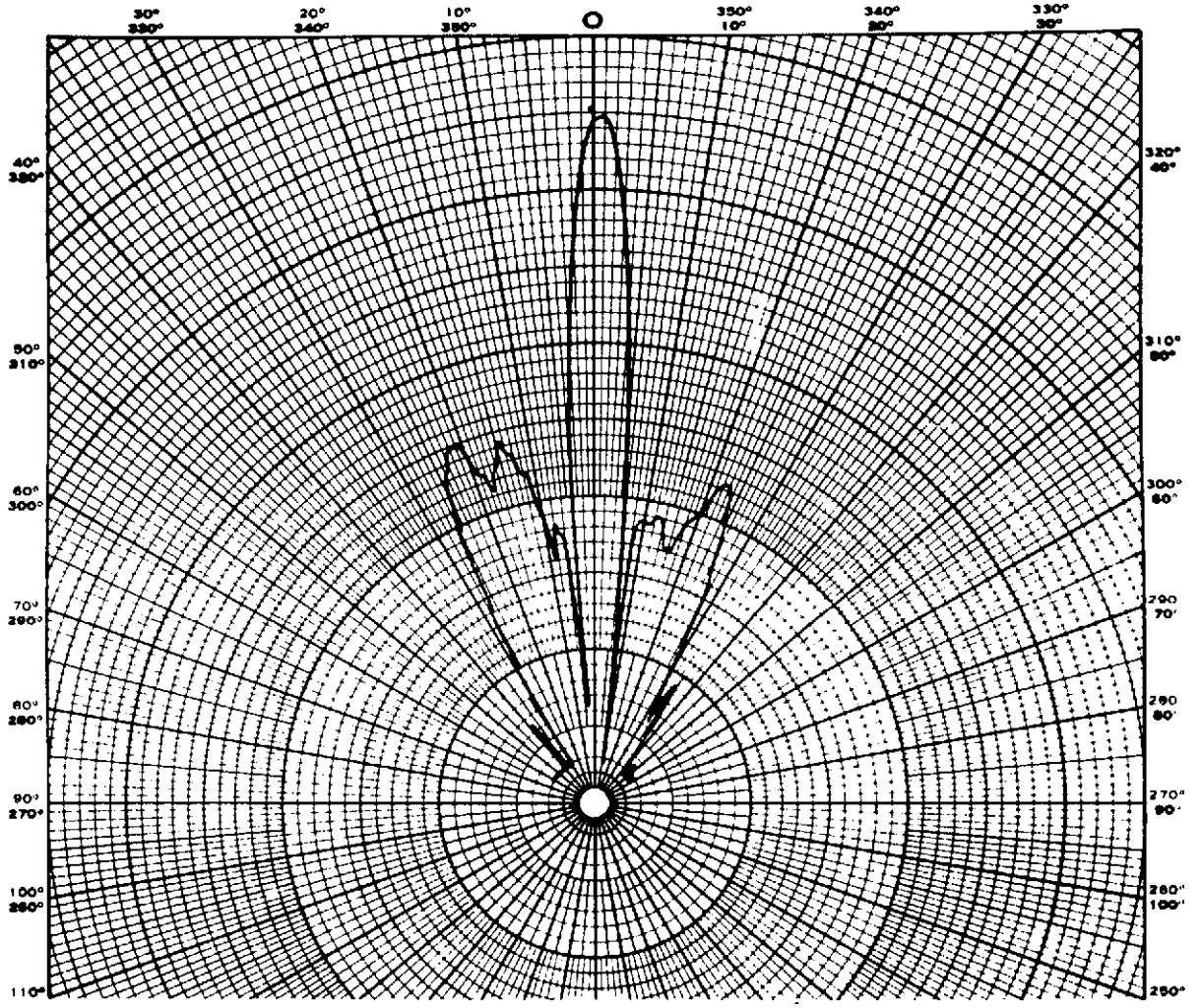

RECEIVE ANTENNA
FREQUENCY = 10 GHz
AZIMUTH PATTERN

D3

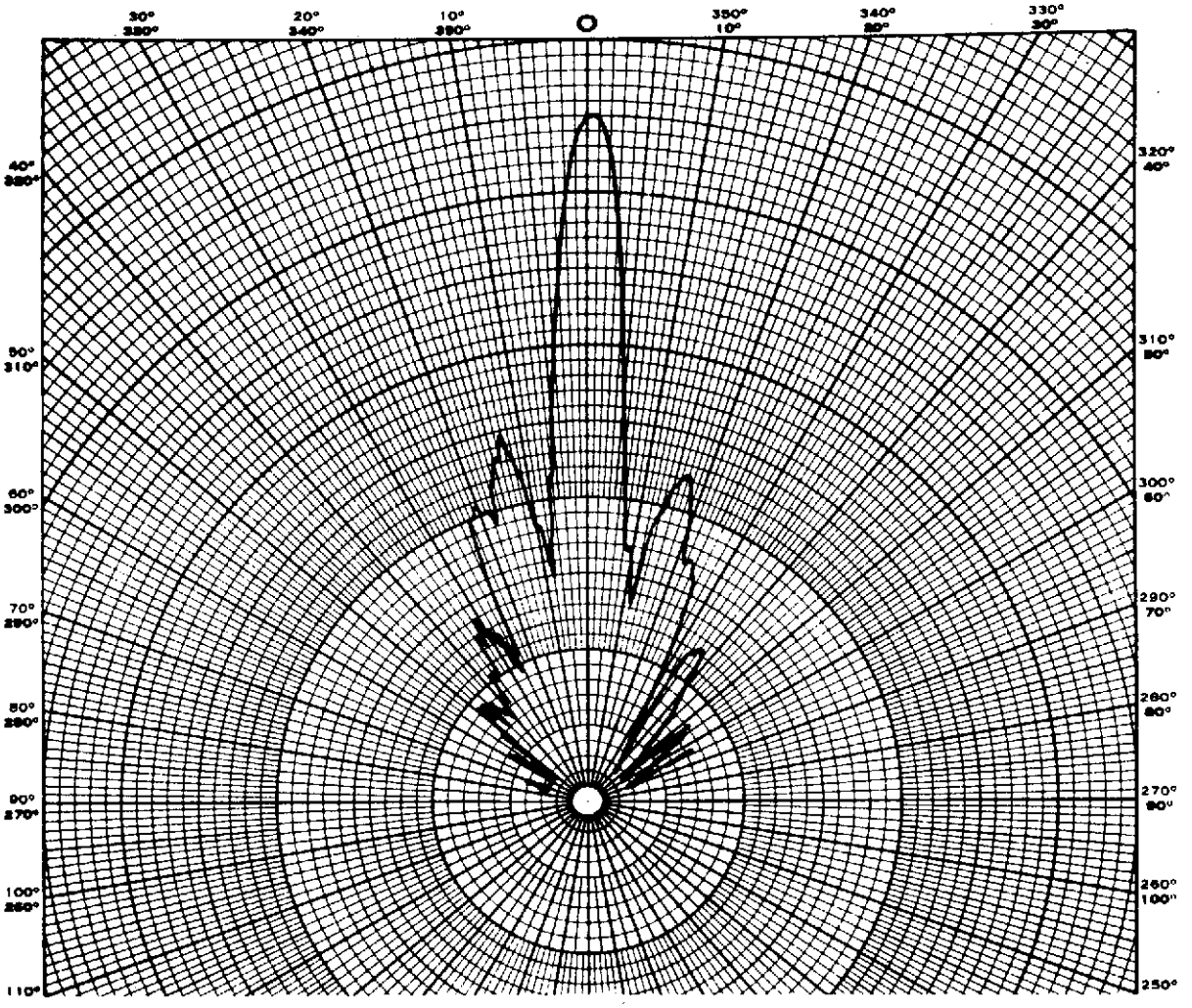

RECEIVE ANTENNA
FREQUENCY = 10 GHz
ELEVATION PATTERN

D4

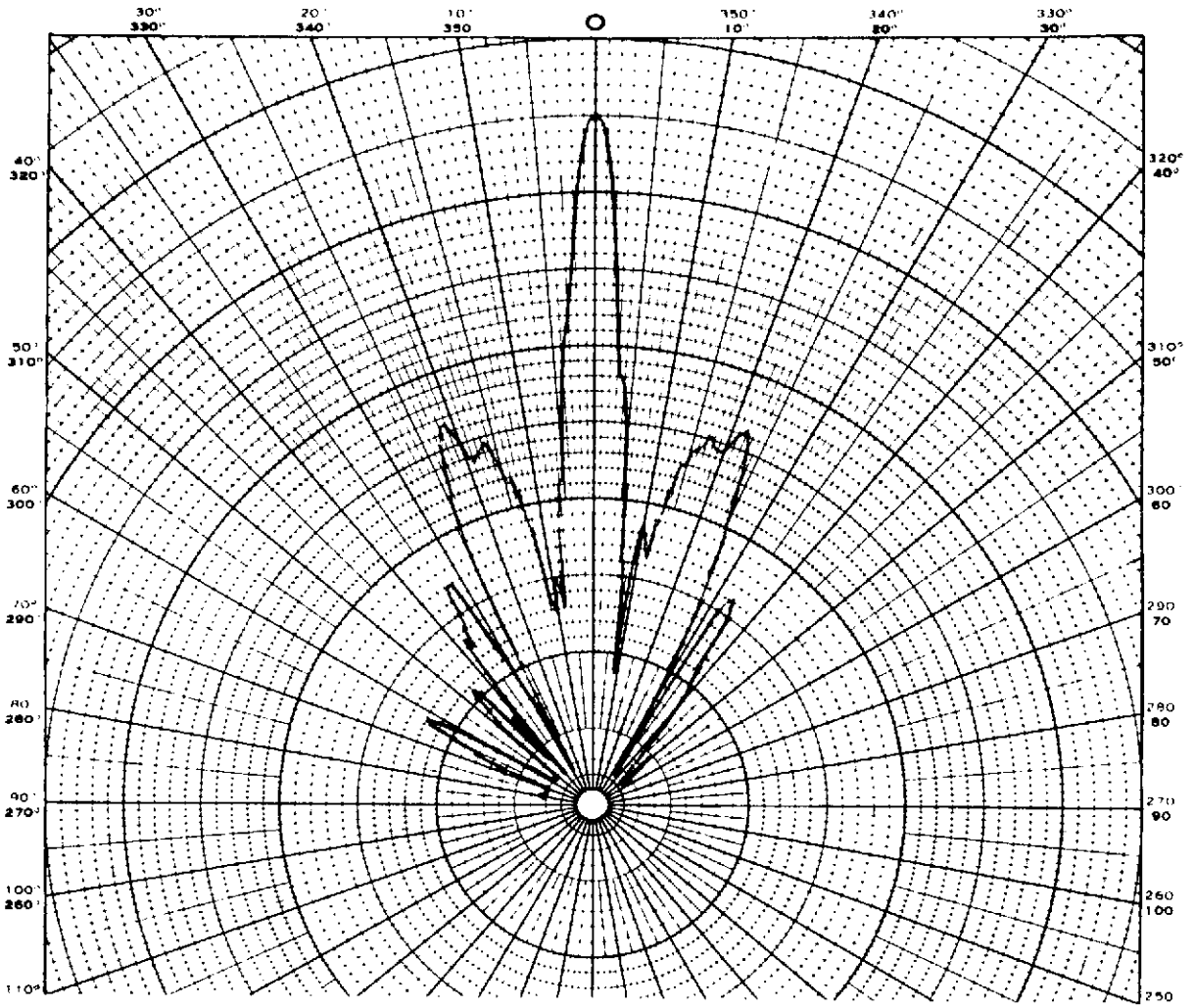

RECEIVE ANTENNA
FREQUENCY = 12 GHz
AZIMUTH PATTERN

D5

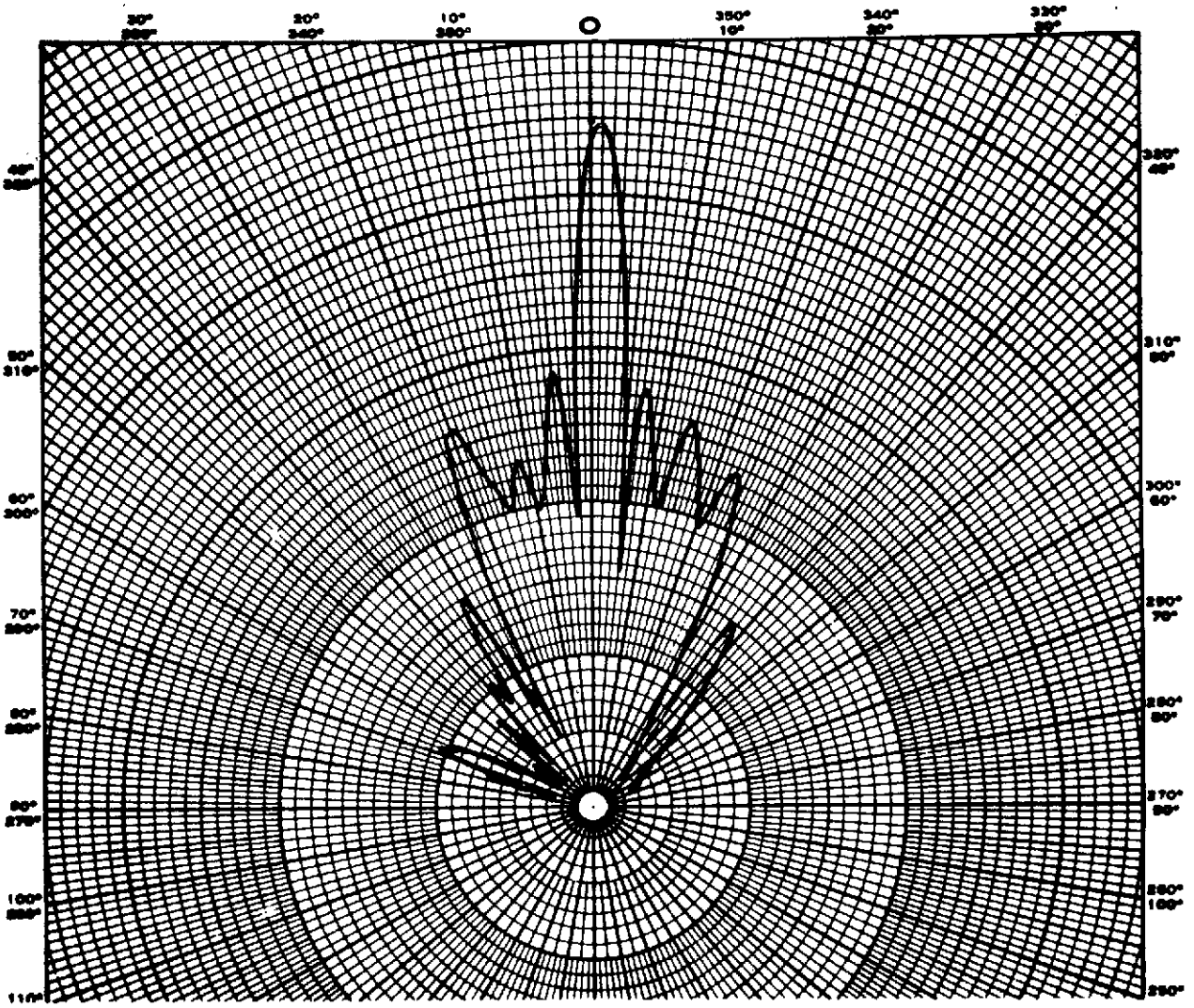

RECEIVE ANTENNA
FREQUENCY = 12 GHz
ELEVATION PATTERN

D6

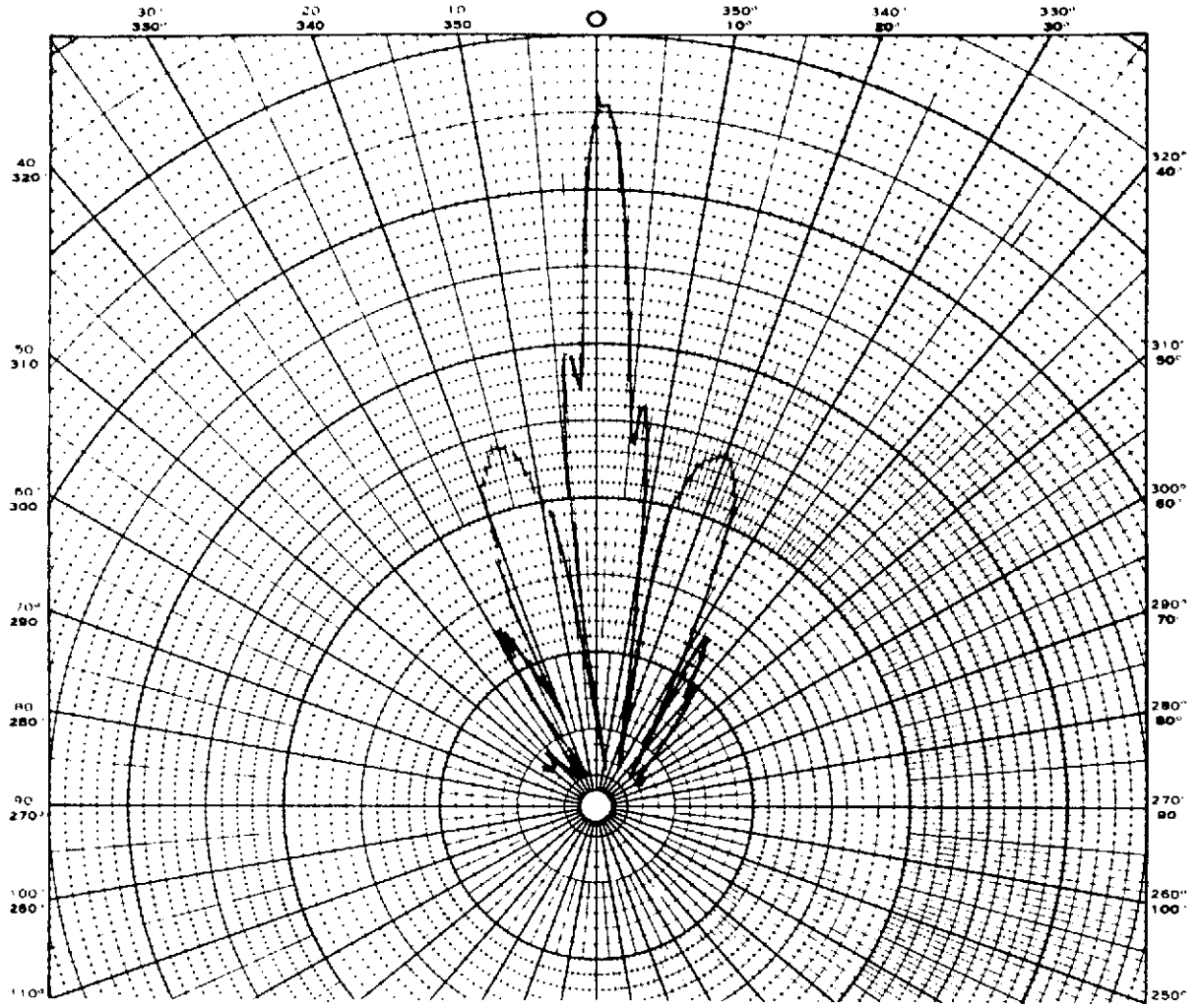

RECEIVE ANTENNA
FREQUENCY = 14 GHz
AZIMUTH PATTERN

D7

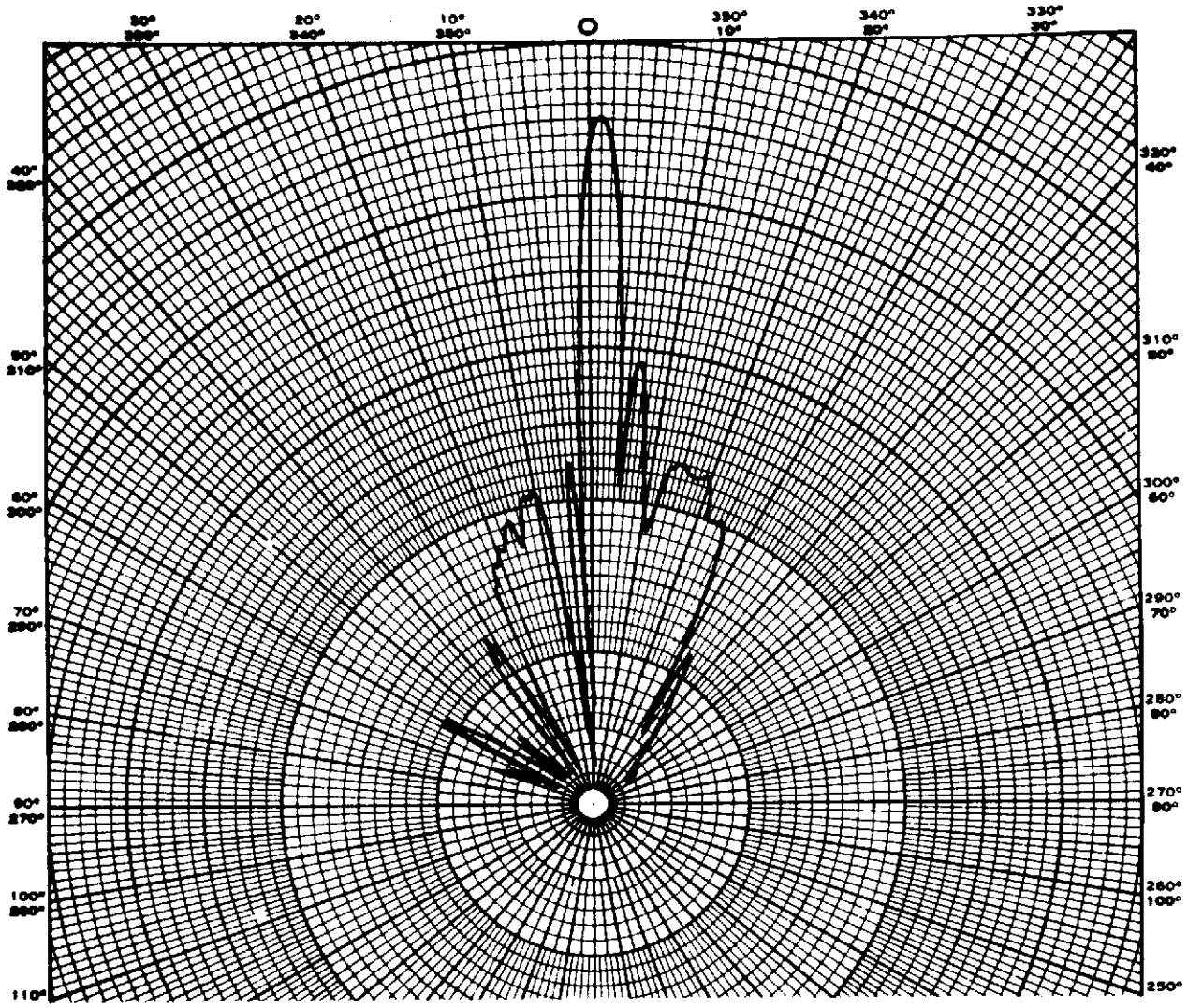

RECEIVE ANTENNA
FREQUENCY = 14 GHz
ELEVATION PATTERN

D8

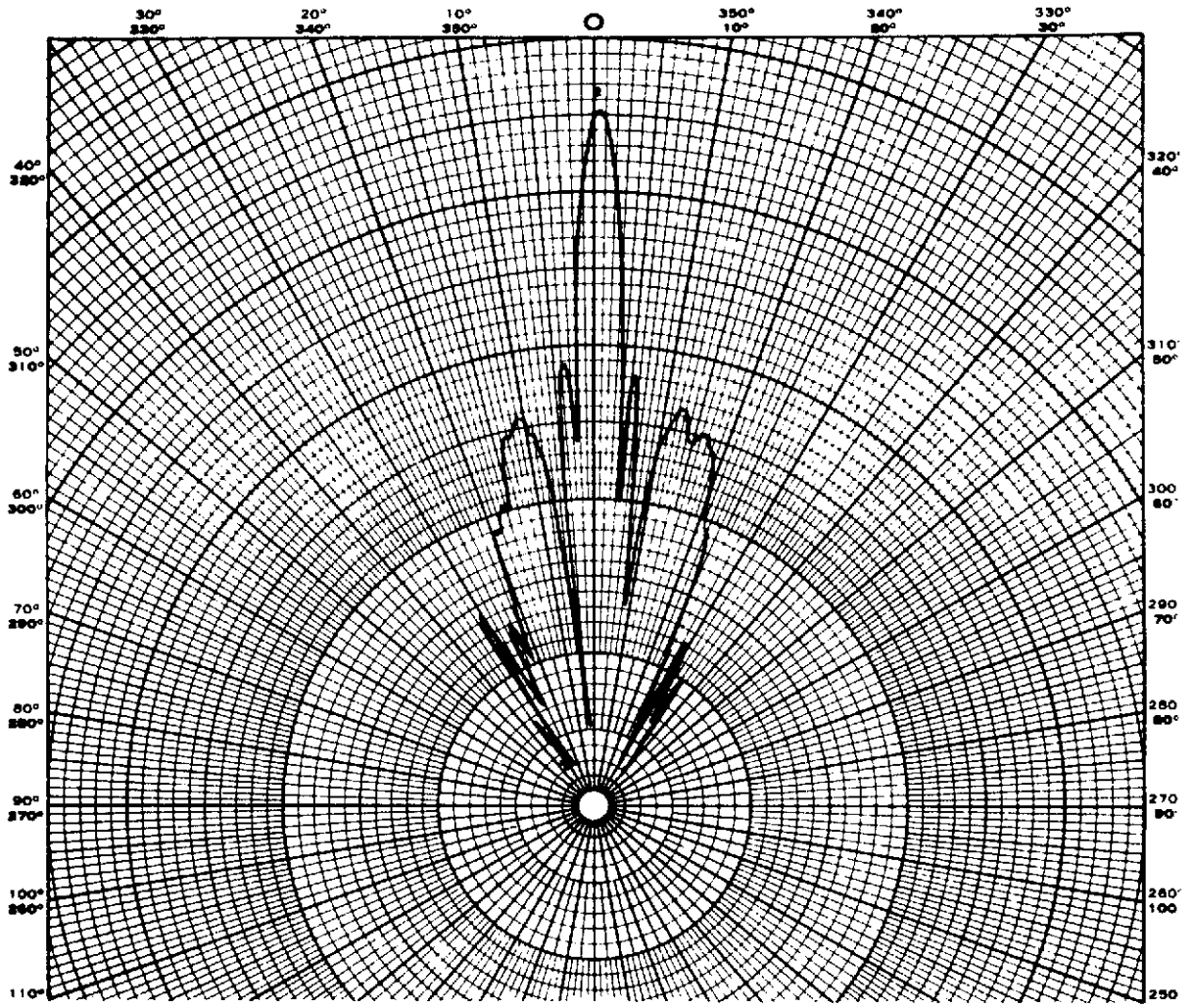

RECEIVE ANTENNA
FREQUENCY = 16 GHz
AZIMUTH PATTERN

D9

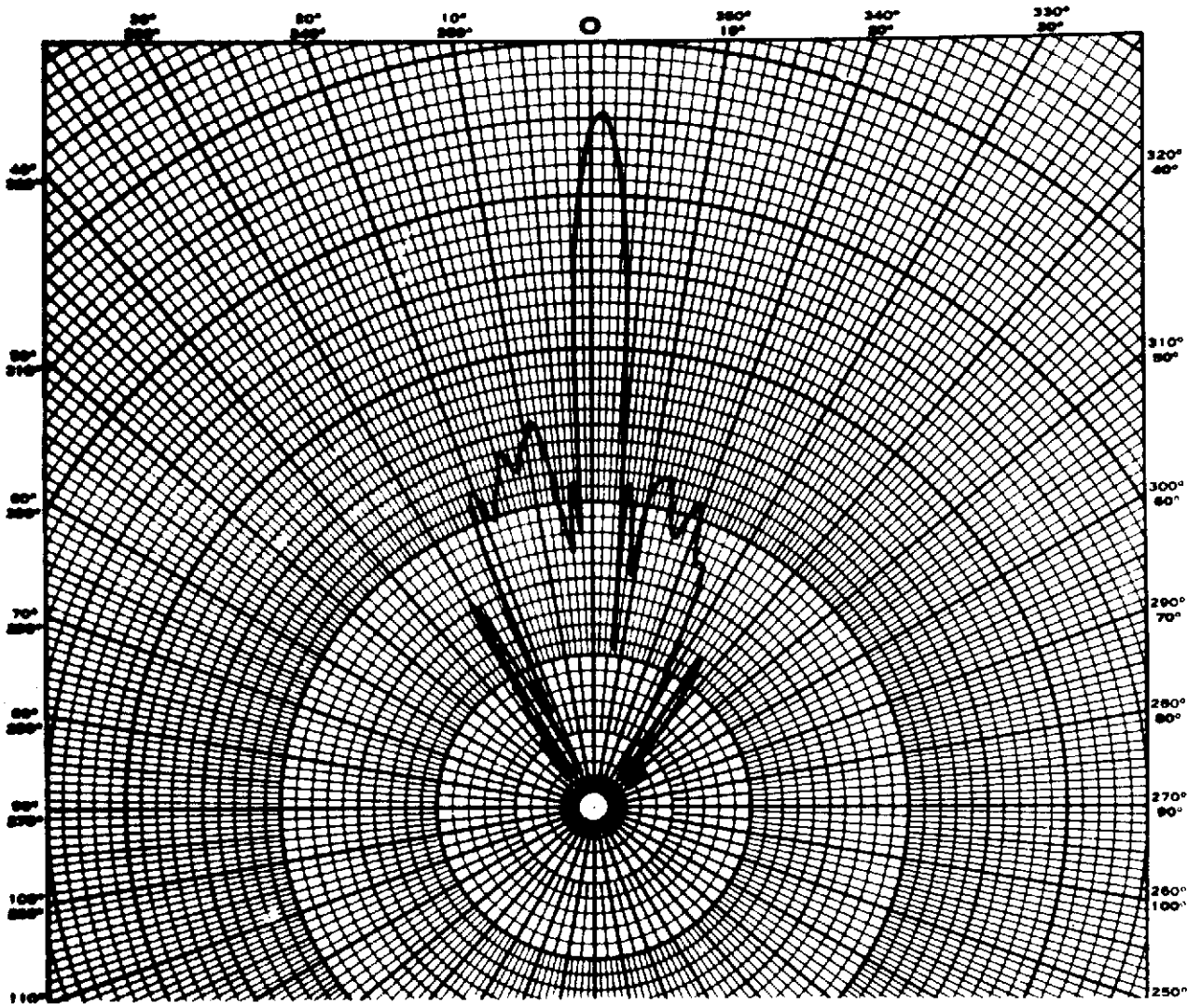

RECEIVE ANTENNA
FREQUENCY = 16 GHz
ELEVATION PATTERN

D10

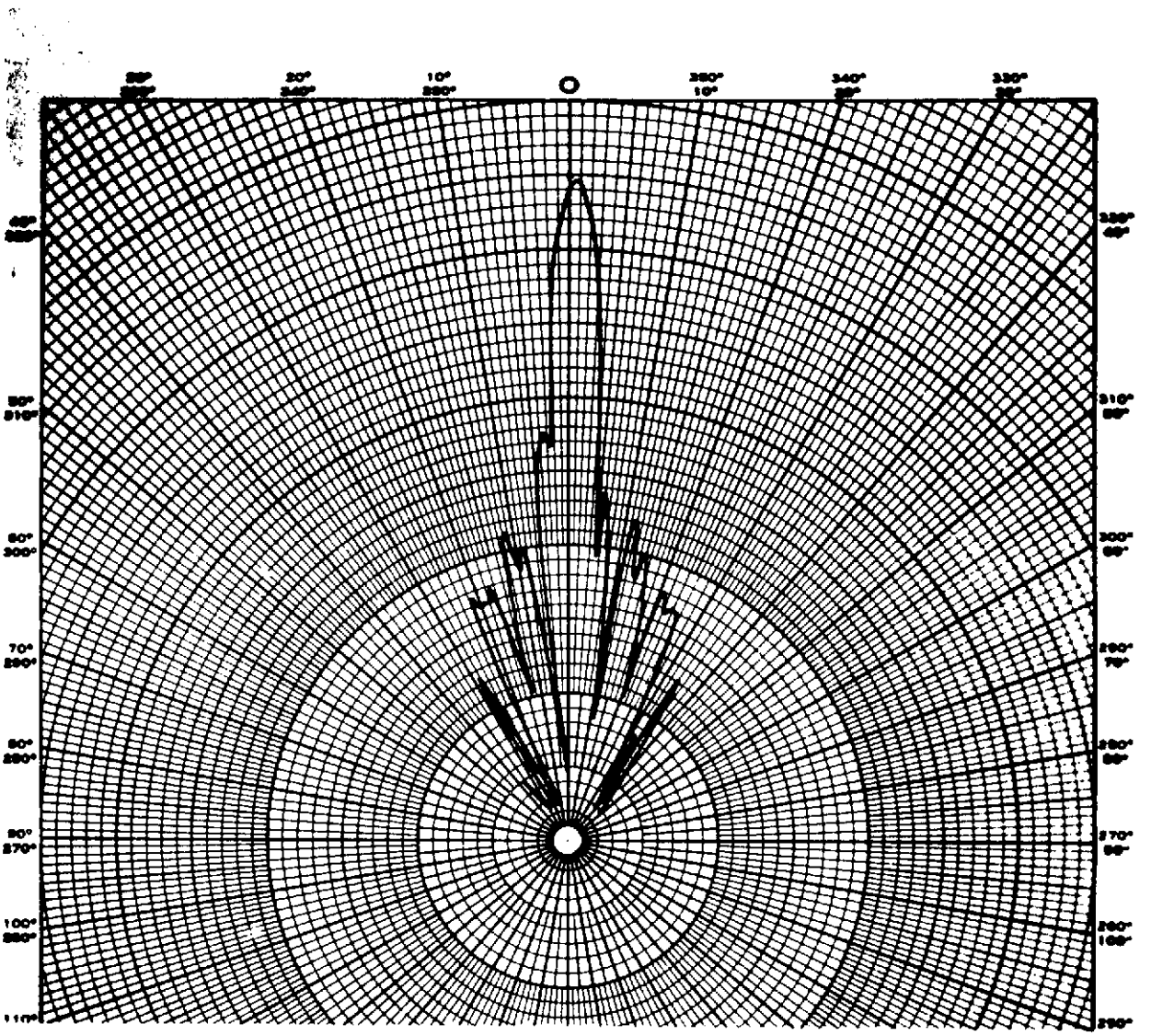

RECEIVE ANTENNA
FREQUENCY = 18 GHz
AZIMUTH PATTERN

D11

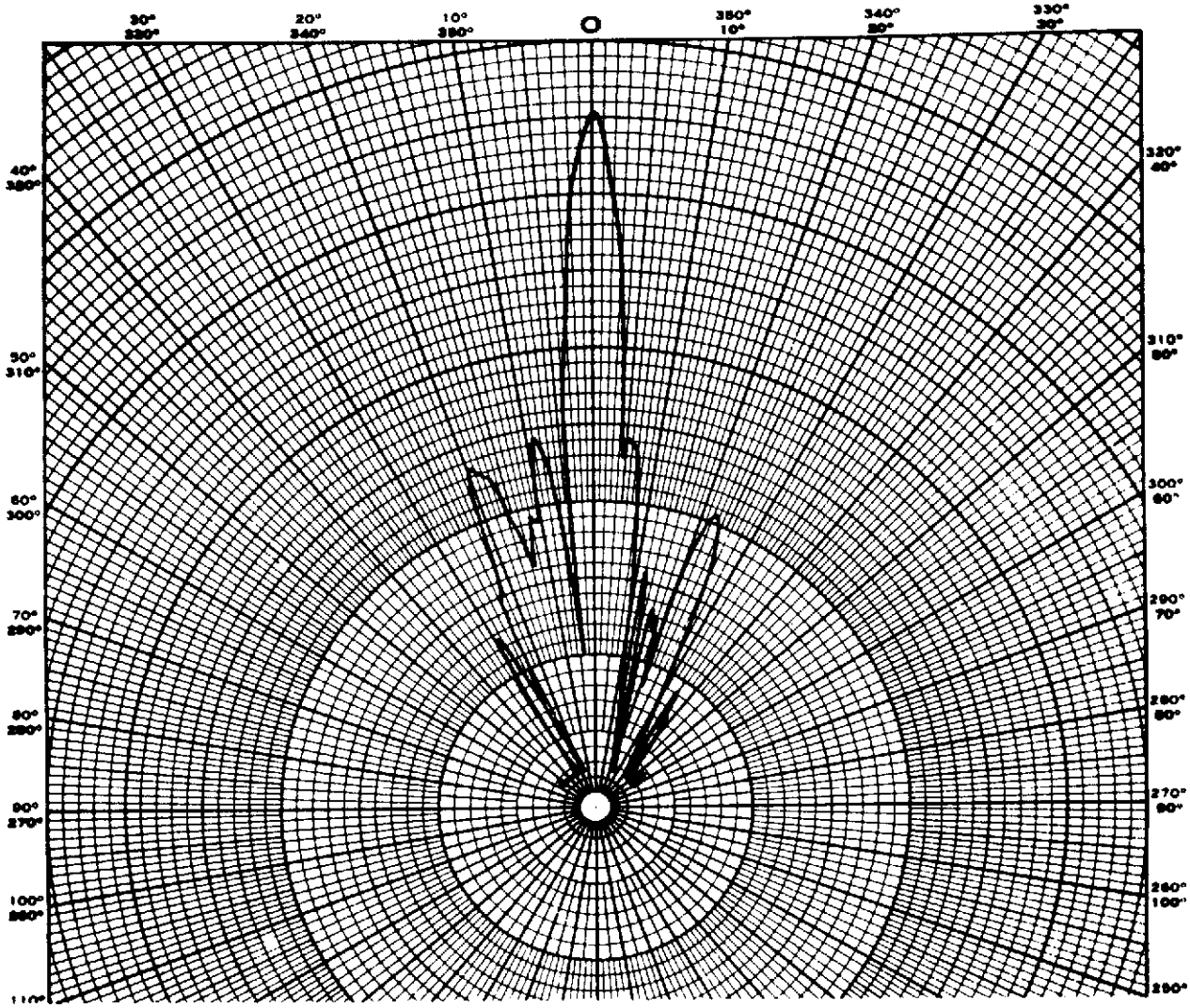

RECEIVE ANTENNA
FREQUENCY = 18 GHz
ELEVATION PATTERN

D12

APPENDIX E

DUAL PRINCIPAL PLANE POWER PATTERNS

4 div. = 3 dB

NOTE: Dark Pattern = Transmit Antenna
Gray Pattern = Receive Antenna

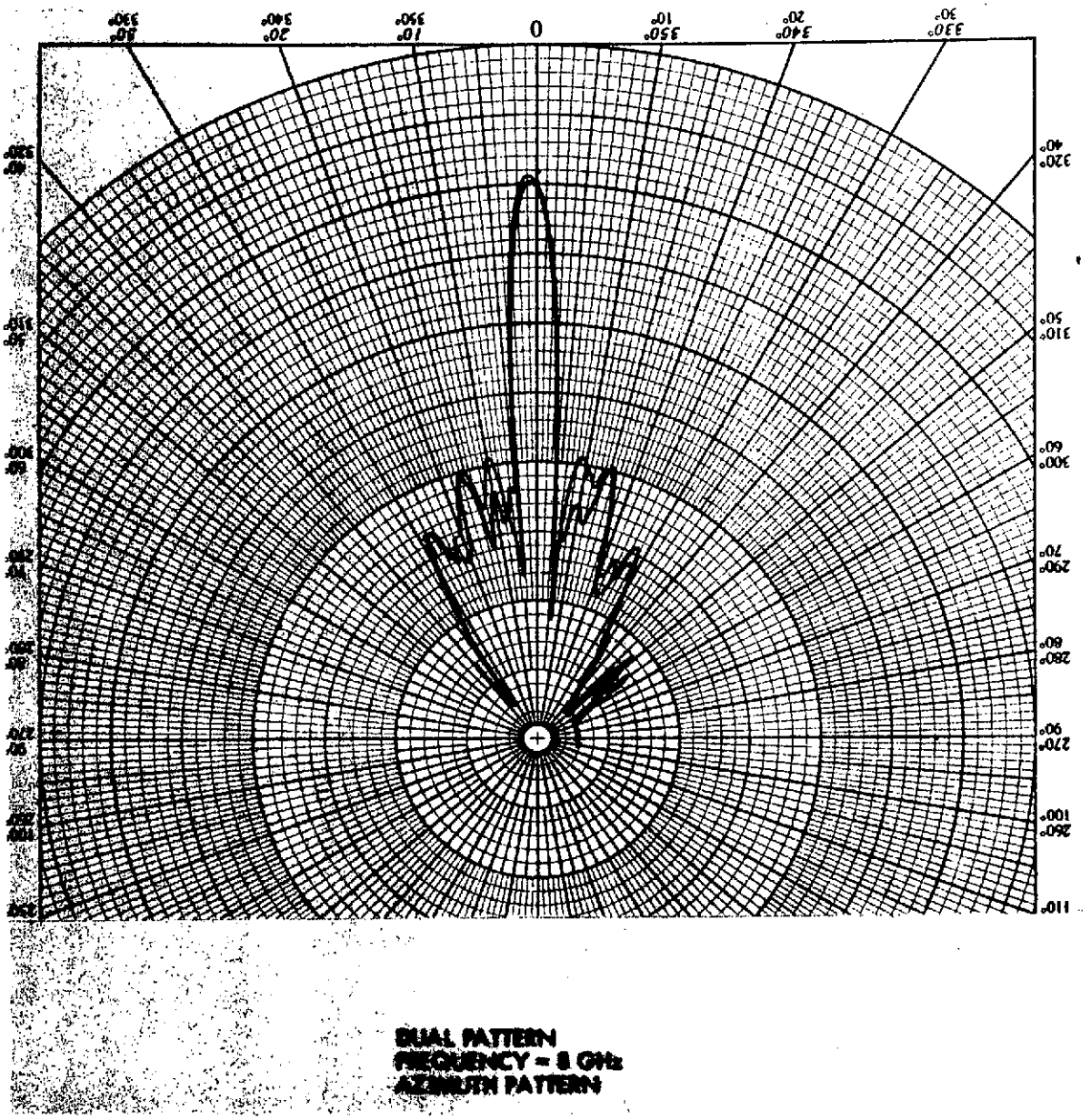

E1

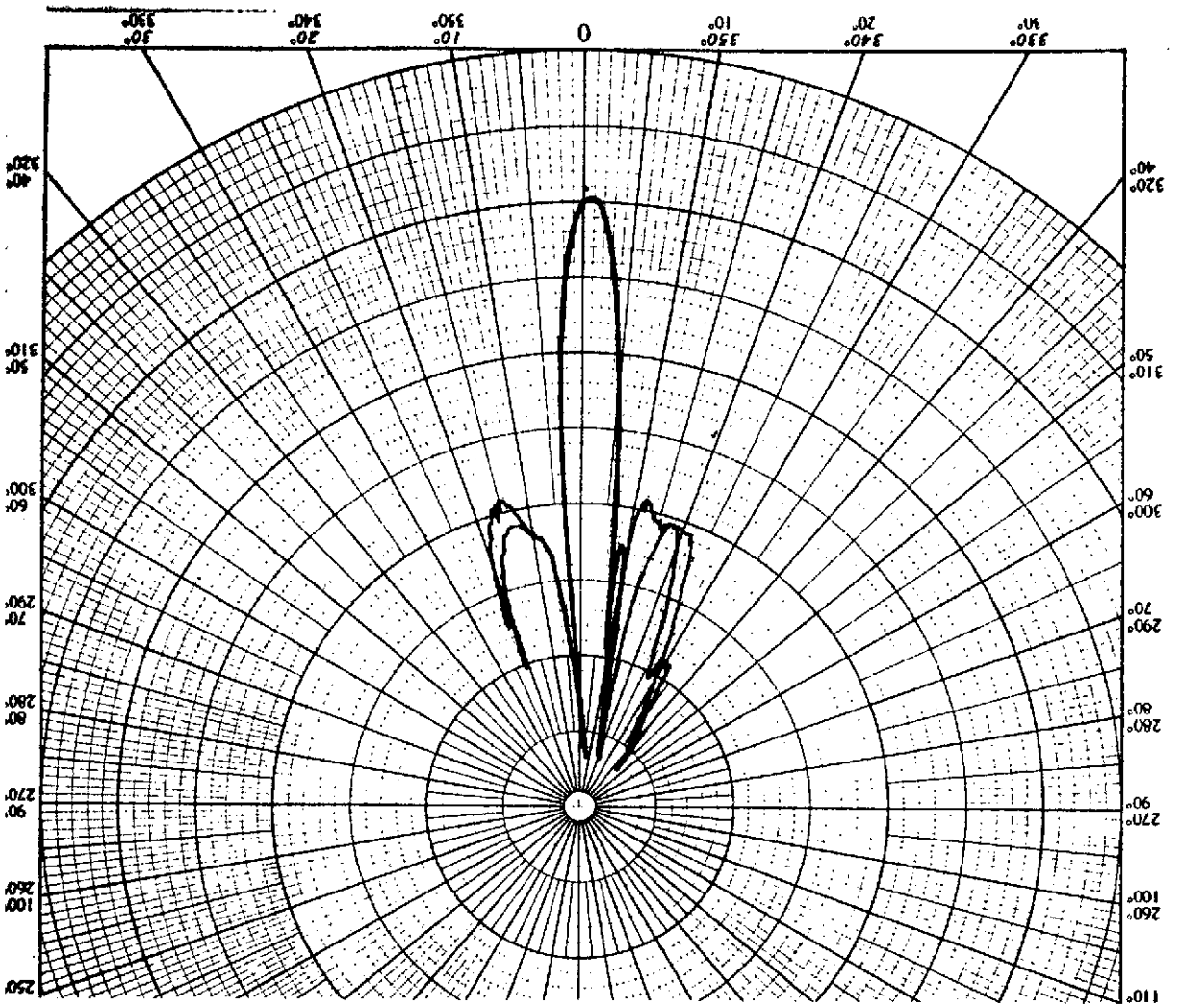

DUAL PATTERN
FREQUENCY = 8 GHz
ELEVATION PATTERN

E2

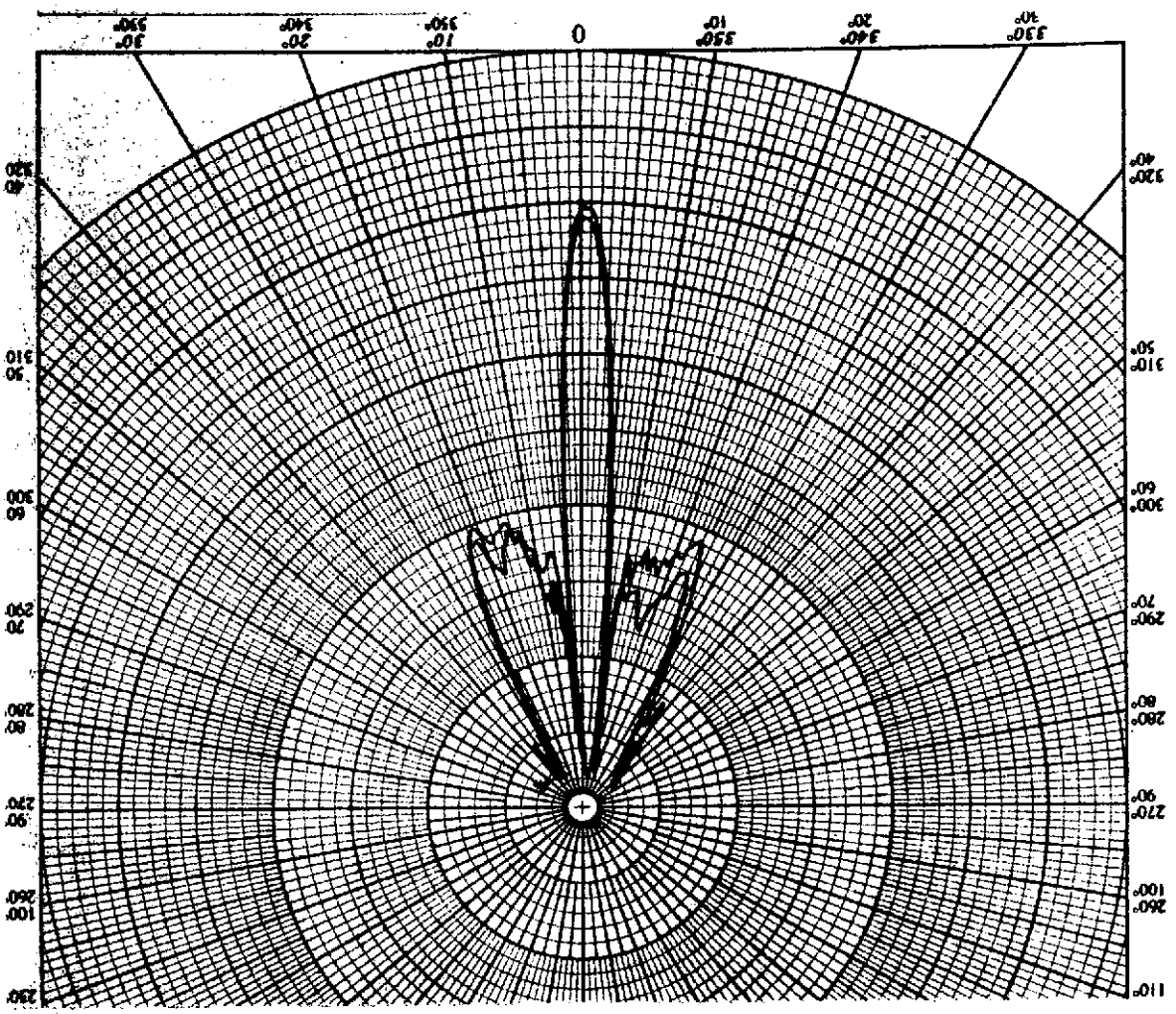

DUAL PATTERN
FREQUENCY = 10 GHz
AZIMUTH PATTERN

E3

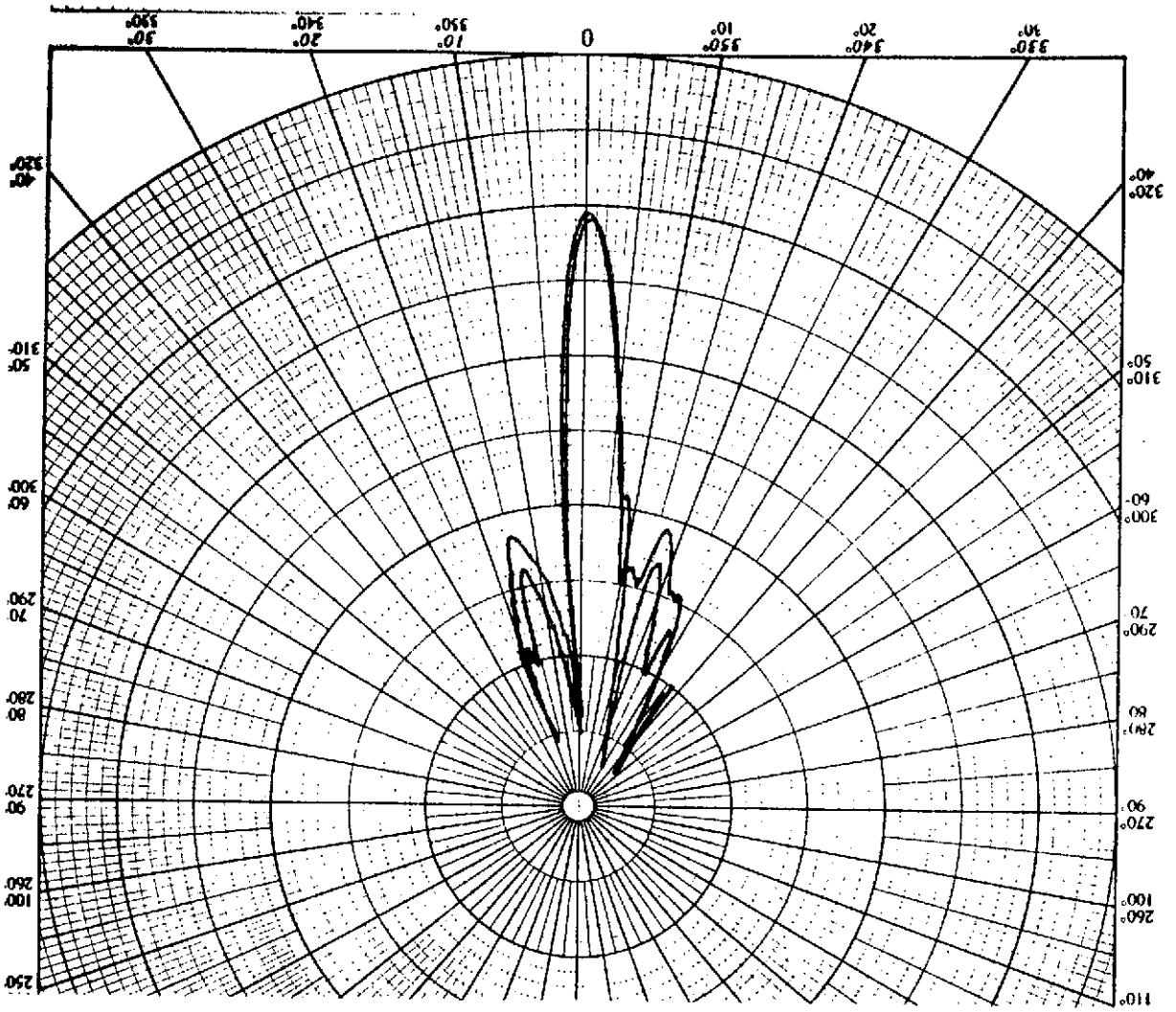

DUAL PATTERN
FREQUENCY = 10 GHz
ELEVATION PATTERN

E4

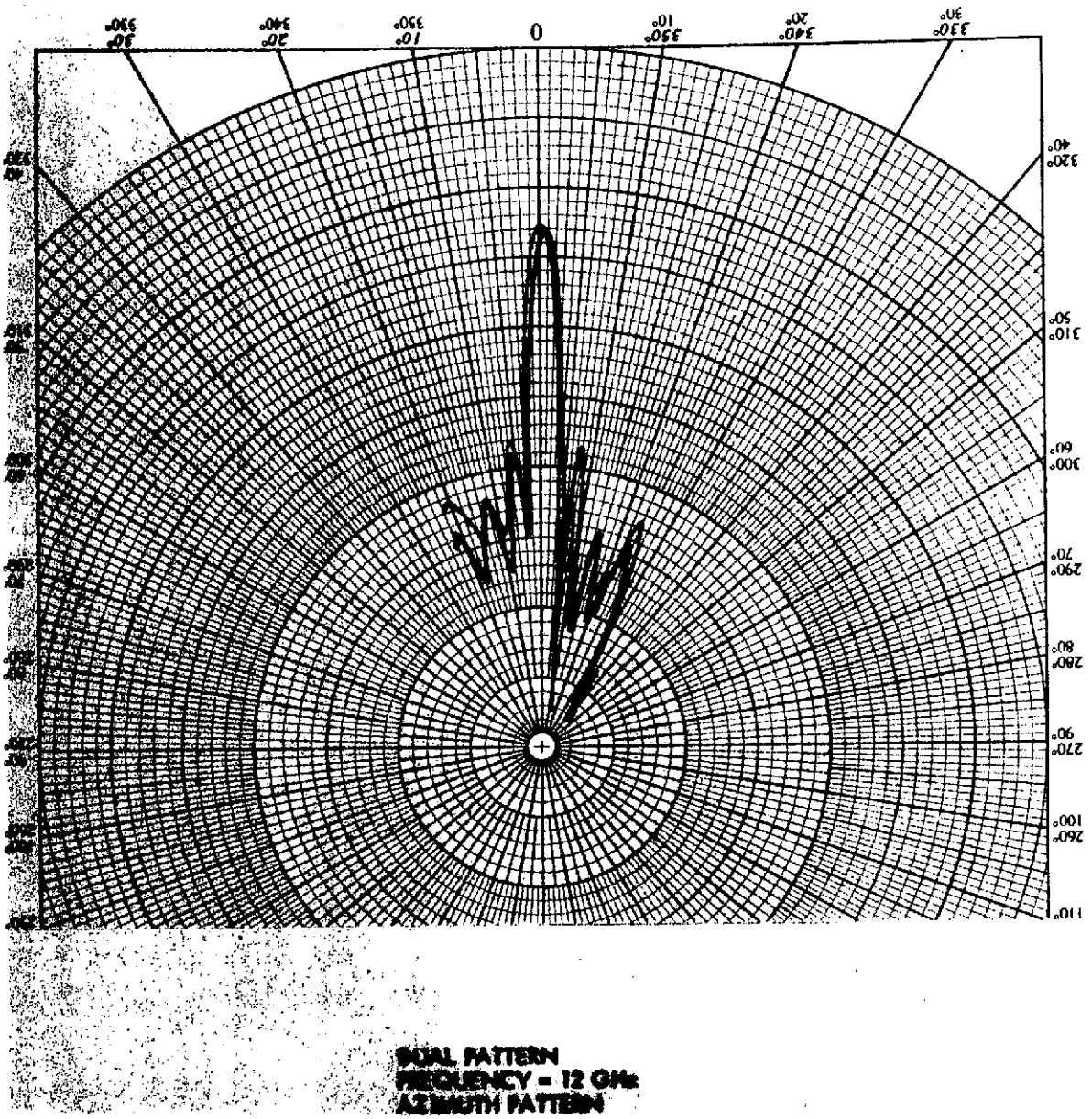

E5

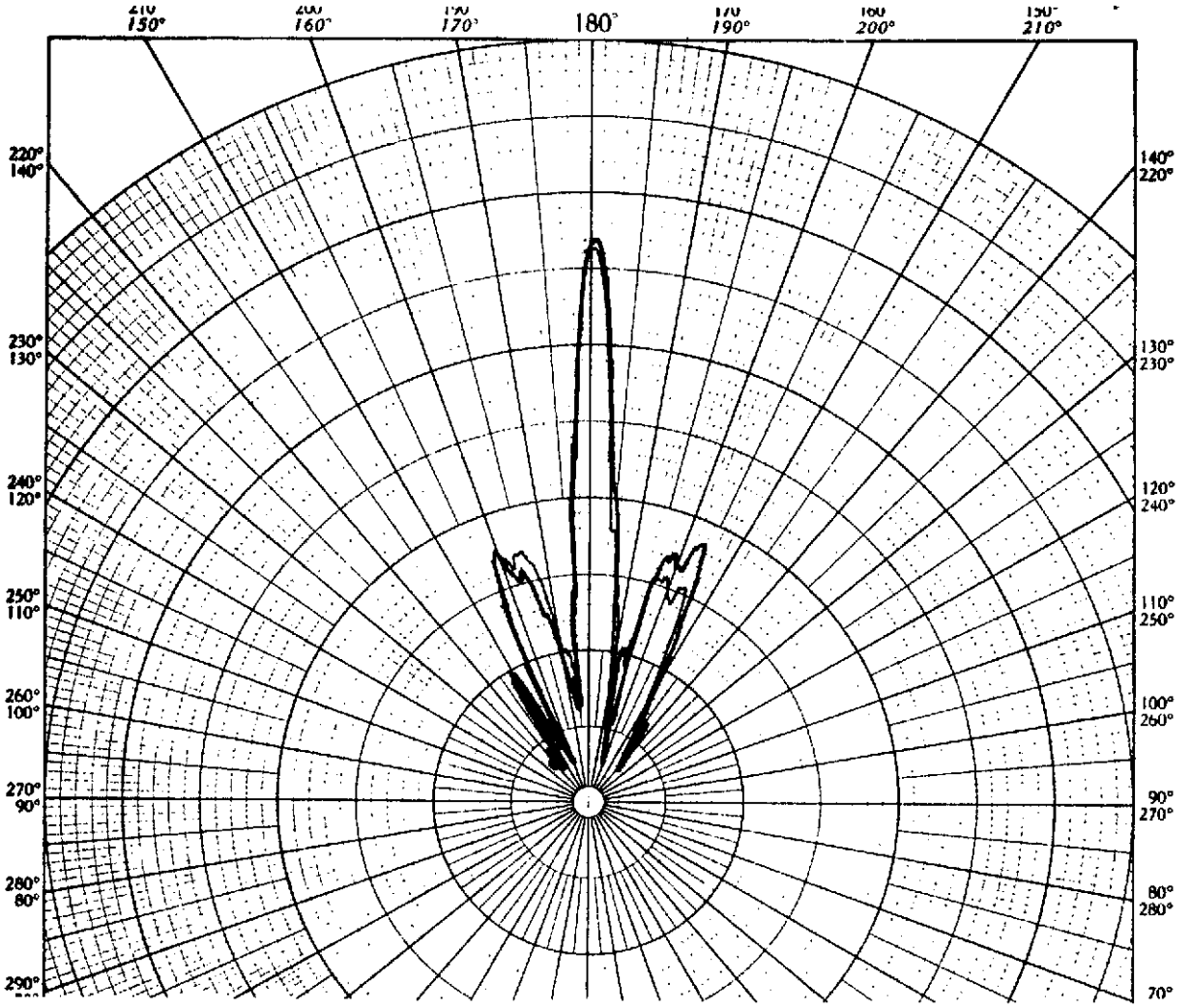

DUAL PATTERN
FREQUENCY = 12 GHz
ELEVATION PATTERN

E6

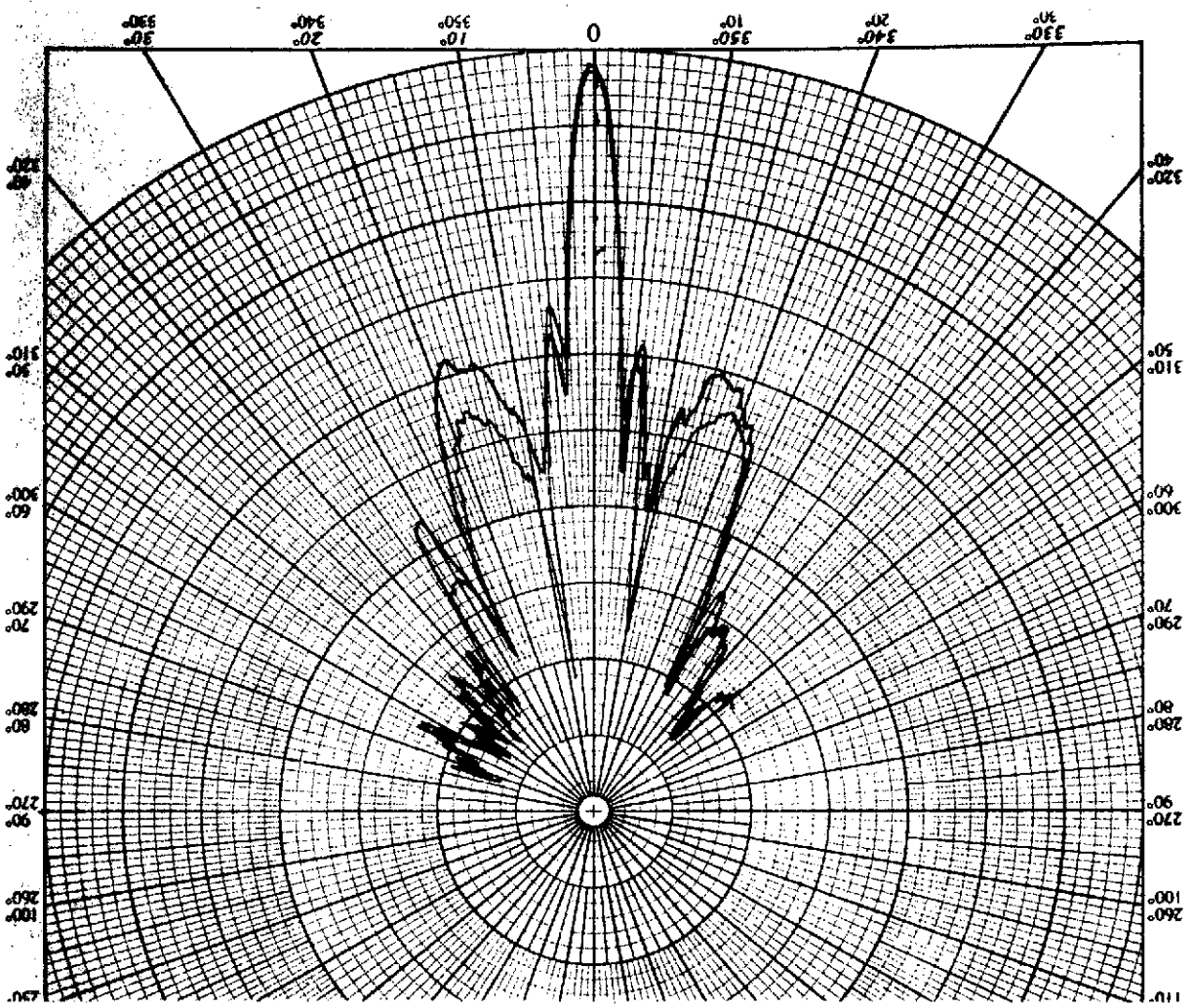

DUAL PATTERN
FREQUENCY = 14 GHz
AZIMUTH PATTERN

E7

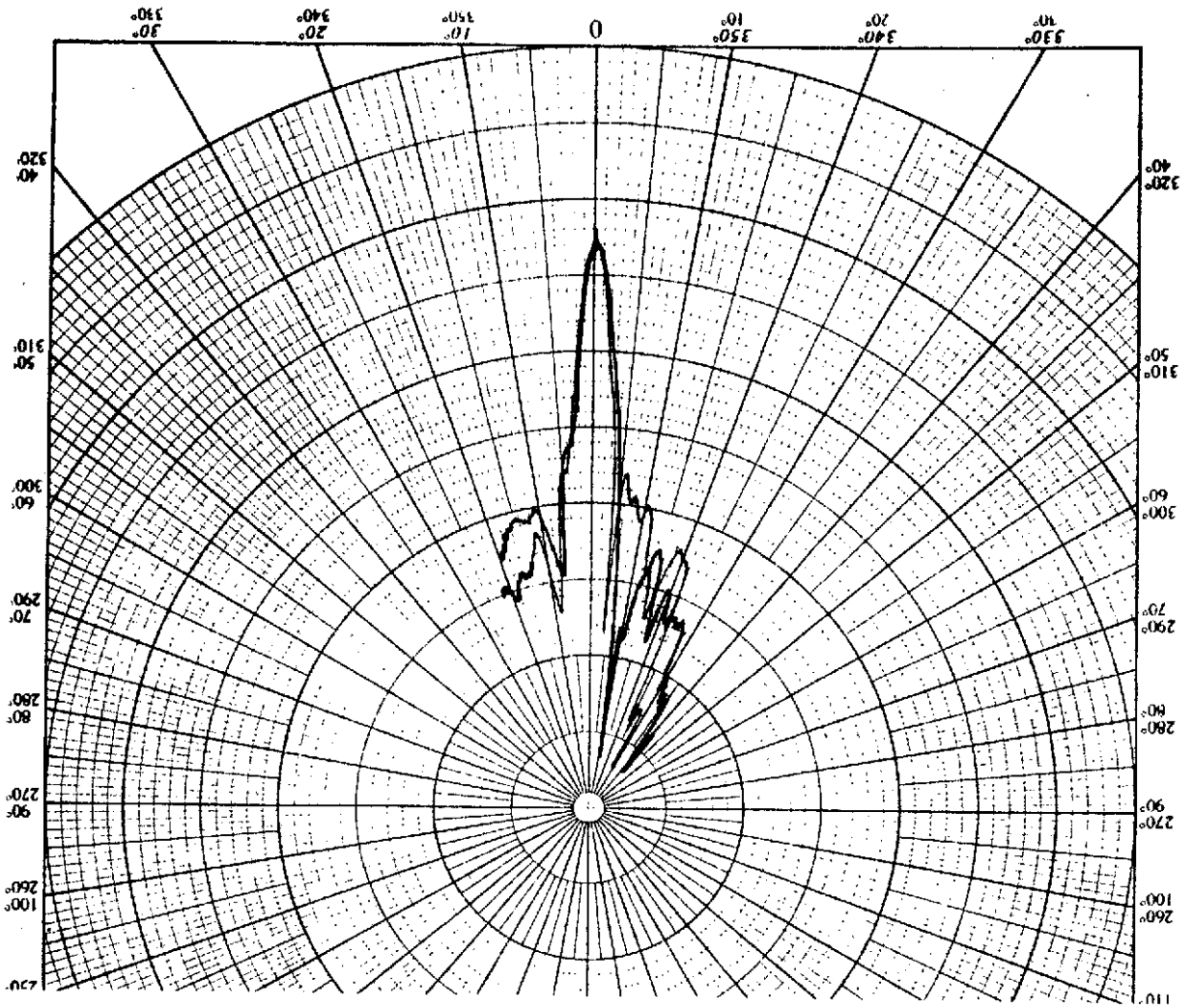

DUAL PATTERN
FREQUENCY = 14 GHz
ELEVATION PATTERN

E8

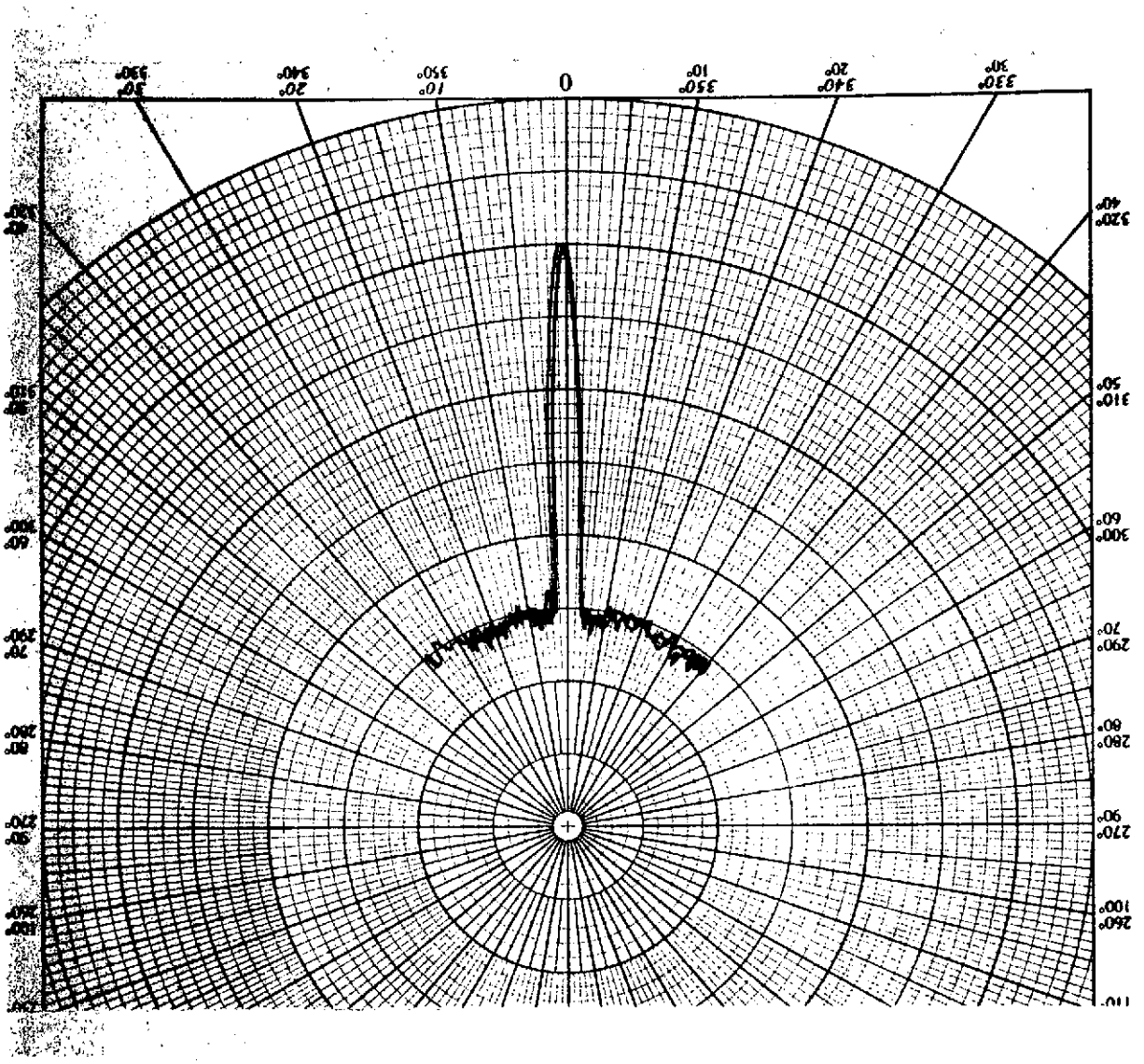

DUAL PATTERN
FREQUENCY = 16 GHz
AZIMUTH PATTERN

E9

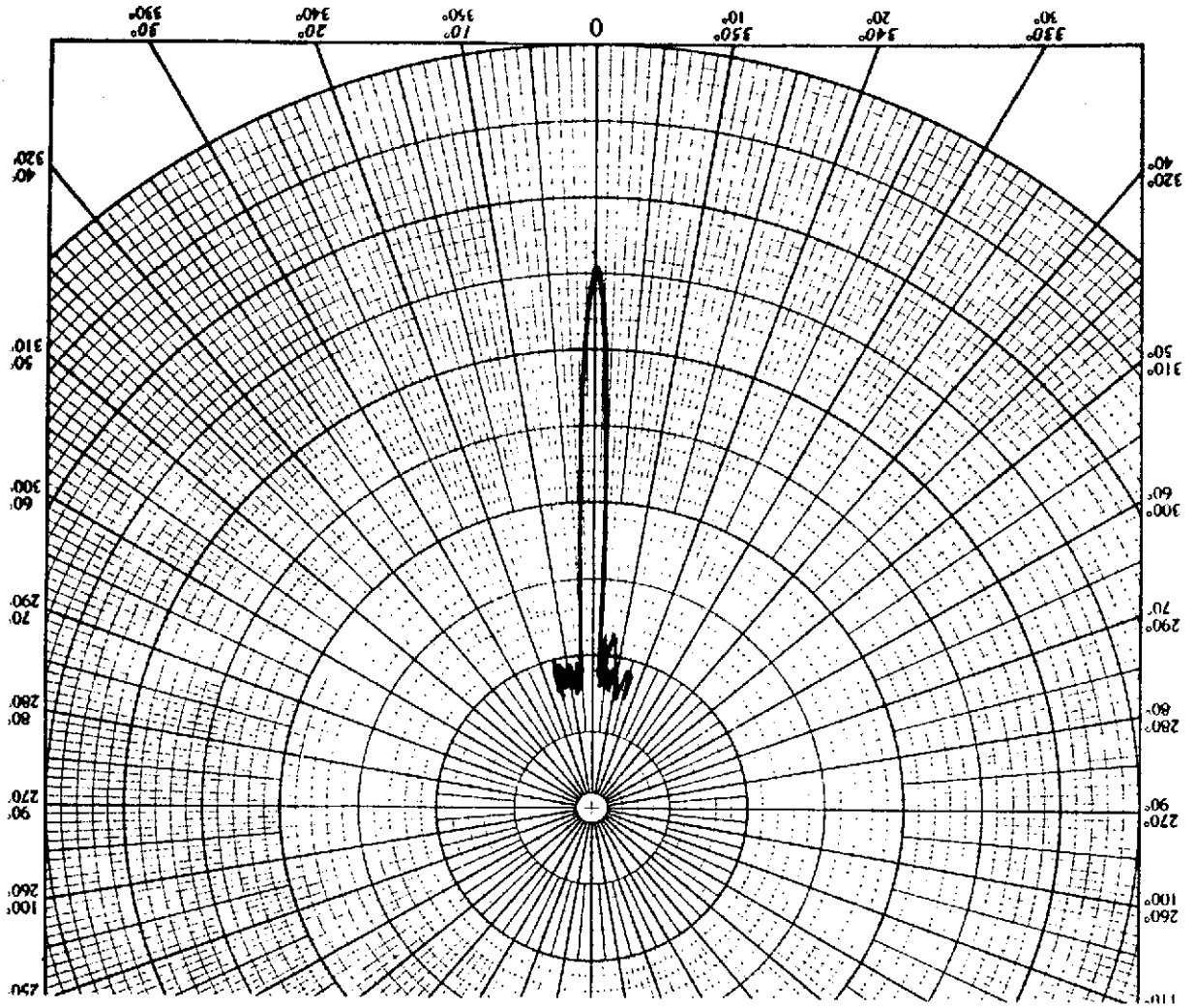

DUAL PATTERN
FREQUENCY = 16 GHz
ELEVATION PATTERN

E10

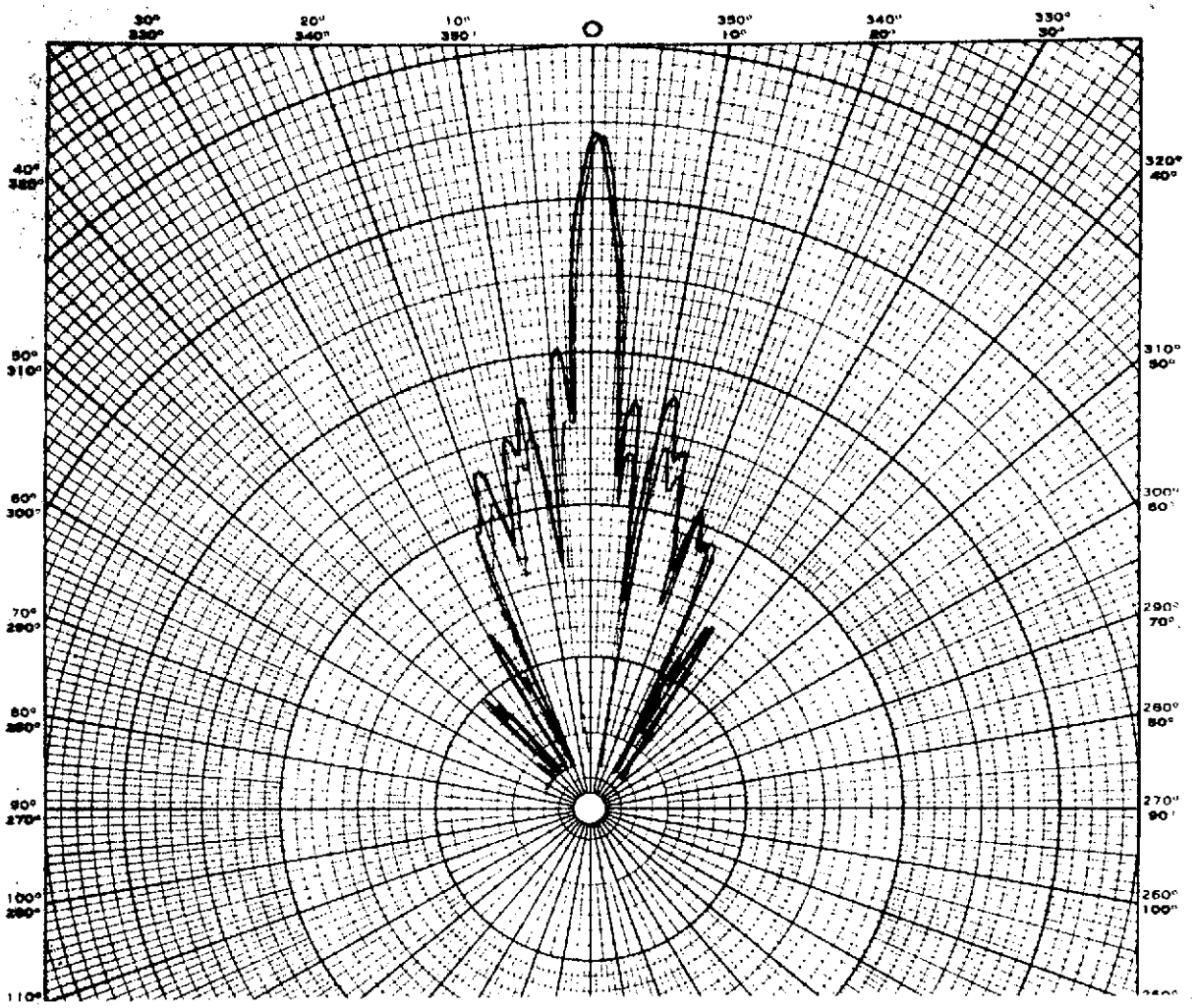

DUAL PATTERN
FREQUENCY = 18 GHz
AZIMUTH PATTERN

E11

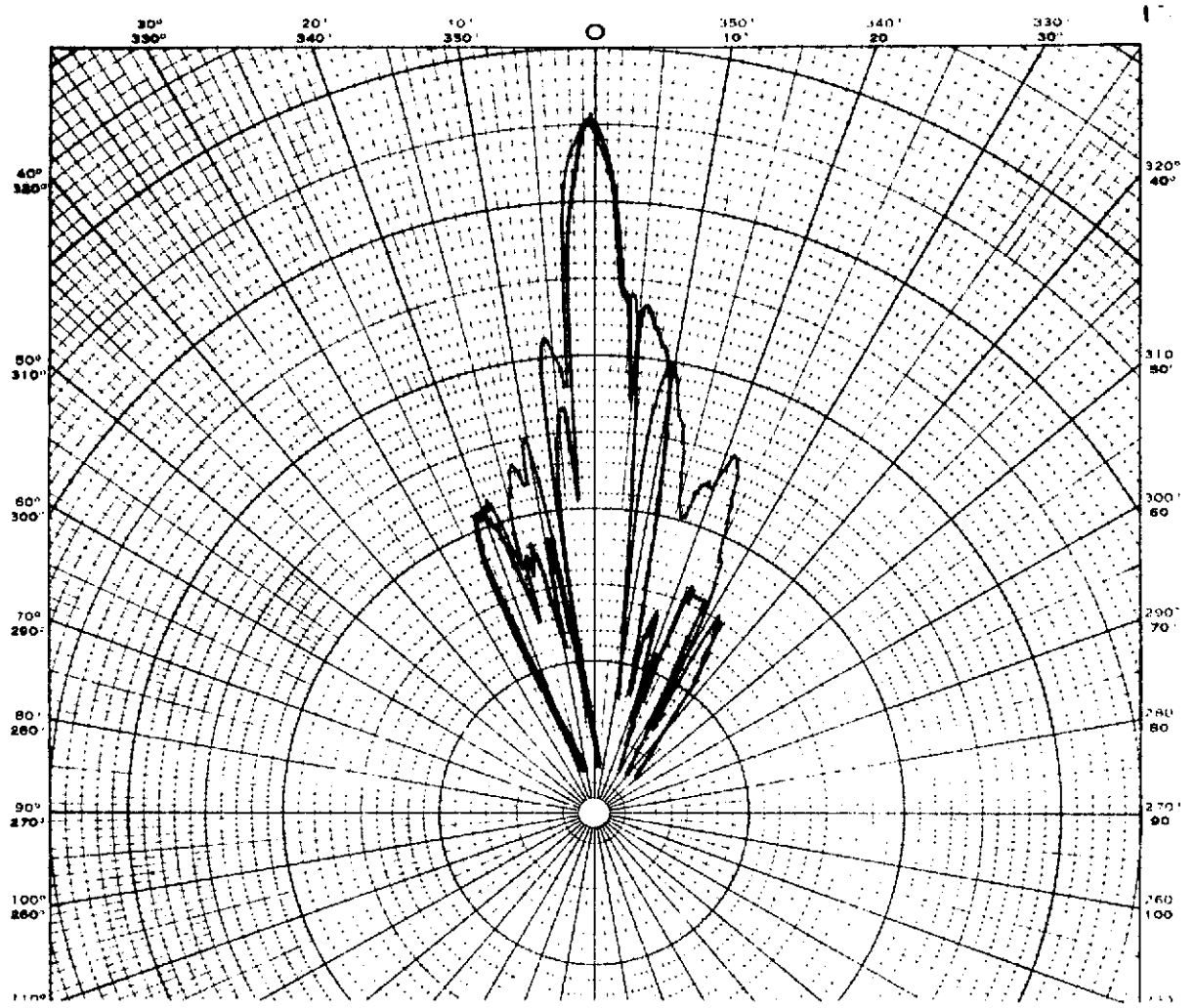

DUAL PATTERN
FREQUENCY = 18 GHz
ELEVATION PATTERN

E12

APPENDIX F

ANTENNA EFFECTIVE PRINCIPAL PLANE POWER PATTERNS

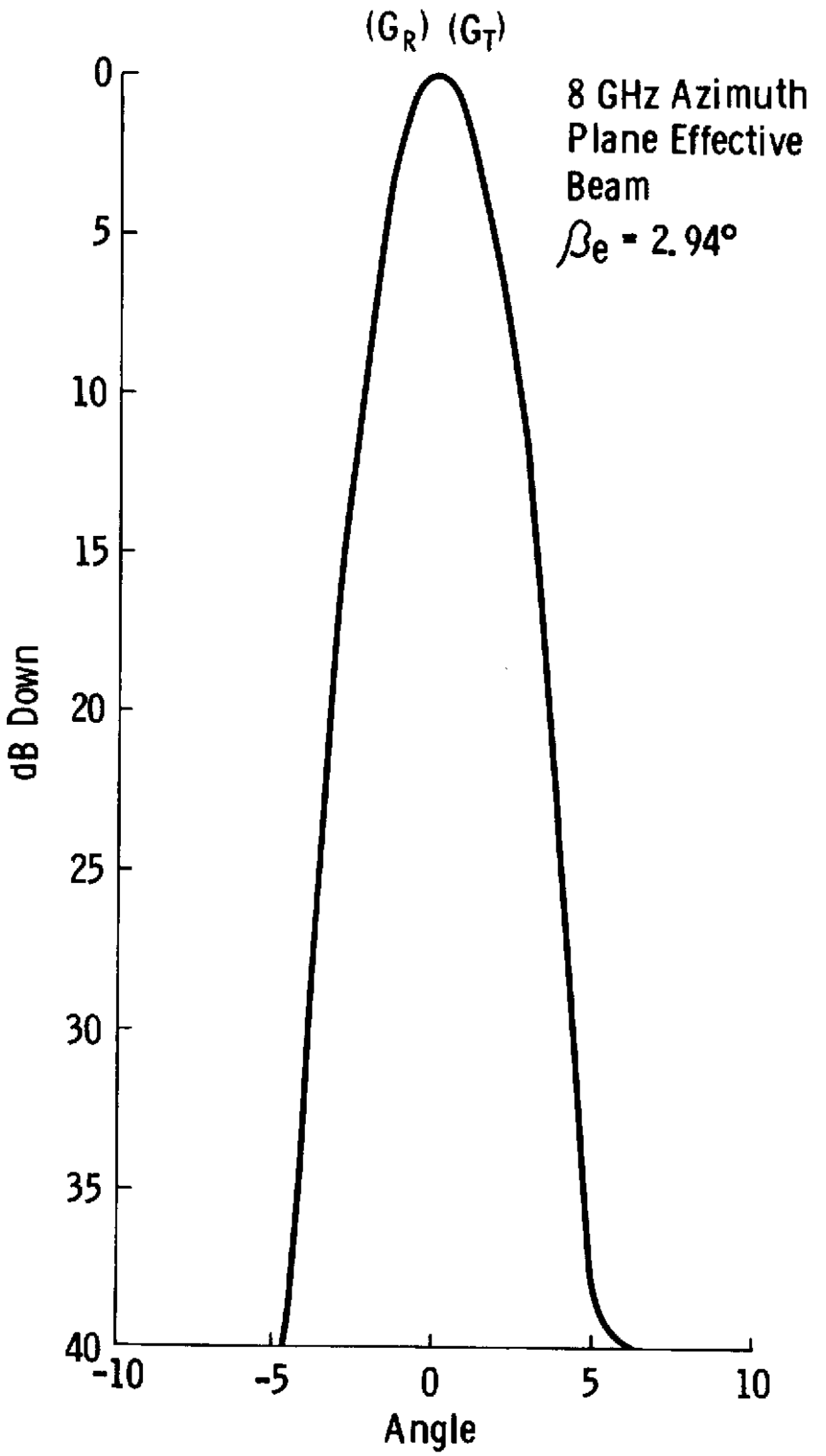
(G_R) (G_T)
8 GHz Azimuth Plane Effective Beam
β_e = 2.94°
dB Down
0
5
10
15
20
25
30
35
40
-10
-5
0
5
10
Angle

F1

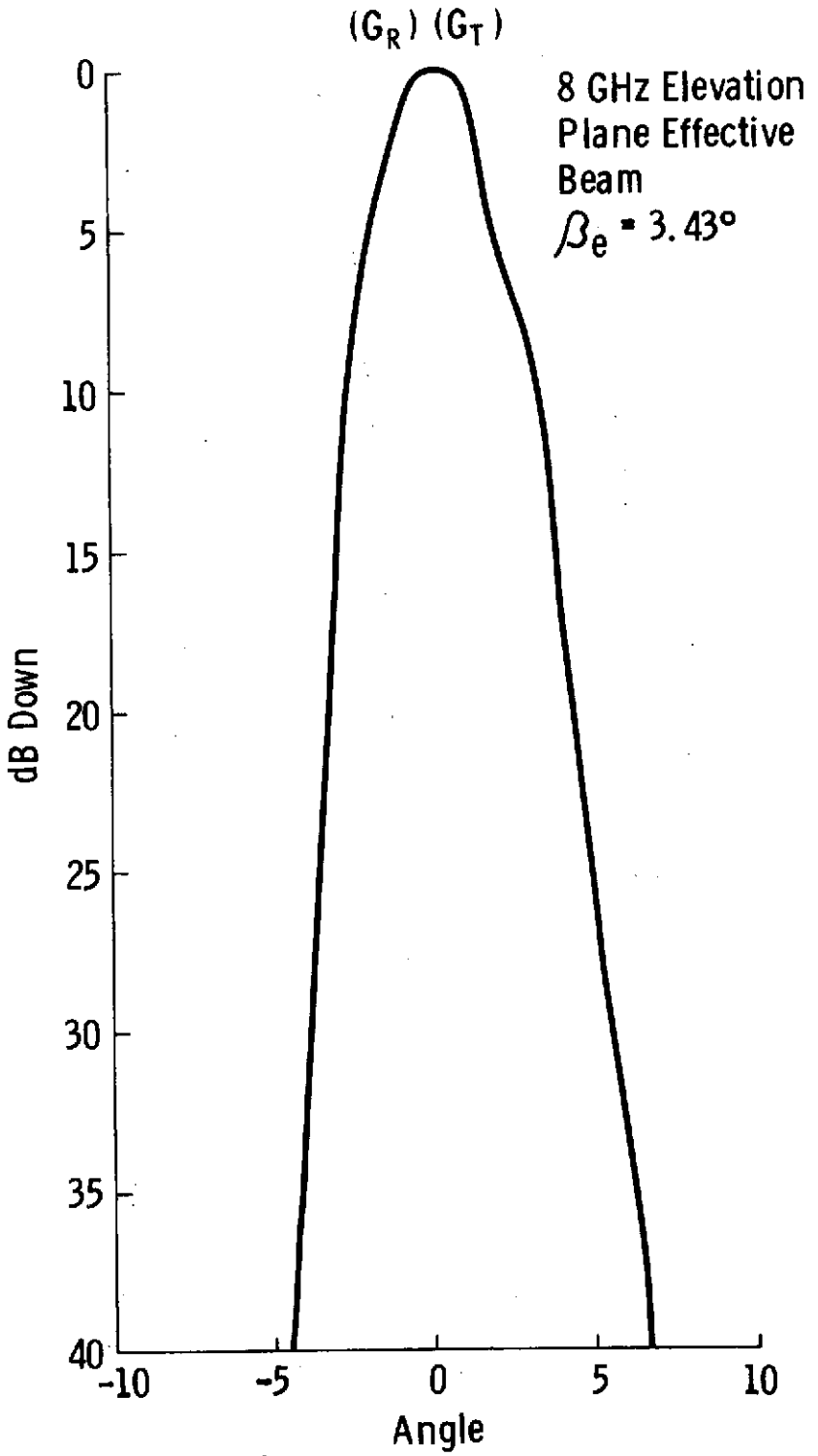
$(G_R)(G_T)$
8 GHz Elevation Plane Effective Beam
$\beta_e = 3.43°$
dB Down
0
5
10
15
20
25
30
35
40
-10
-5
0
5
10
Angle

F2

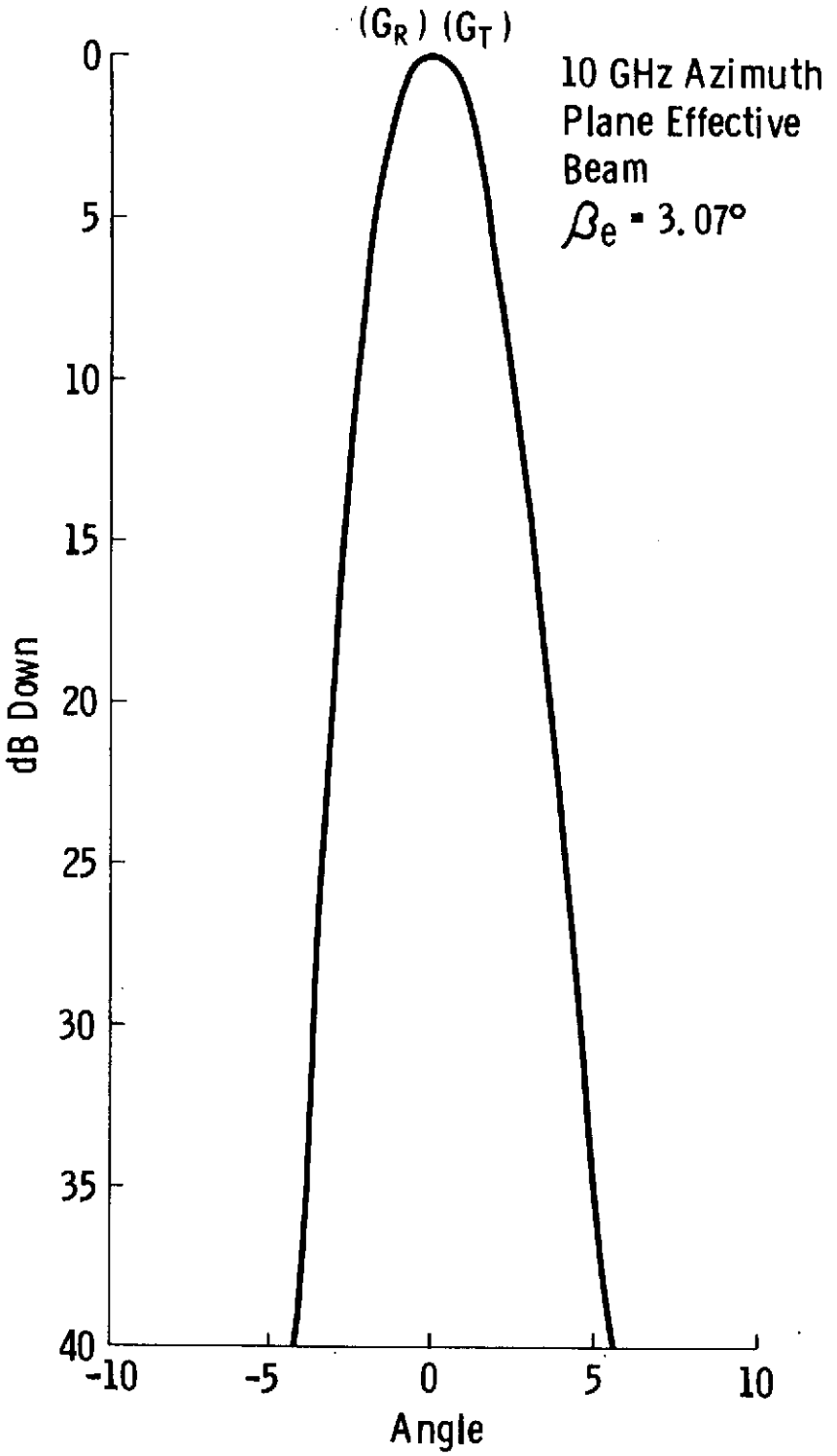
$(G_R)(G_T)$
10 GHz Azimuth Plane Effective Beam
β_e = 3.07°
dB Down
0
5
10
15
20
25
30
35
40
-10
-5
0
5
10
Angle

F3

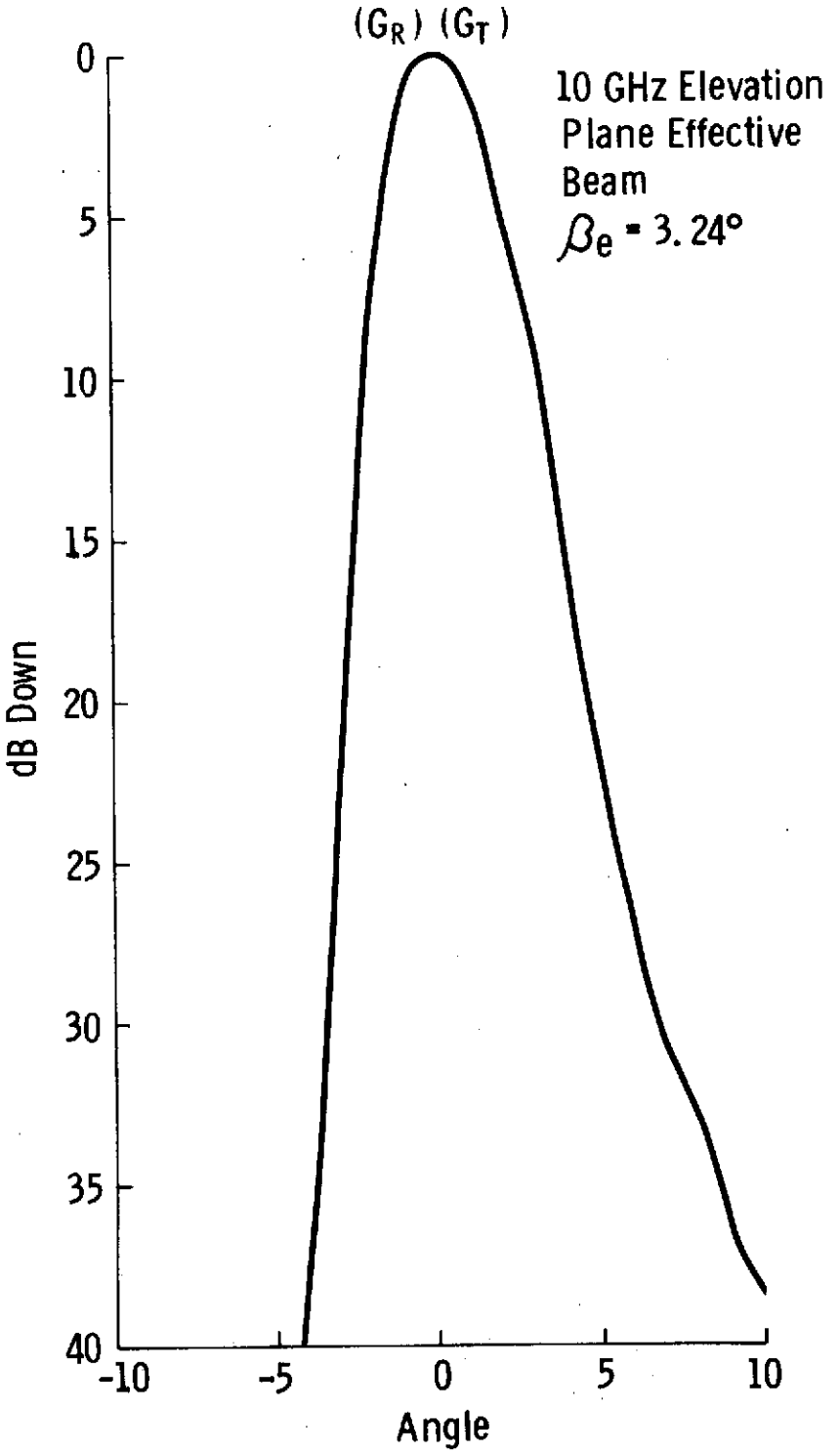
(G_R) (G_T)
10 GHz Elevation Plane Effective Beam
β_e = 3.24°
dB Down
0
5
10
15
20
25
30
35
40
-10
-5
0
5
10
Angle

F4

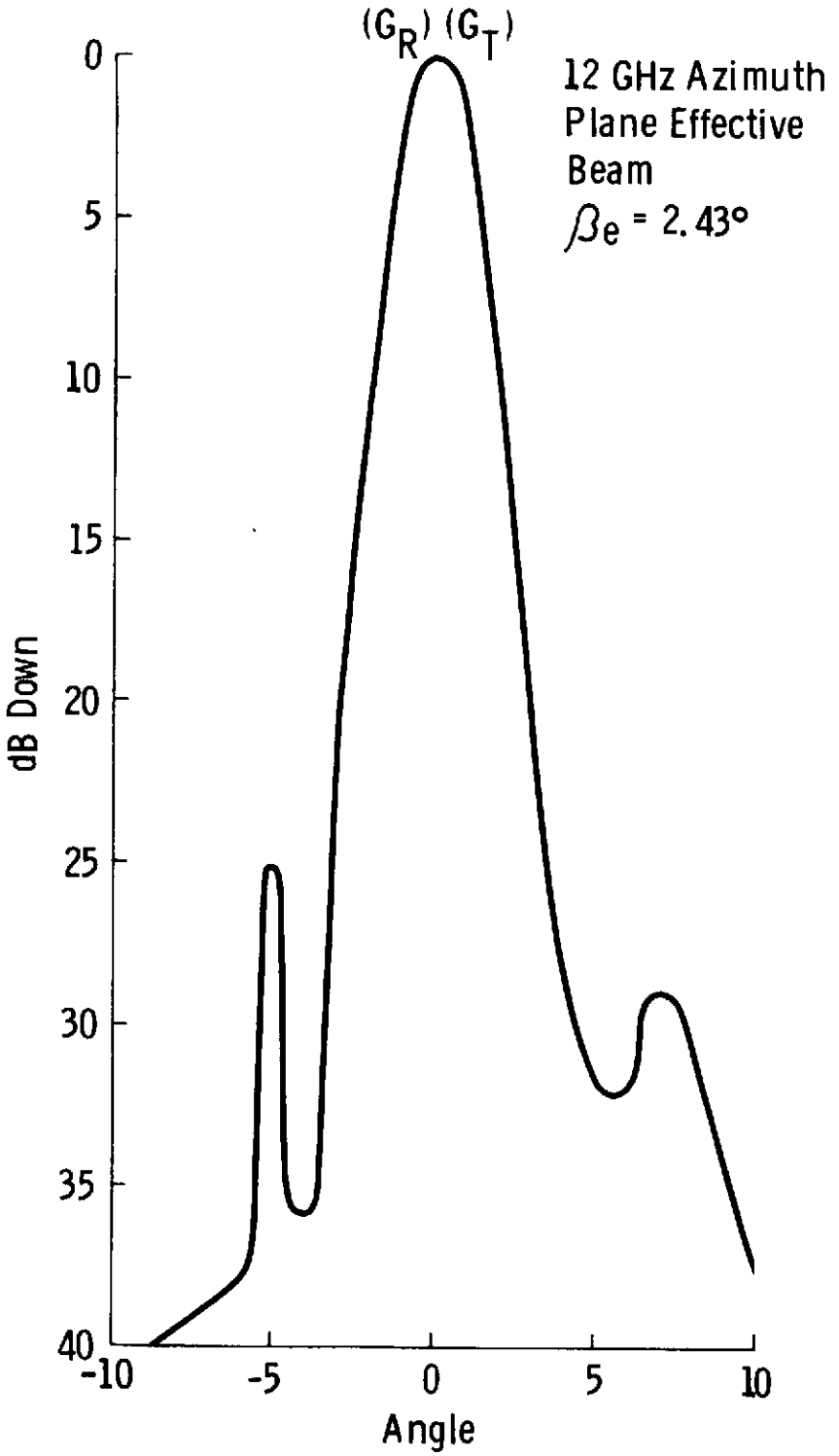
$(G_R)(G_T)$
12 GHz Azimuth Plane Effective Beam
$\beta_e = 2.43°$
dB Down
0
5
10
15
20
25
30
35
40
-10
-5
0
5
10
Angle

F5

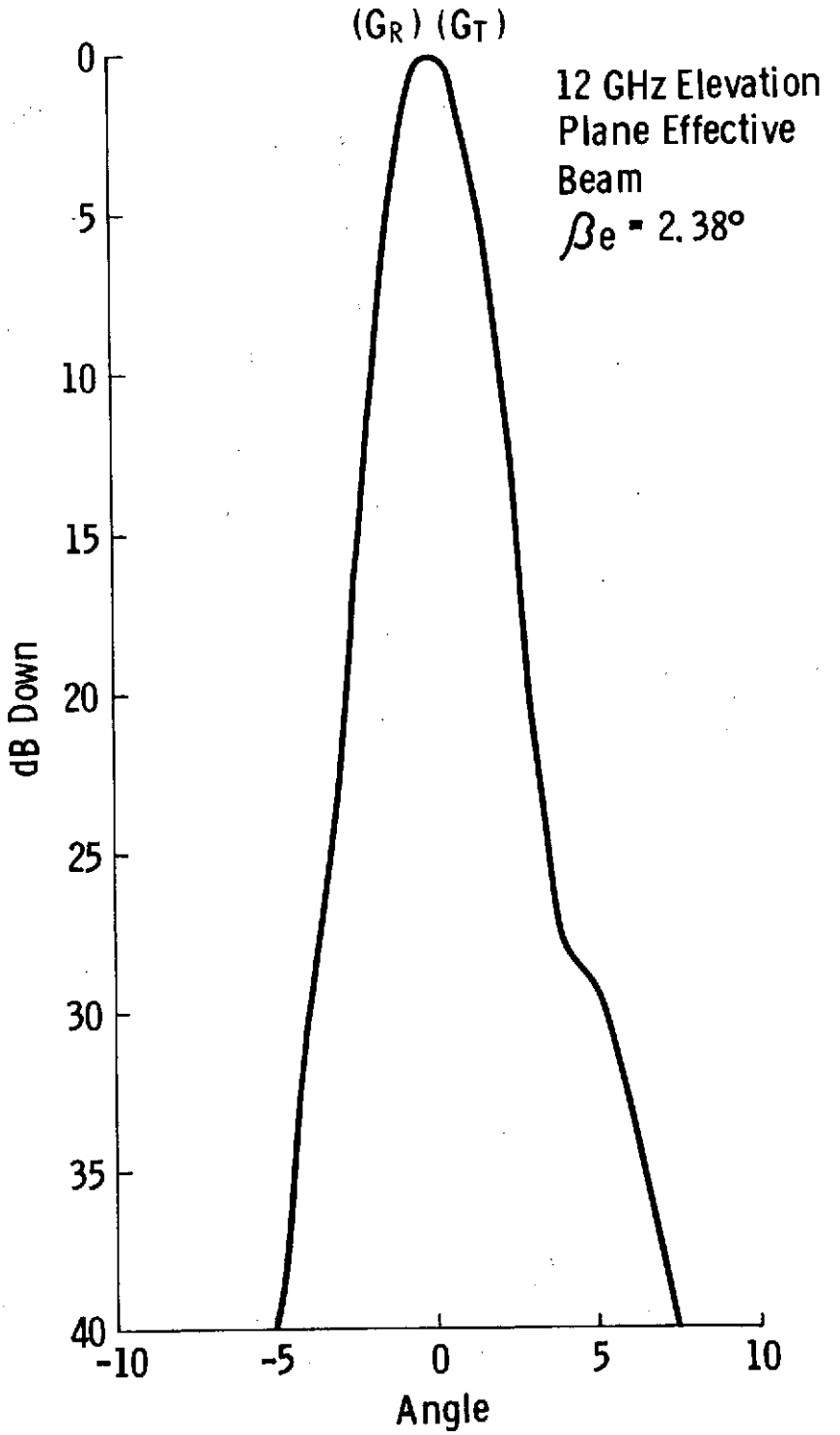
$(G_R)(G_T)$
12 GHz Elevation Plane Effective Beam
$\beta_e = 2.38°$
dB Down
0
5
10
15
20
25
30
35
40
-10
-5
0
5
10
Angle

F6

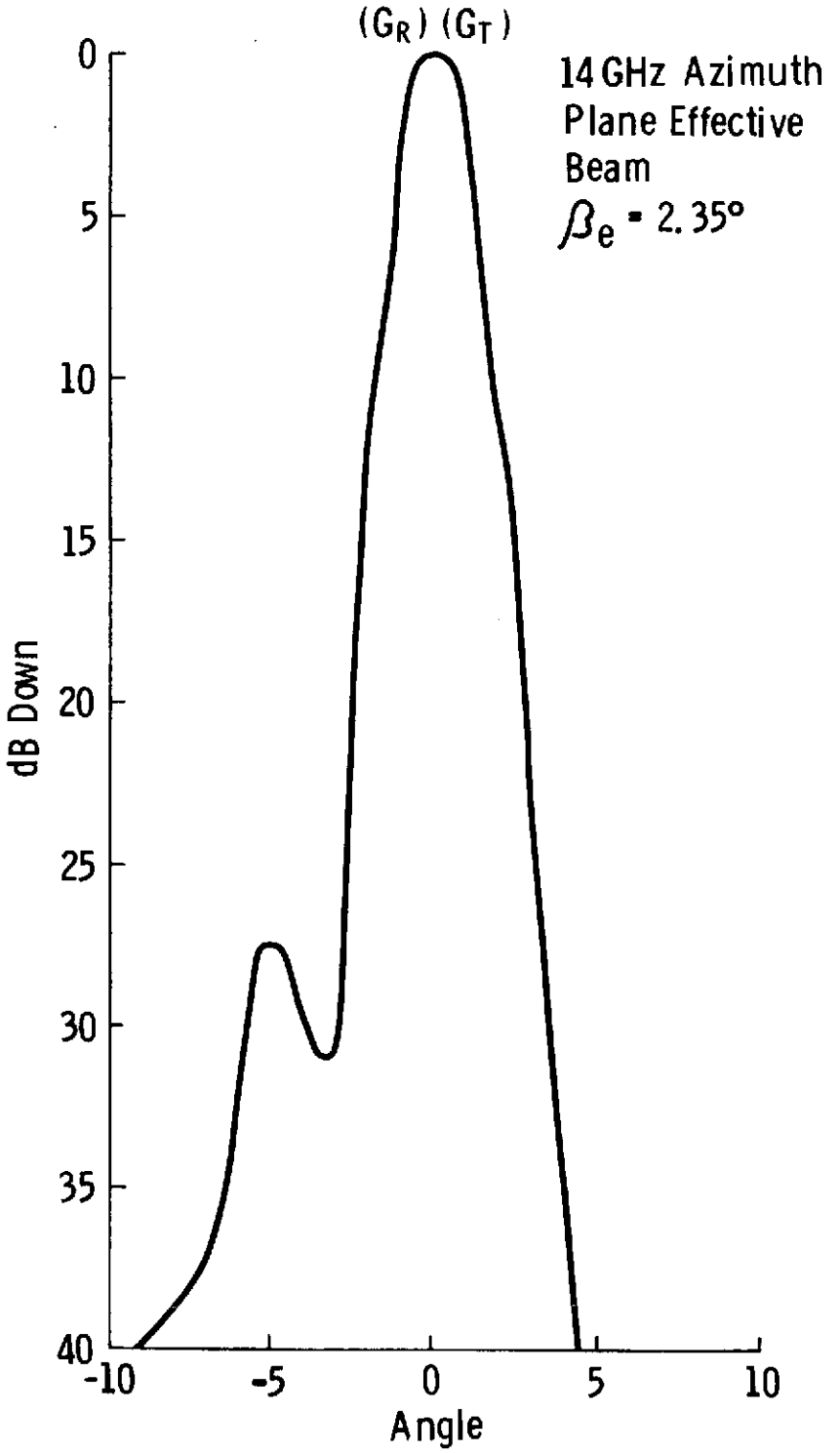
(G_R) (G_T)
14 GHz Azimuth Plane Effective Beam
β_e = 2.35°
0
5
10
15
20
25
30
35
40
dB Down
-10
-5
0
5
10
Angle

F7

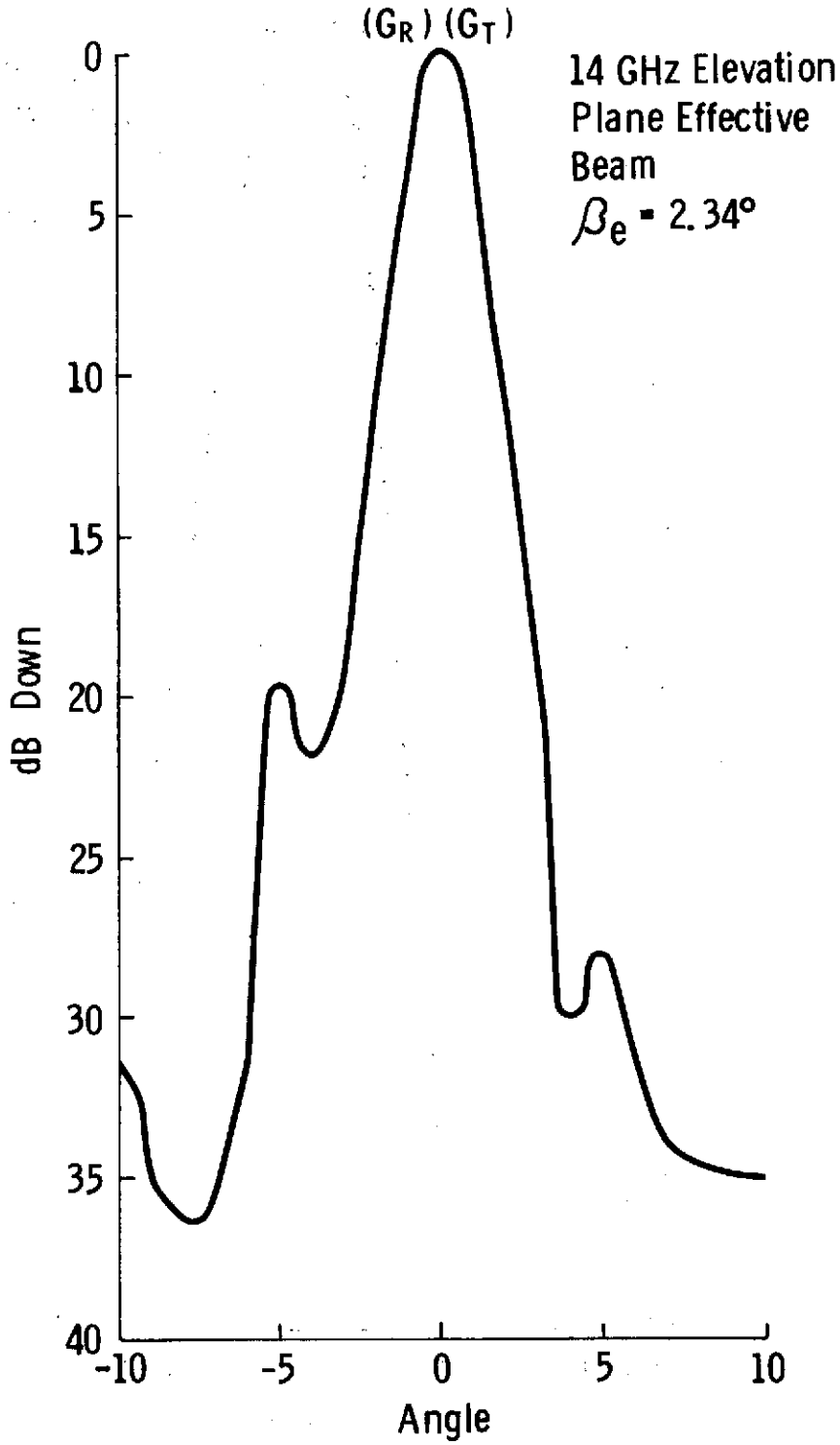
$(G_R)(G_T)$
14 GHz Elevation Plane Effective Beam
β_e = 2.34°
dB Down
0
5
10
15
20
25
30
35
40
-10
-5
0
5
10
Angle

F8

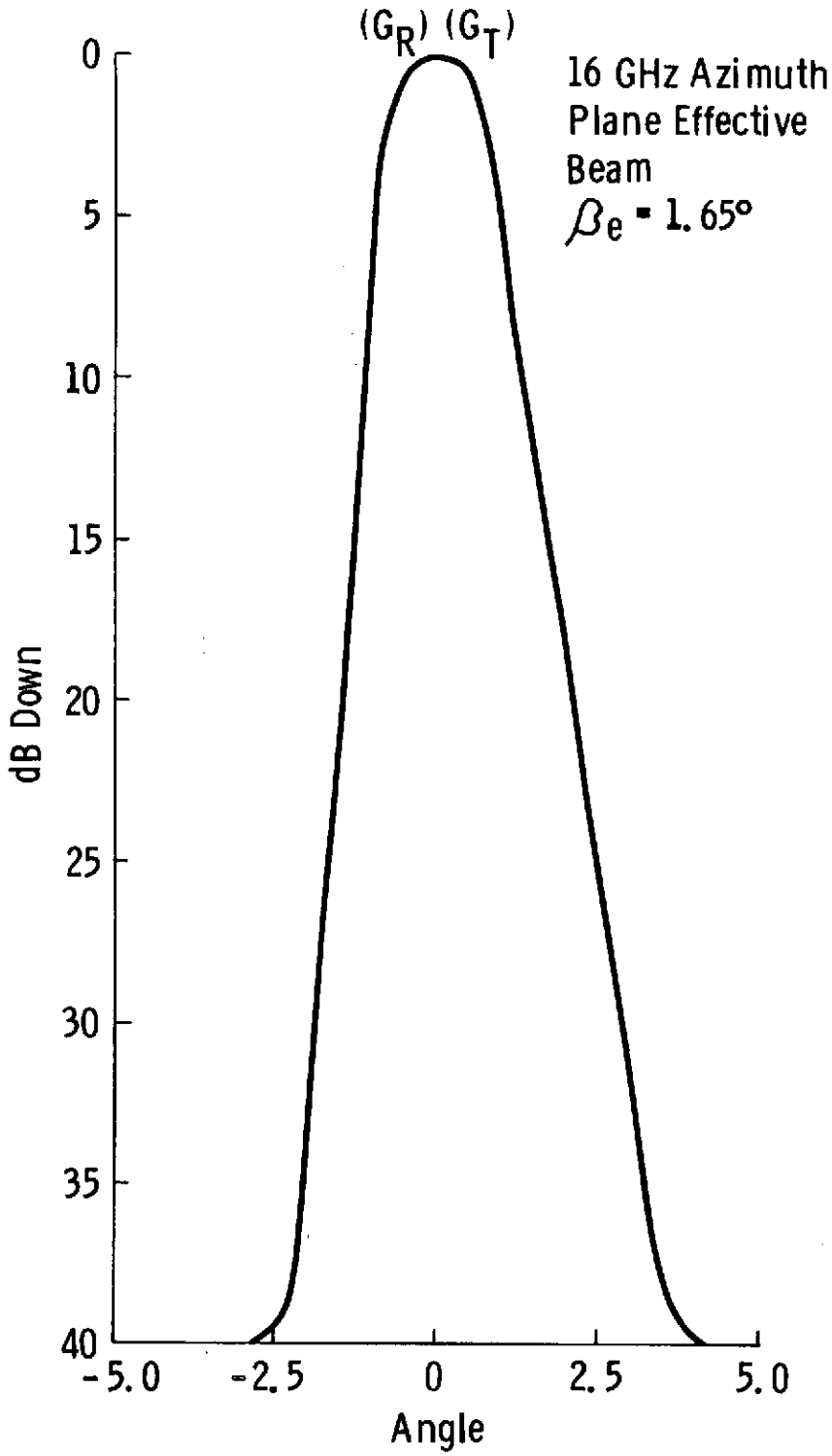
(G_R) (G_T)
16 GHz Azimuth Plane Effective Beam
β_e = 1.65°
0
5
10
15
20
25
30
35
40
dB Down
-5.0
-2.5
0
2.5
5.0
Angle

F9

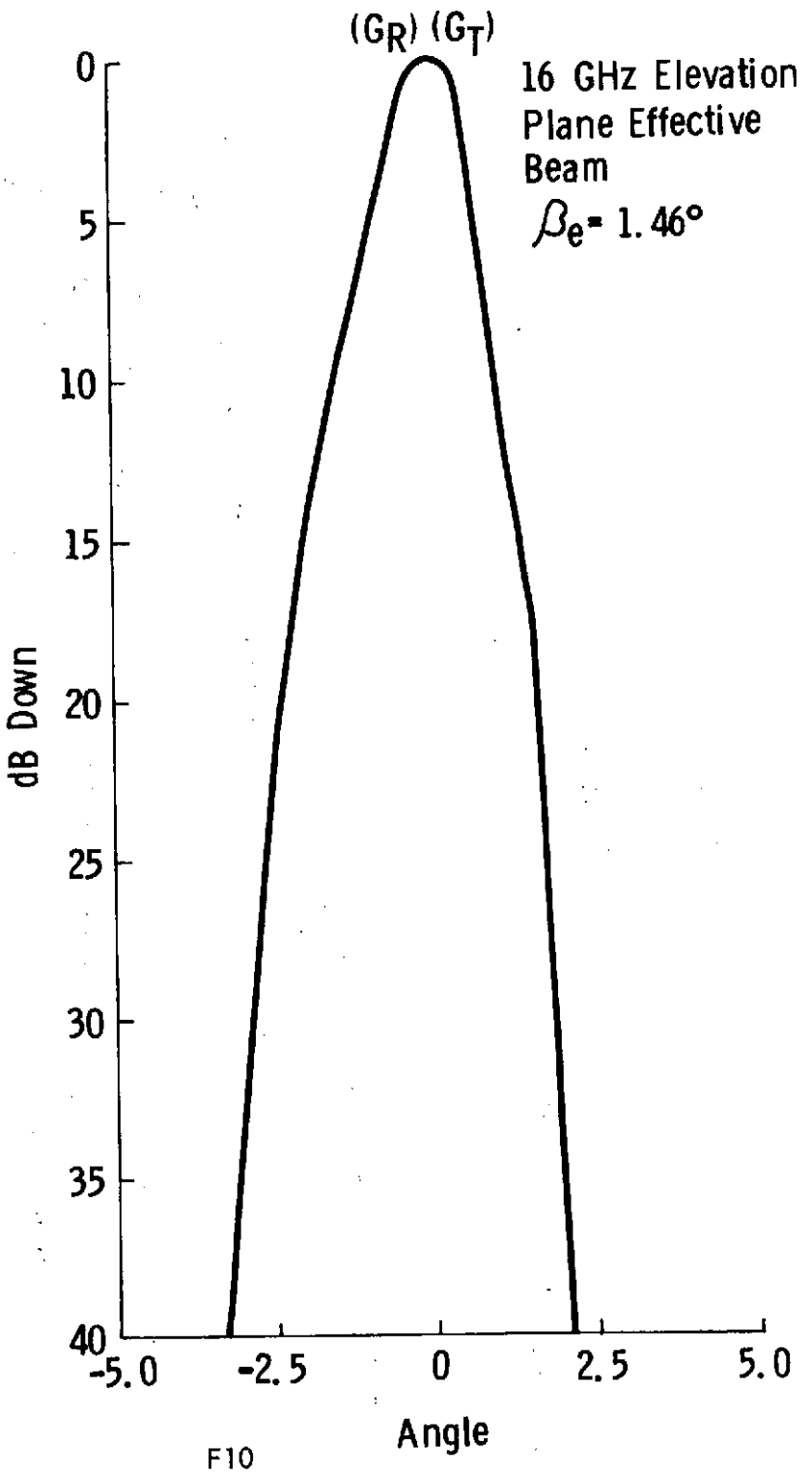
(G_R) (G_T)
16 GHz Elevation Plane Effective Beam
β_e = 1.46°
0
5
10
15
20
25
30
35
40
dB Down
-5.0
-2.5
0
2.5
5.0
Angle

F10

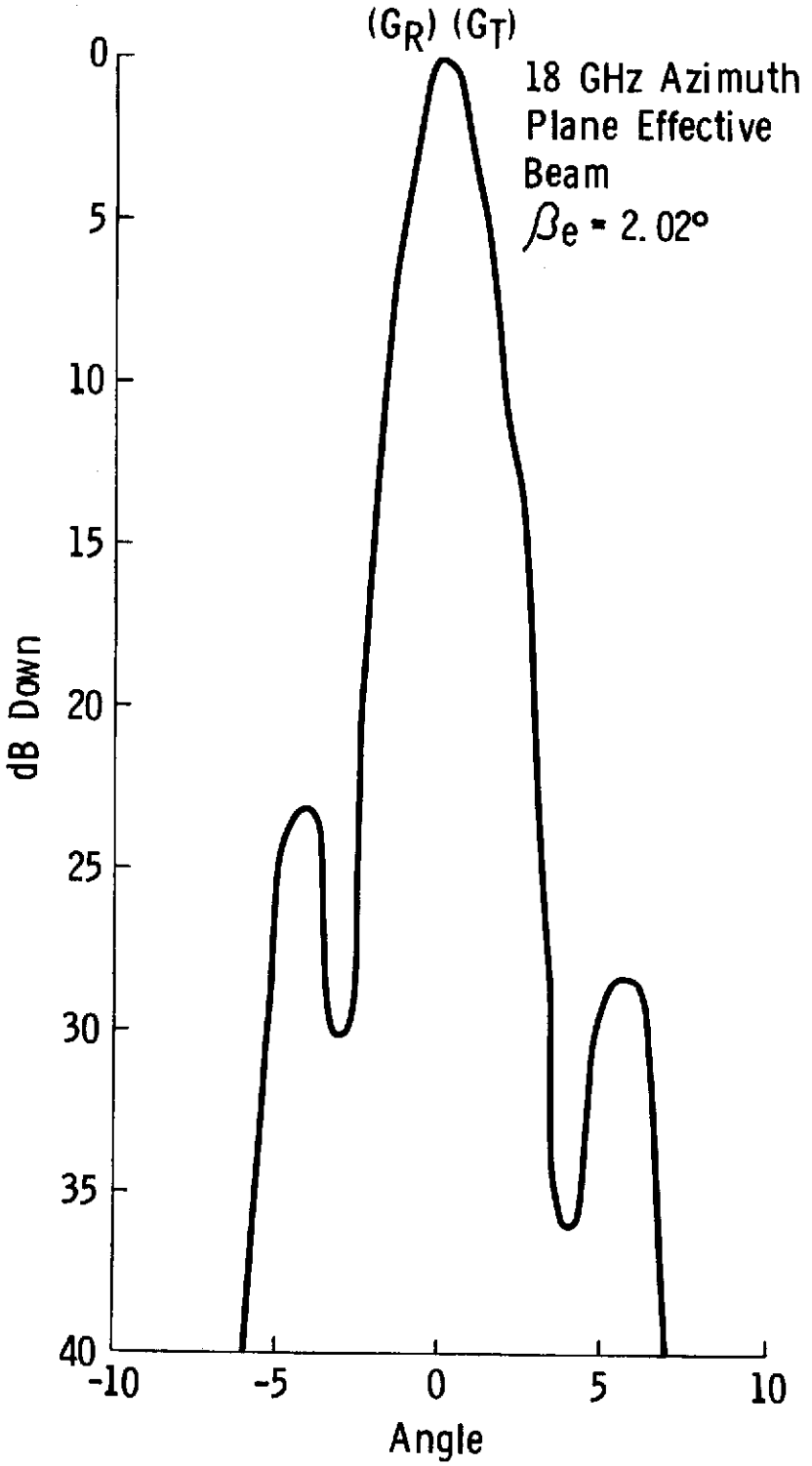
$(G_R)(G_T)$
18 GHz Azimuth Plane Effective Beam
$\beta_e = 2.02°$
dB Down
0
5
10
15
20
25
30
35
40
-10
-5
0
5
10
Angle

F11

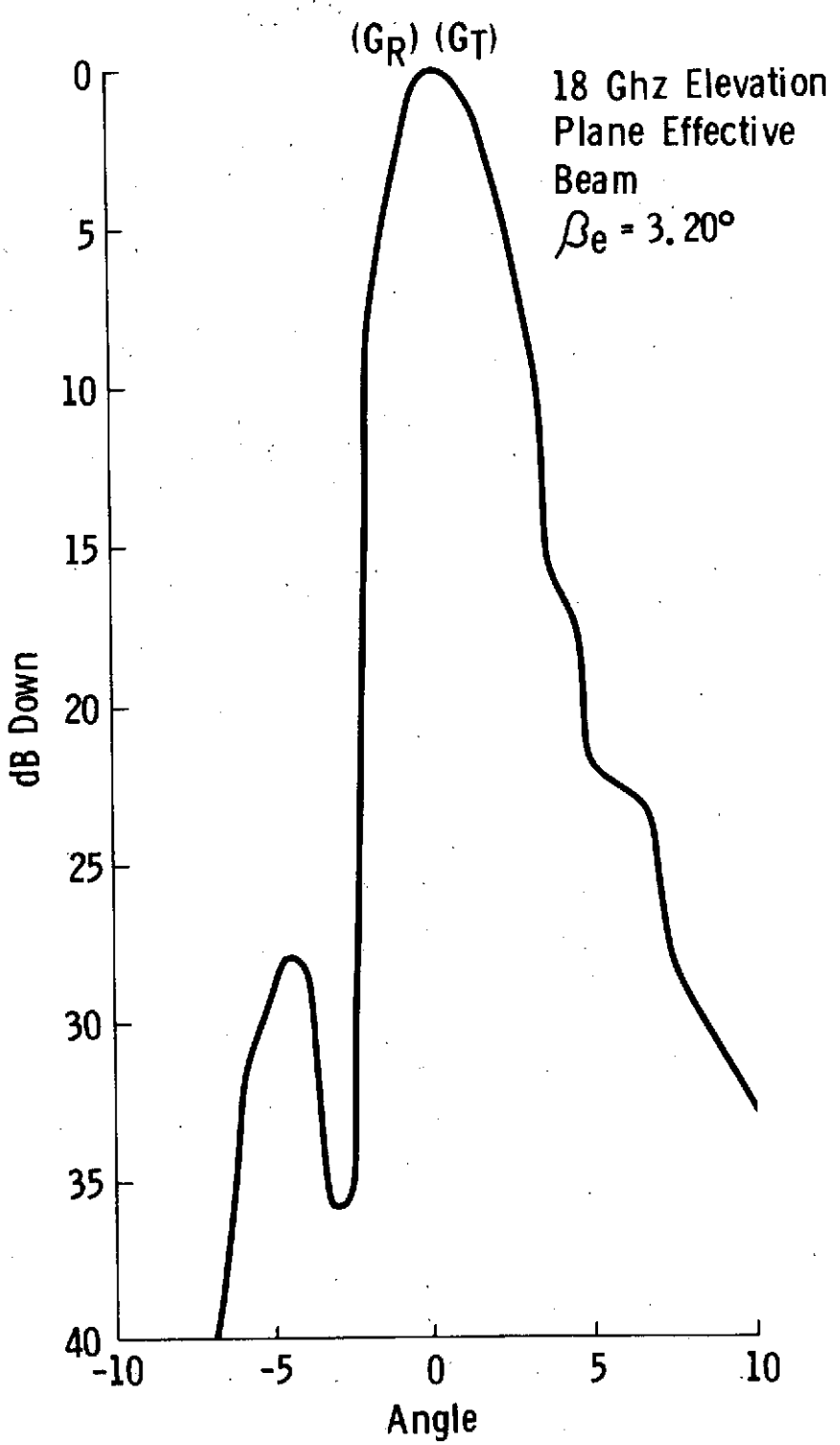
(G_R) (G_T)
18 Ghz Elevation Plane Effective Beam
β_e = 3.20°
dB Down
0
5
10
15
20
25
30
35
40
-10
-5
0
5
10
Angle

F12

REFERENCES

(1) Link, D. J., "Statement on Current Capabilities, State of the Technology and Future Requirements for Remote Sensing of Earth Resources," Presented to the Committee on Science and Astronautics, U. S. House of Representatives, 92nd Congress, January, 1972.

(2) Luney, P. R., and H. W. Dill, Jr., "Uses, Potentialities and Needs in Agriculture and Forestry," in Remote Sensing, Washington, D. C. National Academy of Sciences, pp. 1-33, 1970.

(3) Dellwig, L. F., H. C. MacDonald, and J. Dirk, "Potential of Radar in Geological Exploration," CRES Technical Report 118-11, The University of Kansas Center for Research, Inc., Lawrence, Kansas, pp. 747-764, April, 1968.

(4) Dellwig, L. F., J. N. Dirk, and R. L. Walters, "Potential of Low Resolution Radar Imagery in Regional Geologic Studies," Journal of Geophysical Research, vol. 77, pp. 4995-4998, 1966.

(5) National Academy of Sciences, Useful Applications of Earth Oriented Satellites, National Research Council, Division of Engineering, NSR-09-012-909, 1969.

(6) Smith, Rao, Koffler and Curtis, "The Determination of Sea Surface Temperature from Satellite High Resolution Infrared Window Radiation Measurements," Monthly Weather Review, vol. 98, no. 8, pp. 604-611.

(7) Avery, T. E., "Photointerpretation for Land Managers," Rochester, New York Eastman Kodak Company, 1970.

(8) American Society of Photogrammetry, Manual of Photographic Interpretation, George Banta Publishing Company, Menesho, Wisconsin, 1960.

(9) Sabatini, R. R., G. A. Rabchevsky and J. E. Sissala, "Nimbus Earth Resources Observations," Technical Report No. 2, Allied Research Associates, Inc., Concord, Massachusetts, November, 1971.

(10) Curtis, W. R. and P. K. Rao, "Gulf Stream Thermal Gradients from Satellite, Ship and Aircraft Observations," Journal of Geophysical Research, vol. 74, no. 28, pp. 6984-6990.

(11) Holter, M. R., et. al., "Research Needs: The Influence of Discrimination, Data Processing, and System Design," in Remote Sensing, Washington, D. C., National Academy of Sciences, pp. 73-161, 1970.

(12) Dellwig, L. F. and C. Burchell, "Side-Look Radar: Its Uses and Limitations as a Reconnaissance Tool," (Abs.) in Highway Research Abstracts, vol. 55, pp. 2064-2055, 1971.

(13) Gillerman, E., "Investigation of Cross-Polarized Radar on Volcanic Rocks," CRES Technical Report 61-25, The University of Kansas Center for Research, Inc., Lawrence, Kansas February, 1967.

(14) Cosgriff, R. L., W. H. Peake and R. C. Taylog, "Terrain Scattering Properties For Sensor System Design," (Terrain Handbook II), Engineering Experiment Station Bulletin 181, Ohio State University, Columbus, Ohio, 1960.

(15) Dellwig, L. F., "An Evaluation of Multifrequency Radar Imagery of the Pisgah Crater Area, California," CRES Technical Report 118-6, The University of Kansas Center for Research, Inc., Lawrence, Kansas, Published in Modern Geology, vol. 1, p. 65, 1969.

(16) Cutrona, L. J., "Synthetic Aperature Radar," in Radar Handbook, M. I. Skolnik, Editor, McGraw-Hill Book Company, New York, pp. 13-23, 1970.

(17) Morain, S. A., and D. S. Simonett, "Vegetation Analysis with Radar Imagery," CRES Technical Report 61-9, The University of Kansas Center for Research, Inc., Lawrence, Kansas, April, 1965.

(18) Coiner, J. C., and L. F. Dellwig, "Similarities and Differences in the Interpretation of Air Photos and SLAR Imagery," Proceedings of the Electro-Optical Systems Design Conference, New York, September, 12-14, 1972.

(19) Lewis, A. J., "Geomorphic Evaluation of Radar Imagery of Southeastern Panama and Northwestern Columbia," CRES Technical Report 133-18, The University of Kansas Center for Research, Inc., Lawrence, Kansas, January, 1971.

(20) Walters, R. L., "Radar Bibliography for Geosciences," CRES Technical Report 61-30, The University of Kansas Center for Research, Inc., Lawrence, Kansas, March, 1968.

(21) Moore, R. K., "Radar Imaging Applications: Past, Present and Future," in AGARD Conference Proceedings No. 90 on Propagation Limitations in Remote Sensing, J. B. Lomax, Editor, NATO, pp. 9-1 to 9-19, 1971.

(22) Claassen, J. P., et. al., "Radar Sea Return and the RADSCAT Satellite Anemometer," Ocean '72 IEEE International Conference Record, Engineering in the Ocean Environment, (IEEE Publication 72 CHO 660-1 OCC), Newport Rhode Island, pp. 180-185, September, 1972.

(23) Moore, R. K., "Ground Return," Chapter 25 in Radar Handbook, M. I. Skolnik, Editor, McGraw-Hill Book Company, New York, p. 25-2, May, 1970.

(24) Janza, F. J., "The Analysis of a Pulsed Radar Aquisition System and a Comparison of Analytical Models for Describing Land and Water Radar Return Phenomena, Ph.D. Dissertation, The University of New Mexico, Albuquerque, New Mexico, 1963; also Published as Sandia Corp. Monograph, SCR-533, 1963.

(25) Lundien, J. R., "Terrain Analysis by Electromagnetic Means," U. S. Army Engineer Waterways Experiment Station, Technical Report 3.693, 1971.

(26) Roberts, S. and A. Von Hippel, "A New Method for Measuring Dielectric Constant and Loss in the Range of Centimeter Waves," Journal of Applied Physics, vol. 17, July, 1946.

(27) Vickers, R. S., and G. C. Rose, "The Use of Complex Dielectric Constant as a Diagnostic Tool for the Remote Sensing of Terrestrial Material," Colorado State University, Department of Electrical Engineering, Fort Collins,Colorado, Project No. 7260, Scientific Report No. 5.

(28) Wiebe, M. L., "Laboratory Measurement of the Complex Dielectric Constant of Soils," Texas A&M University Remote Sensing Center, College Station, Texas, Technical Report RSC-23, 1971.

(29) Waite, W. P., "Broad Spectrum Electromagnetic Backscatter," CRES Technical Report 133-17, The University of Kansas Center for Research, Inc., Lawrence, Kansas, August, 1970.

(30) Skolnik, M. I., Introduction to Radar Systems, McGraw-Hill, Inc., New York, p. 264, 1962.

(31) Ulaby, F. T., "4-8 GHz Microwave Active and Passive Spectrometer (MAPS)," Volume I, Radar Section, CRES Technical Report 177-34, The University of Kansas Center for Research, Inc., Lawrence, Kansas, January, 1973.

(32) Taylor, J. W., Jr., and J. Mattern, "Receivers," in Radar Handbook, M. I. Skolnik, Editor, McGraw-Hill Book Company, New York, p. 5-5, 1970.

(33) Kell, R. E., and R. A. Ross, "Radar Cross Section of Targets," in Radar Handbook, M. I. Skolnik, Editor, McGraw-Hill Book Company, New York, pp. 27-11, 16, 1970.

(34) Ulaby, F. T. and R. K. Moore, "Radar Spectral Measurements of Vegetation," CRES Technical Report 177-40, The University of Kansas Center for Research, Inc., Lawrence, Kansas, April, 1973.

(35) Reitz, E. A., et. a., "Radar Terrain Return Study, Final Report: Measurement of Terrain Backscattering Coefficients with an Airborne X-Band Radar," Goodyear Aerospace Corporation Department, Report GERA - 463, 1959.

(36) de Loor, G. P., and A. A. Gurriens, "The Radar Backscatter of Vegetation," AGARD Conference Proc. No. 90 on Propagation Limitations of Remote Sensing, NATO, pp. 12-1, 12-7, 1971.

(37) Moore, R. K., W. P. Waite and J. W. Rouse, Jr., "Panchromatic and Poly-panchromatic Radar," Proc. IEEE, vol. 57, pp. 590-593, April, 1969.

(38) Thomann, G.C., "Panchromatic Illumination for Radar; Acoustic Simulation of Panchromatic Radar," CRES Technical Report 177-11, The University of Kansas Center for Research, Inc., Lawrence, Kansas, September, 1970.

(39) Ulaby, F. T., R. K. Moore, R. Moe, and J. Holtzman, "On Microwave Remote Sensing of Vegetation," Proceedings 8th Symposium of Remote Sensing of Environment, University of Michigan, Ann Arbor, Michigan, 1972.

(40) Fisz, M., Probability Theory and Mathematical Statistics, John Wiley and Sons, Inc., New York, 1963.

(41) Hersey, D. F., Editor, Water Resources Research Catalog, U. S. Department of the Interior, Office of Water Resources Research, Water Resources Scientific Information Center, Washington, D. C., 1972.

(42) Rouse, J. W., Jr., "Broad Spectrum Backscatter Acoustic System," CRES Technical Memorandum 133-2, The University of Kansas Center for Research, Inc., Lawrence, Kansas March, 1968.

(43) Cramer, H., Mathematical Methods of Statistics, Princeton University Press, Princeton, New Jersey, p. 234, 1946.